Mitochondrial Actions and Structure Activity Relationships of Cytotoxic Ionic Liquids

Meryem-Nur Duman

Thesis submitted in fulfilment of the requirements for

the degree of Doctor of Philosophy

Supervisor: Associate Professor Tristan Rawling

Co-Supervisor: Associate Professor Andrew McDonagh

University of Technology Sydney

Faculty of Science

February 2023

Declaration

I, Meryem-Nur Duman declare that this thesis, is submitted in fulfilment of the requirements for the award of Doctor of Philosophy (Science) in the School of Mathematics and Physical Sciences at the University of Technology Sydney.

This thesis is wholly my own work unless otherwise referenced or acknowledged. In addition, I certify that all information sources and literature used are indicated in the thesis. This document has not been submitted for qualifications at any other academic institution. This research is supported by the Australian Government Research Training Program.

Meryem-Nur Duman

February 2023

COVID-19 impact statement

The work involved for this thesis was impacted by the COVID- 19 pandemic during 2020 and through to 2021. Progress was affected and delayed during this period due to several factors including:

1- Extended periods of time (months) waiting for orders and delivery of consumables such as biological laboratory consumables and/or chemical reagents.

2- Lockdown for 4 months and access to laboratories and experimental facilities was limited and/or restricted.

These factors resulted in some experiments in Chapter 3 not being able to be completed within the time of my candidature. This is a result of the experiments being laboratory-based activities and could not be transitioned to an online format. Unfortunately, the level of detail and experiments preformed for this thesis was less than originally intended for the full scope of this study.

Acknowledgments

Firstly, I would like to thank my supervisor Associate Professor Tristan Rawling for his help and guidance throughout this project, and his constant excitement and enthusiasm which has allowed me to learn so much. I would also like to thank my co-supervisor Associate Professor Andrew McDonagh for all his help and guidance.

Secondly, I would like to thank Dr. Alexander Angeloski for his constant help throughout this project and teaching me so much. Next, I would like to thank Dr Ariane Roseblade for her constant help in the biology lab, thank you for teaching me all I know about cell work and for constantly answering my questions. A big thank you to Dr. Mike Johnson and Associate Professor Charles Cranfield. Mike for this constant help with microscopy and Charles for all he has provided for the tBLMs.

I would also like to thank my research group, Ethan Pacchini, Ritik Roy, Freddy Ha and Edward York, without you guys the time during my PhD would not have been the same. Also, I would like to thank Dr Ronald Shimmon for the NMR training he provided and the general assistance within the laboratory, along with Dr. Alexander Angeloski and Dr. Iurii Bodachivskyi for their technical support throughout the years.

Lastly, I would like to thank my sister Merve for providing moral support and constant encouragement throughout my PhD. I hope to have made you proud with this accomplishment.

Table of Contents

List of Figures

List of Schemes

List of Tables

Publications, Presentations and Awards

Publications (related to this thesis)

M.-N. Duman, A. Angeloski, M. S. Johnson and T. Rawling. (2023). "Aromatic long chain cations of amphiphilic ionic liquids permeabilise the inner mitochondrial membrane and induce mitochondrial dysfunction at cytotoxic concentrations", *Green Chemistry,* **25**, 6067-6076.

Publications (not related to this thesis)

C. I. Gallagher, Z. J. Frangos, D. Sheipouri, S. Shimmon, M.-N. Duman, S. Jayakumar, C. L. Cioffi, T. Rawling and R. J. Vandenberg. (2023). "Novel Phenylene Lipids That Are Positive Allosteric Modulators of Glycine Receptors and Inhibitors of Glycine Transporter 2", *ACS Chemical Neuroscience*, 14, 2634-2647.

E. York, D. A. McNaughton, M. -N. Duman, P. A. Gale and T. Rawling. (2023), "Fatty Acid-Activated Proton Transport by Bisaryl Anion Transporters Depolarises Mitochondria and Reduces the Viability of MDA-MB-231 Breat Cancer Cells", *Biomolecules*, 13.

A. Angeloski, K. Flower-Donaldson, F. Matar, D. Hayes, M. Duman, D. Oldfield, M. Westerhausen and A. McDonagh. (2023) "Gold microstructures by thermolysis of isomeric gold (III)-di-isopropyldithiocarbamate complexes", *ChemNanoMat*. DOI: 10.1002/cnma.202300514.

Presentation

M.-N. Duman "Aromatic long chain cations of amphiphilic ionic liquids permeabilise the inner mitochondrial membrane and induce mitochondrial dysfunction at cytotoxic concentrations", Poster presentation, 8th Asia-Oceania Conference on Green and Sustainable Chemistry, 29th November 2023, Auckland, New Zealand.

Awards

8th Asia-Oceania Conference on Green and Sustainable Chemistry: Highly Commended Poster Presentation.

List of Abbreviations

qNMR	Absolute quantitative ^1H nuclear magnetic resonance
ADP	Adenosine diphosphate
ATP	Adenosine triphosphate
br s	Broad singlet (NMR)
^{13}C NMR	Carbon nuclear magnetic resonance
FCCP	Carbonyl cyanide-4-(trifluoromethoxy)phenylhydrazone
$CHCl_3$	Chloroform
J	Coupling constant (NMR)
^{o} C	Degrees Celsius
DLC	Delocalised lipophilic cation
δ	Delta (Chemical Shift, NMR)
$CDCl_3$	Deuterated chloroform
DCFDA	2',7'-dichlorofluorescein diacetate
DCM	Dichloromethane
DMSO	Dimethyl sulfoxide
MTS	3-(4,5-dimethylthiazol-2-yl)-5-(3-carboxymethoxyphenyl)-2-(4-sulfophenyl)-2H-tetrazolium
DOPC	1,2-dioleoyl-*sn*-glycero-3-phosphocholine
d	Doublet (NMR)
dd	Doublet of doublets (NMR)
FBS	Fetal bovine serum
IC_{50}	Half maximal inhibitory concentration
Hz	Hertz

HRMS	High resolution mass spectroscopy
IS	Internal standard
IL	Ionic liquid
MIM	Methylimidazolium
IMM	Inner mitochondrial membrane
MS	Mass spectrometry
m/z	Mass to charge ratio
m.p.	Melting point
μM	Micro-molar
mg	Milligrams
mL	Millilitre
mmol	Milli mole
$\Delta\Psi_m$	Mitochondrial membrane potential
DMEM	Mulbecco's modified eagle's medium
m	Multiplet (NMR)
NMR	Nuclear Magnetic Resonance
OXPHOS	Oxidative phosphorylation
OCR	Oxygen consumption rate
PBS	Phosphate buffered saline
$[M + H]^+$	Protonated molecular ion
PMF	Proton motive force
^{1}H NMR	Proton nuclear magnetic resonance
ROS	Reactive oxygen species
Py	Pyridinium

Quin	Quinolonium
S	Singlet (NMR)
SEM	Standard error of mean
SAR	Structure-activity relationship
JC-1	1,1',3,3'-tetraethyl-5,5',6,6'-tetrachloroimidacarbocyanine iodide
tBLM	Tethered bilayer lipid membrane
BF_4	Tetrafluoroborate
TMA	Trimethyl ammonium
t	Triplet (NMR)

Abstract

Ionic liquids (ILs) are a group of ionic compounds that are typically comprised of an inorganic anion and an organic cation that is substituted with an *N*-alkyl chain. The physicochemical properties of ILs can be readily controlled through different combinations of cations and anions, which have allowed for the development of task specific ILs with a wide variety of applications. ILs were once touted as environmentally friendly and safe alternatives to organic solvents, however recent research has shown that ILs are toxic towards a variety of organisms such as microbes, plants, aquatic life, and mammalian cells. The understanding of the cellular mechanisms and structural features of ILs that promote cytotoxicity is incomplete, and this may limit the wide scale adoption of ILs. Thus, the aims of this thesis were to provide new insights into the mechanism by which ILs induce toxicity and the structure-activity relationship (SAR) governing IL cytotoxicity.

The first stage of this thesis investigated the cytotoxic mechanism of ILs. Current evidence suggests that ILs kill cells by disrupting cellular membranes and/or inducing mitochondrial dysfunction. ILs share structural features with lipophilic cations such as triphenylphosphonium salts, which are known to accumulate in mitochondria in response to the membrane potential across the inner mitochondrial membrane (IMM). Therefore, it was hypothesised that ILs exert their cytotoxic effects by disrupting the IMM, the integrity of which is critical to several important cellular processes. To investigate this, a library of ILs bearing aromatic or aliphatic cationic headgroups substituted with butyl or decyl chain were prepared and their effects on HeLa cell viability and mitochondrial function were assessed. Mitochondrial accumulation was established using fluorescence microscopy, where a quinolinium-based IL was shown to rapidly partition to mitochondria of HeLa cells. It was found that IL cytotoxicity correlated to their capacity to disrupt lipid bilayers, and that ILs

produce a range of cellular effects consistent with permeabilisation of the IMM. ILs depolarise the IMM, inhibit oxidative phosphorylation and ATP synthesis, and induce ROS formation at cytotoxic concentrations. These effects were only induced by ILs with aromatic cations substituted with long (decyl) alkyl chains, as these features promote accumulation in, and permeabilisation of, the IMM. These mechanistic insights help explain the structure-activity relationship governing IL cytotoxicity and may be used to rationally design either safe or cytotoxic ILs.

The second stage of this thesis sought to expand the SAR governing IL cytotoxicity by assessing the impacts of headgroup substitution. To achieve this a series of quinolinium-based ILs (**29-32**) were synthesised with various substituents at the C-3 position of the headgroup. The substituted ILs killed HeLa cells with similar potency to their unsubstituted counterpart, which suggests that substitution on the quinolinium headgroup does not significantly affect cytotoxicity. The diversity of the quinolinium IL library was limited by commercial availability of appropriate quinolines, so a second series of substituted ILs were prepared with pyridyl-headgroups (**35-44**). From this series it was shown that while substituent lipophilicity and electronic properties had minimal effect on cytotoxicity, the capacity of the substituent to act as a hydrogen bond donor did. Thus, ILs substituted with hydroxyl or primary amide substituents were 2-3 fold less cytotoxic than those bearing other substituents. A preliminary investigation aimed at understanding the role of hydrogen bond donating substituents in governing cytotoxicity was conducted. It was shown that the presence of hydrogen bond donating groups decreased the capacity of the ILs to permeabilise lipid bilayers. Further studies are required to understand the hydrogen bonding that occurs between these ILs and membrane phospholipids, and what impact this has on the mitochondrial actions of substituted ILs.

Chapter 1 - Introduction

1.1 Ionic Liquids

Ionic liquids (ILs) are a group of ionic compounds which typically contain a positively charged organic cation and a negatively charged inorganic anion. Common IL cations and anions structures are shown in **Figure 1A**. In the case of ILs bearing aliphatic cationic headgroups such as PIP the positive charge is localised on a single atom, whilst in ILs with aromatic headgroups such as MIM the positive charge is delocalised across the headgroup *via* resonance stabilisation.[1] IL cationic headgroups are also typically substituted with an *N*-alkyl chain as shown in **Figure 1B**.
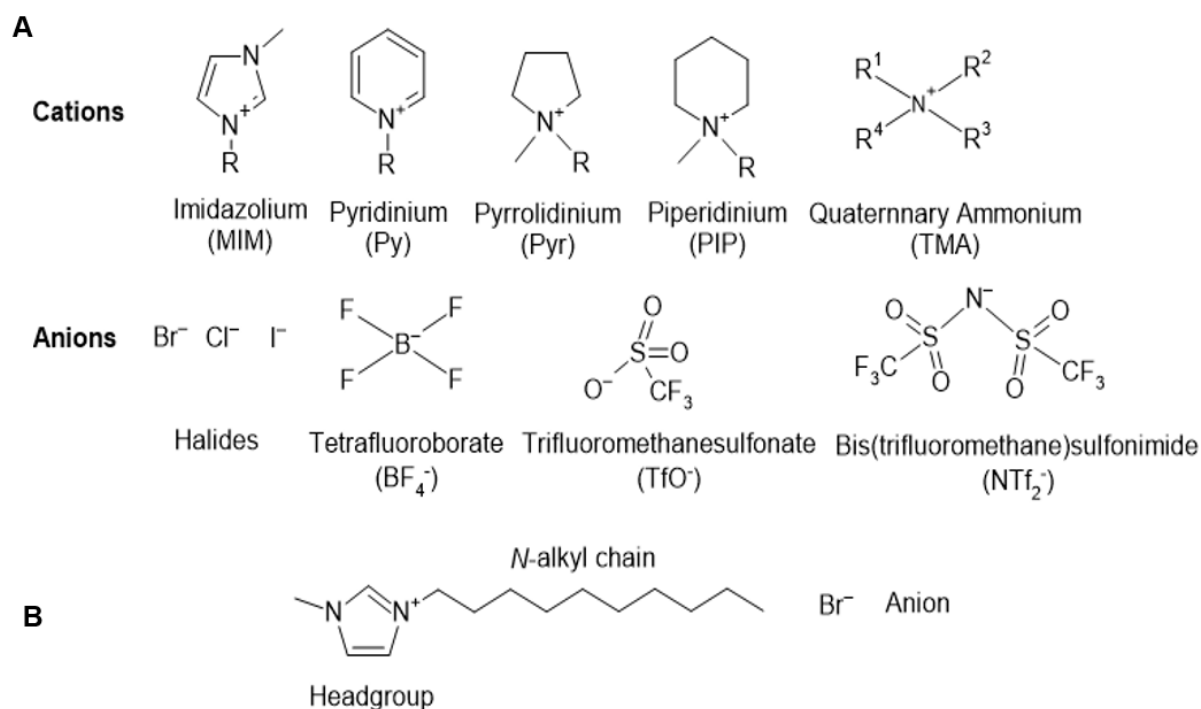
Figure 1 A) Chemical structures of common cationic headgroups (upper) and anionic (lower) components of ILs. B) Structural components of the IL 1-decyl-3-methylimidazolium bromide (**[C10Mim][Br]**).

IL research has steadily increased over the last two decades, since their initial report in 1914 by Paul Walden, who synthesised the first room temperature IL ethylammonium nitrate

([CH$_3$CH$_2$NH$_3$]$^+$ [NO$_3$]$^-$) with a melting point of 12 °C. [2-4] Recently, ILs have gained significant attention in the scientific community as the diverse combination of ILs cations and anions allows access to a vast range of possible structures with a tunable nature. This allows the physicochemical properties of ILs to be readily controlled for the development of task-specific ILs with a wide range of potential applications as [5]solvents and catalysts in areas such as food processing, battery and energy research, and pharmaceutics.[6-10] ILs also posess favourable pharmacological characteristics such as aqueous solubility and membrane premeabilty that makes them suitable for applications in biological systems.[11]

1.2 Applications of ILs

Following on from their discovery, ILs were initially considered environmentally friendly and safe alternatives to conventional organic solvents due to their high thermal stability and low flammability owing to their negligible vapour pressure.[4,12-14] These properties can increase their safety and potential use in high temperature processes, which has led many investigators to explore their use in a variety of applications, which will be discussed in the following section. More recently concerns have arisen regarding IL toxicity towards a variety of organisms, and these concerns may hinder the widespread adoption of ILs.[1,11,15-17] Regardless, ILs show promise in many areas and as their applications are explored further research is required to develop safe ILs for their commercial use.

1.2.1 IL use in electrochemical applications

ILs have gained interest in electrochemical applications such as catalysts and solvents due to their low volatility and ionic conductivity. These desired properties initiated the use of ILs as electrolytes in energy storage devices such as batteries, sensors, solar cells and fuel cells.[18-20] Compared to common electrolyte systems, IL-based devices have a lower risk of

leakage and explosion, which allows energy storage devices to have improved conductivity and performance.[18] Hence the uses of ILs in electrochemical applications are focused on the development of safer energy storage devices.

ILs properties have contributed to their potential use as electrolytes in the development of safer and more efficient batteries.[20-23] Several types of batteries including lithium-ion, lithium metal, aluminium and redox flow batteries have been undergoing research to improve their efficiency and performance. Lithium metal battery peformance has been improved by incorporation of modifed ILs that contain inorganic polymer electrolytes, which modification has led to improved safety and stability of the batteries.[24,25] For example, Li *et al.* introduced *N*-methyl-*N*-propyl-pyrrolidinium bis(fluorosulfonyl)imide (Pyr$_{13}$FSI) into a hybrid network to obtain a series of gel polymer electrolytes (GPEs). The electrochemical properties of GPEs were altered by controlling the network structure and IL, which led to significant improvement in electrochemical and thermal stability.[20,26] A study by Angell *et al.* demonstrated the use of *N*-methyl urea and *N*-ethyl urea mixed with aluminium chloride (AlCl$_3$) as a low-cost electrolyte for use in aluminium batteries.[27] These electrolytes were shown to have significantly lower viscosities and the associated batteries had higher intrinsic discharge voltages, providing battereis with excellent performance and efficincy.

ILs have also been utilised in various types of electrochemical sensing devices such as humidity sensors, gas sensors and chemical sensors.[20,28,29] For example, Zhao *et al.* synthesised hydrophobic ILs in polymer composites which were composed of 1-ethyl-3-methylimidazolium bis(trifluo- romethylsulfonyl) imide ([EMI][TFSI]) and poly(vinylidene fluorideco-hexafluoropropylene) (PVDF-HFP). These composites demonstrated a highly sensitive and ultrafast linear response to humanity which has led to their use as humidity

sensors.[30] The use of ILs in other gas sensers have recently been investigated. A study by Yu *et al.* reported the synthesis of a metal oxide with reduced graphene oxide ($NiCo_2O_4$/rGO) combined with 1-butyl-3-methylimidazolium hexafluorophosphate ([BMIM][PF_6]) to form a composite material $NiCo_2O_4$/rGO/[BMIM][PF_6]. When employed as an oxygen sensor, electrochemical tests showed that the composite material exhibit response current, long-term stability in an oxygen-rich environment and significantly enhanced electrochemical oxygen sensing performance..[31] Additionally, D'Anna *et al.* demonstrated the interactions between ILs and tungsten trioxide (WO_3) could be used as the basis for producing pollutant gas sensor and for the removal of sulfur from crude fossil fuels. This was achieved as ILs are able to disperse WO_3 in composites consequently enhancing the contact surface and the catalytic ability of the metal oxide.[32]

1.2.2 ILs use as solvents

The ability of ILs to remain in a liquid state over a wide temperature range has led to their use as solvents in various fields such as organic and nanoparticle synthesis and in extraction processes with industrial significance.[20,33-35] ILs are being used as alternative solvents in organic and enzymatic reactions as they facilitate the purification and isolation of reaction products, which lowers their environmental impact compared to conventional solvents.[20,36,37] Additionally their ease of recovery by distillation or extraction for further use contributes to reduced costs and enhances their utilisation in various industrial processes.[38,39] ILs have been explored to improve extraction and separation processes for biomass and flavonoids, dissolution of wood and water treatment to aid in the removal of water pollutants.[20] Biomass extraction has recently been utilised for clean and renewable energy sources. For example, Tan *et al.* utlised ILs as solvents for the extraction of high-value bio-compounds such as lipids, proteins, and carbohydrates from microalgae biomass for their potential use in large-

scale production of biofuels, food additives, and nutritive supplements.[40] In addition, Rodrigues *et al.* used ultrasonic treatment of 25kHz on *Spirulina platensis* suspended in a mixture of the ILs 2-hydroxyethylammonium acetate and 2-hydroxyethylammonium formate in a 1:1 ratio. The ILs mixture solution demonstrated a higher extraction efficiency of phycocyanin, allophycocyanin, and phycoerythrin compared to the conventionally used sodium phosphate buffer and 1-butyl-3-methylimidazolium chloride.[41] ILs have also been utilised as solvents for the extraction of flavonoids, which are a class of naturally occurring polyphenolic compounds that possess several benefitcial properties such as anticancer, anti-inflammatory, antioxidant and antibacterial activity.[20] For example, Rahmi *et al.* used imidazolium based ILs as solvents to improve the extraction of quercetin (a flavonoid) from Nothopanax scutellarium leaves.[42] The use of ILs as solvents in these processes are favoured compared to conventional solvents as they have lower environmental impacts, however due to their amphiphilic nature ILs are more water soluble than conventional solvents, and although this can be advantageous in certain applications it may also lead to the accumulation of ILs in the environment through wastewater.[43] Given their potential cytotoxicity (see **Section 1.3**), this may pose a risk to the environment.

1.2.3 ILs in the pharmaceutical industry

ILs have favourable pharmacological properties such as aqueous solubility due to their ionic nature and lipophilicity depending on their structure and the combination of headgroup and anion used. This provides ILs the ability to diffuse through cellular membranes and be readily absorbed into the gastrointestinal tract. These properties have allowed for their potential development in pharmaceutical and medical applications.[44-46]

One promoising application of ILs is to improve the aquenous soltubilty and oral bioavailability of drugs with difficult physicocohemcial properties. This is achieved by forming ILs with active pharmaceutical ingredients (APIs).[47-49] For example, nalidixic acid, a relatively water insoluble quinolone was incorporataed into a cholinium-based IL. The resulting IL, cholinium nalidixate, was 5000 times more water soluble than the parent API, nalidixic acid.[50] Similarly, the aqueous solubility of pure salicylic acid was significantly increased when coupled with 1-alkyl-3-methylimidazolium.[51] These studies show that incorporation of APIs into ILs can be used to improve drug efficacy by increasing their solubility in aqueous media, which overcomes an important problem in the pharmaceutical industry.

Additionally, ILs have been utilised for better drug delivery and permeability. For example, Moshikur *et al.* synthesised fatty acid based amino acid ILs (FAAAE-ILs) and their use in transdermal drug delivery of ibuprofen was investigated. FAAAE-ILs were found to provide excellent ibuprofen solubility and were also more effective in enhancing the permeability of drugs.[52] The same group also developed an IL based API using *N*-methyl-2-pyrrolidone (NMP) for effective topical drug delivery. They found the NMP cation presented lower toxicity when compared to conventional IL cations and when ILs were coupled with the NMP cation they exhibited better physico-thermal stability and enhanced skin penetration comapred to conventional IL. Lastly, they demonstrated ILs coupled with NMP presented higher drug accumulation when compared to Cho-IL in target tissue.[53]

1.2.4 ILs as anticancer agents

Cancer is a disease in which there is an abnormal uncontrolled growth of cells which can form a mass called a tumor. Growth of the primary tumor, or its spread to other regions of the body, can lead to organ damage and eventually death. According to the World Health

Organization (WHO), cancer is a leading cause of death worldwide with nearly 10 million deaths in 2020 and is a prominent cause of economic expenditure (**Table 1**).[54] The most common forms of cancer in men include lung, prostate, stomach and liver cancer, whilst breast, lung, and cervical cancer are the most common amongst women. Since cancer involves the uncontrolled proliferation of cancer cells, treatments are aimed at killing cancer cells using cytotoxic chemotherapeutic agents. These drugs have significantly reduced the mortality of cancer, however issues regarding their efficacy and their capacity to produce severe side effects mean that there is still a need for the development of selective chemotherapy drugs with a new mechanism of action.

Table 1 Most common forms of cancer and number of deaths in 2020.

Cancer type	Number of deaths
Lung	1, 800, 000
Breast	685, 000
Colon and rectum	916, 000
Liver	830, 000
Stomach	769, 000

Given that ILs have the correct balance of lipophilicity and polarity required of pharmaceutical agents as well as a capacity to incduce cell death, they have the potentialto be developed into novel anticancer agents. Recent research has shown ILs are cytotoxic and lead to the reduction of cell viability in a range of cancer cell lines, including breast (MCF-7, MDA-MB-231), cervical (HeLa), leukemia (IPC-81) and colon cancer (HT-29 and CaCo-2),[16,55-58] and that ILs may be suitable replacements for current chemotherapeutic drugs.[11,59-61] For example, Zhong-bo *et al.* found the C_{12} guanidinium-based ILs (GIL12) to be approximatly

10-fold more potent than Mitomycin C (a chemotherapy drug) when tested in HeLa299 cells.[62] ILs tested in various cancer cell lines and their half maximal effective concentration (EC$_{50}$), which is a measure of the concentration of a drug required to induce a biological response halfway between the baseline and the maximum, values are summarised in **Table 2**. Commonly IL cytotoxicity is reported with either EC$_{50}$ or IC$_{50}$ values (half-maximal inhibitory concentration).

Table 2 IC$_{50}$ or EC$_{50}$ concentrations of ILs tested as anticancer agents in human cancer cell lines.

IL	Cell line	EC$_{50}$ (mM)	IC$_{50}$ (mM)	Ref
[C$_4$MIM] [Br]	HeLa	2.75	-	17
[C$_4$MIM][PF$_4$]	HeLa	11.2	-	15
[C$_4$MIM][Cl]	B-13	-	1.5	63
[C$_8$MIM] [Br]	HeLa	0.30	-	17
[C$_8$MIM] [Br]	HepG2	-	0.440	59
[C$_8$MIM] [PF$_6$]	CaCo-2	-	0.003	64
[C$_{10}$MIM][Cl]	IPC-81	0.00134	-	55
[C$_4$Py] [Br]	HeLa	3.19	-	17
[C$_4$Py][Tf$_2$N]	HeLa	1.67	-	17
[C$_8$Py] [Br]	HeLa	0.28	-	17
[C$_4$Pip] [Br]	MCF-7	-	14	57
[C$_8$Pip] [Br]	MCF-7	-	0.54	57
[C$_4$TMA] [Br]	HeLa	8.00	-	17
[C$_8$TMA] [Br]	HeLa	0.33	-	17

Imidazolium-based ILs are the most commonly explored class of ILs as anticancer agents, which are nitrogen-rich heterocyclic compounds with favourable properties.[65] Imidazolium-based ILs **[C$_4$MIM][Br]** and **[C$_{12}$MIM][Br]** have been reported to decrease the cell viability in PC12 cells, with EC$_{50}$ concentartions of > 10 mM to 24 μM, respectively.[66]

It is important to compare the toxic effects of ILs towards cancerous cells and non-cancerous cells to understand their potential as anticancer agents. A study by Kaushik *et al.* showed ILs **[C$_1$MIM][Cl]**, **[C$_4$MIM][Cl]** and triethylammonium sulfate were more toxic towards T98G brain cancer cells when compared to non-cancerous human embryonic kidney (HEK) cells.[11] These findings suggest ILs are potentially selective towards cancerous cells compared to normal cells which is important for potential anticancer drugs.

1.3 IL Cytotoxicity

ILs have been shown to be cytotoxic towards a wide range of organisms including fish (CCO, a channel catfish ovary cell line),[15] insects,[67] bacteria (*Aliivibrio fischeri*),[68] plant cells (pine trees, eucalyptus and rice seedlings)[69] and mammalian cells (HEK, embryonic kidney and HeLa, cervical cancer cells).[16,17,70] For example, Huijun Liu *et al.* found the ILs **[C$_8$MIM][Cl]**, **[C$_{10}$MIM][Cl]** and **[C$_{12}$MIM][Cl]** inhibit the growth of rice seedings, where an increase in IL concentration decreased the stem and root size of the plant.[69] Due to ILs high water solubility they have been identified as an emerging environmental problem due to their ease of penetration in waterways and particularly due to their cytotoxicity towards aquatic organisms. Several studies have been conducted to determine ILs cytotoxicity, for example imidazolium-based ILs were found to cause oxidative stress and inhibit growth in aquatic algae[71-74] and terrestrial plants.[75-77] Comparable results were obtained when plants were treated with ammonium based ILs.[78,79] ILs have been observed to present high antimicrobial, antifungal and antibacterial cytotoxicity, due to their long alkyl chain being able to destabilise

the membrane by inserting into the lipid bilayer and causing structural damage.[80-82] For example, when bacteria (*Aliivibrio fischeri)* was exposed to 1-butyl-4-methylpyridinium tetrafluoroborate **[C₄mpy][BF₄]**, a high toxicity with an $EC_{50}= 45.3$ mg·L^{-1} was observed.[68]

1.4 IL cytotoxicity structure-activity relationships

Numerous studies have revealed the structural features of ILs which promote cytotoxicity in one organism are also common to other organisms, hence an overall structure activity relationship (SAR) can be derived which describes the general cytotoxicity of ILs. This SAR will be detailed in the following section and supported by examples across different classes of organisms. It should be noted that the SAR information regarding IL cytotoxicity is limited by the low structural diversity of ILs assessed in toxicity studies. This shortfall will be investigated later in this thesis.

1.4.1 *N*-alkyl chain length

The length of the *N*-alkyl chain on the cation is a major determinant of cytotoxicity, with numerous studies showing IL cytotoxicity increases as the alkyl chain length increases.[15,16,55,58,61,66,83-86] For example, Malhotra *et al.* found that the *in vitro* cytotoxicity of imidazolium based ionic liquids against 60 human cancer cell lines was significantly enhanced where the alkyl chain length was increased to 12 or more carbons. This is exemplified by 1-methy-3-dodecylimidazolium (**[C₁₂MIM][Cl]**) which showed activity against all cancer cell lines tested with overall potency in terms of GI_{50} values ranging from 0.109 to 22.60 μM whilst 1-methy-3-hexadecylimidazolium (**[C₁₆MIM][Cl]**) had increased activity with GI_{50} values ranging from 0.092 to 2.10 μM. In contrast, when the alkyl chain lengths ranged between 4 to 8 carbons, the compounds were considered inactive as they showed less than 60 % growth inhibition.[61] This dependence on chain length was also observed in bacteria (*Aliivibrio fischeri)*

where a pyridinium-based ILs bearing a 2 carbon *N*-alkyl chain had an EC_{50} value of ~3400 mg·L^{-1}. When the chain length was increased to 4 carbons, this caused an increase in cytotoxicity as shown by a 6-fold decrease in the EC_{50} value to ~500 mg·L^{-1}.[87] There have also been reports on the influence of chain polarity on cytotoxicity by functionalising the *N*-alkyl chain with polar substituents such as hydroxyl or ether groups. For example, Frade *et al.* found that imidazolium based ILs with polar hydroxyl and ether groups in the alkyl chain were less cytotoxic towards CaCo-2 colon cancer cells .[83]

1.4.2 Headgroup

The nature of the IL headgroup appears to modulate IL cytotoxicity, although the effect headgroup structure has is lower in magnitude than that of the *N*-alkyl chain. Headgroup aromaticity promotes IL cytotoxicity, with several studies finding that ILs containing aromatic headgroups were significantly more cytotoxic towards cancerous cells than aliphatic ILs.[11,17,88] For example, studies by Wang *et al*. and Kumar *et al*. showed imidazolium and pyridinium-based ILs were more cytotoxic to HeLa and MCF-7 cells than aliphatic (pyrrolidinium, piperidinium, ammonium) ILs of equivalent *N*-alkyl chain length.[17,57] Similar findings have been observed by Costa *et al.* in bacteria (*Vibrio fischeri*) where the aromatic imidazolium IL was more cytotoxic than the aliphatic IL choline acetate.[68] Interestingly, headgroup aromaticity only appears to increase the cytotoxicity of ILs with longer ($\geq$ C8) alkyl chains; in ILs with shorter chains aromaticity does not change activity.[57] For example [C$_8$Py][Br], an IL with an octyl-substituted pyridinium headgroup, decreased the viability of MCF-7 breast cancer cells with 25-fold greater potency than its piperidinium-based counterpart, while [C$_3$Mim][NTf$_2$] was equipotent to its pyrrolidinium counterpart.[57]

Several groups have suggested that headgroup aromaticity promotes cytotoxicity by increasing the hydrophobicity of the IL cation. Headgroup hydrophobicity is correlated with increased cytotoxicity as supported by studies by Kumar *et al.* which showed that when the aliphatic piperidinium based IL was changed to the more hydrophobic pyridinium headgroup caused a 25-fold increase in cytotoxicity.[57] Importantly, hydrophobic substituent effects on the pyridinium headgroup were also assessed. Kumar *et al.* found the substitution of a methyl group on the *para*, *ortho* and *meta* positions on the pyridinium headgroup was equipotent when tested in MCF-7 cells. This suggests headgroup substitution has negligible effects on cytotoxicity.[57]

1.4.3 Anion

The effect of the anion on IL cytotoxicity is less clear, with some studies suggesting that the anion effects cytotoxicity and others indicating there to be negligible effect.[15,89,90] In general it appears that the bis(trifluoromethane)sulfonimide (NTf$_2$) anion has the greatest impact on IL toxicity. For example, Dzhemileva *et al.* found ILs with a NTf$_2$ anion were more cytotoxic towards HEK293 and A549 cells than ILs with an acetate (OAc) anion. It should be noted however that the NTf$_2$ anion is cytotoxic in its own right (MTT IC$_{50}$ of LiNTf$_2$ in HeLa cells = 4.24 μM), and that this may be causing the observed changes in IL cytotoxicity.[17,70] Additionally, a study by Kumar *et al.*[57] studied the effect of ILs with various anions on MCF-7 breast cancer cells. They found that small and hydrophilic anions such as bromide, hexafluoroarsenate and tetrafluoroborate had higher EC$_{50}$ values compared to the bulky and hydrophobic anions tested including trifluoromethanesulfonate and bis(trifluoromethylsulfonyl)imide anions.[65] There is some evidence that the influence of the anion on IL cytotoxicity is dependent on the nature of the cation, and that the anion does not affect the cytotoxicity of ILs with longer alkyl chains or aromatic cationic headgroups.[57]

1.5 Mechanism/s of cytotoxicity

While the SAR regarding IL cytotoxicity is well established, the precise cellular mechanism/s by which ILs exert cytotoxicity has not been fully elucidated. This is significant as a knowledge of the mechanism/s by which ILs induce toxicity would aid in the rational design of ILs with tailored cytotoxicty. Indeed, the lack of clarity has been identified as a major hurdle in the development of ILs as anticancer agents,[91] and potential non-toxic ILs for industrial applications. Current evidence suggests that ILs kill cells by either disputing cellular membranes or inducing mitochondrial dysfunction.[1]

1.5.1 ILs effect on cellular membranes

Cellular membranes consist of two layers of phospholipids, an inner core which is made up of hydrophobic fatty acid tails and a hydrophilic membrane surface made up of polar phosphate headgroups (**Figure 5)**.
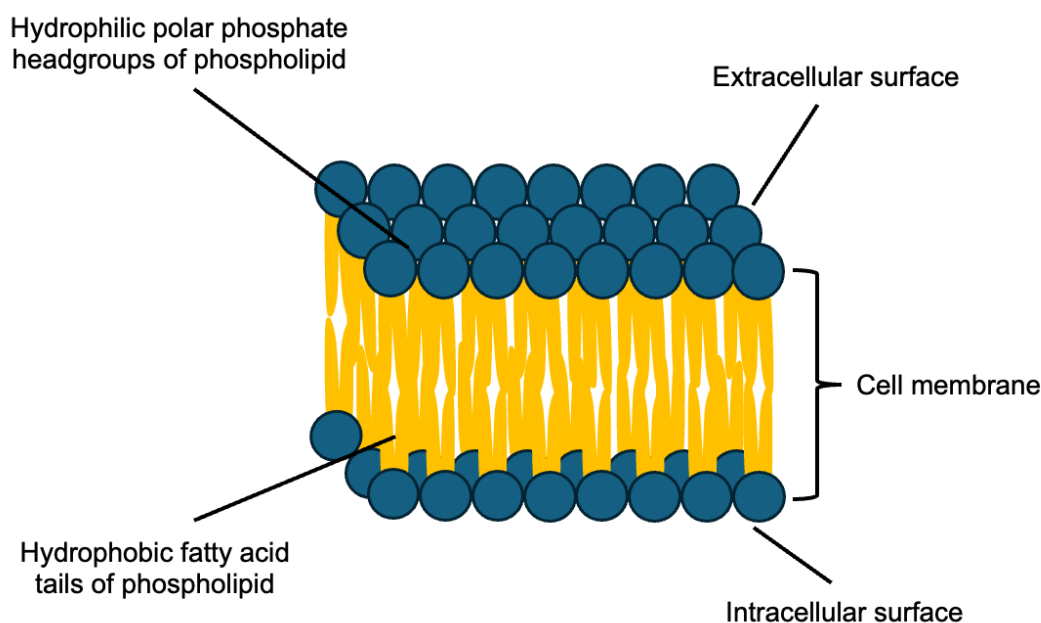
Figure 2 Labelled diagram of the cellular membrane.

Cellular membranes are biological barriers which separate the interior of the cell from extracellular environments. It is crucial for cellular membranes to maintain their integrity to allow for proper cell function and health,[92] and alterations to the structural integrity of the cell membrane may lead to cell death.[93] Numerous studies have shown that ILs effectively partition into lipid bilayers and disrupt membrane integrity.[94-96] For example, Jing *et al*. found that increasing the *N*-alkyl chain of MIM based ILs (eg: **[C$_{12}$MIM][Cl]** compared to **[C$_4$MIM][Cl]**) were able to cause greater lipid bilayer disruption and swelling.[97] Jing *et al*. suggested that IL cytotoxicity is governed by IL-induced perturbation of membrane structure and insertion of ILs in lipid bilayers, which resulst in membrane. MIM-based ILs were found to be able to insert into lipid bilayers at the lipid-water interface to cause membrane disruption due to the electrostatic attraction between the positive charge of the cationic headgroup and negatively charged regions of phospholipid headgroups. Once ILs lodge into a membrane, the headgroup remains at the lipid-water interface while the *N*-alkyl chain inserts into the hydrophobic core of the membrane. This causes membrane permeabilisation as it loses its structural integrity.[94,98,99] Importantly, a trend between the hydrophobicity of ILs and their ability to disrupt cell membranes have been shown in several studies, where increasing the *N*-alkyl chain length leads to greater membrane disruption and cytotoxicity.[16,55,58,85,96,98-100]

Supprting the conclusions gained from studies in model membranes, cell-based studies indicate that disruption of the plasma membrane may account for IL cytotoxicity. For example, Kumar *et al.* showed increasing the hydrophobicity of MIM based ILs by extending the *N*-alkyl chain length from C$_8$ to C$_{16}$ caused greater disruption to the membrane integrity of POPC bilayers and also led to increased permeabilisation, which was correlated with their cytotoxicity towards HeLa cells.[94] Additionaly, the greatre hydrophobicity of aromatic ILs relative to aliphatic ILs allows for enhanced membrane insertion and could account for their greater

cytotoxicty.[70,96,101-106] For example, Kaur *et al.* found lipid packing was affected based on hydrophobicity of the headgroup, where the aliphatic ammonium IL did not affect lipid bilayer dynamics whilst the aromatic benzimidazolium IL increased lipid chain synamics by enhacing interlipid spacing. In response to these structural changes the lipid bilayer becomes more permeable and was expected to induce high cellular cytotoxicity.[96]

1.5.2 ILs induce mitochondrial dysfunction

ILs have also been shown to cause mitochondrial dysfunction, which is important as mitochondria are involved in several processes that determine cell health and function.[107,108] Mitochondria are small membrane bound organelles found in eukaryotic cells with the primary function of generating chemical energy to the cell in the form of adenosine triphosphate (ATP) which is vital in maintaining normal cell function and survival.[107,108] Mitochondria consist of two distinct membranes, a permeable outer membrane, and a relatively impermeable inner mitochondrial membrane (IMM) which encloses the mitochondrial matrix (**Figure 3).** These two membranes are separated by the intermembrane space.
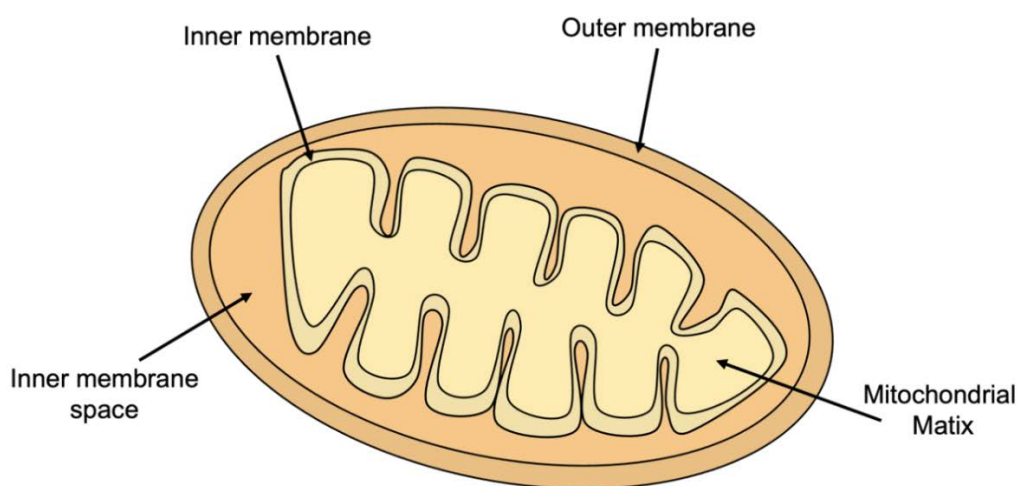
Figure 3 Structure of mitochondria with an outer and inner membrane.

In addition to ATP production, mitochondria have many roles within the cell to maintain normal cell function such as thermal regulation, cell signalling pathways, apoptosis regulation, and reactive oxygen species (ROS) containment.[109, 110] Mitochondria produce ATP via oxidative phosphorylation (OxPhos), a metabolic pathway that takes place in the inner mitochondrial membrane (IMM) and uses the energy released by nutrient oxidation to produce large amounts of cellular energy in the form of ATP. The OxPhos pathway is able to efficiently provide energy as one glucose molecule yields up to 36 molecules of ATP.[110] OxPhos is driven by the movement of electrons through the electron transport chain (ETC), a series of protein complexes (Complexes I-IV) embedded in the IMM which shuttle electrons via sequential redox reactions, as shown in **Figure 4**. The high energy electron carriers NADH and $FADH_2$ donate electrons to the ETC at either Complex I or II, and are carried through to Complex IV where oxygen serves as the final electron acceptor to produce molecular water.[111,112] The ETC uses energy derived from nutrient oxidation to pump protons from the matrix, across the IMM and into the intermembrane space. As the IMM is relatively impermeable an electrochemical proton gradient is established, referred to as the proton motive force (PMF). The PMF drives the flow of protons through the ATP synthase to re-enter the matrix, which catalyses the synthesis of ATP from adenosine diphosphate (ADP) and inorganic phosphate (P_i) (**Figure 4**).[111] In addition, mitochondria have other fundamental roles including the production of ROS as leakage of protons from the ETC can cause the reduction of molecular oxygen.[110,113]
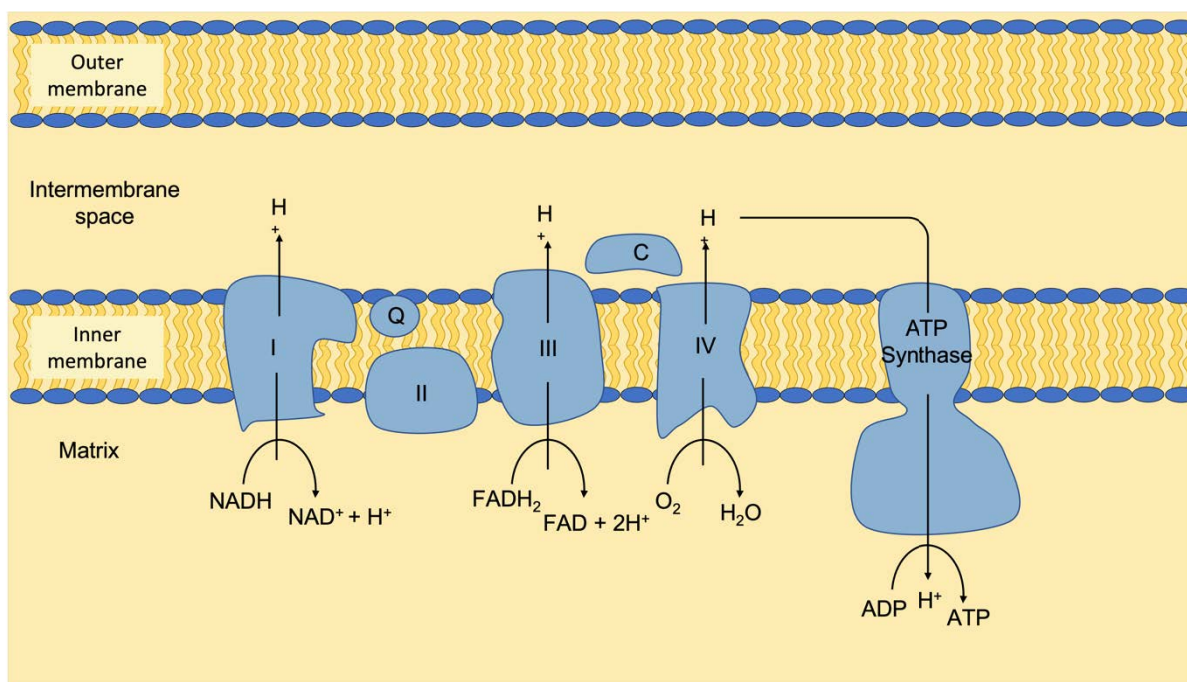
Figure 4 The electron transport chain, complexes I-IV and the ATP synthase embedded within the inner mitochondrial membrane.

Several studies have found that ILs induce mitochondrial dysfunction.[17,59,66,114] For example, Li *et al*. showed **[C₈MIM][Cl]** caused a collapse in the mitochondrial membrane potential ($\Delta\Psi_M$) and reduced intracellular ATP levels in PC12 cells.[104] This is due to the fact that mitochondria utilises the $\Delta\Psi_M$ for the production of ATP via OxPhos.[115] Other mitochondrial affects were also observed such as the induction of apoptosis via a mitochondrial-mediated pathway, DNA damage, an increase in intracellular calcium (Ca^{2+}) and the overproduction of ROS.[104] Similarly, Wang *et al.* found that **[C₂MIM][BF₄]** decreased mitochondrial membrane potential in HeLa cells. They also observed an increase in ROS production, intracellular calcium and cells undergoing apoptotosis in the presence of this IL. Similar findings were observed by Hu *et al*. who showed that **[C₁₀MIM][Cl]** caused an increase in ROS production, induced apoptosis and caused mitochondrial swelling in HeLa cells. These effects are consistent with IL induced mitochondrial dysfunction.[116] Ma and Li observed **[C₈MIM][Br]** to increase Cytochrome C content, and increase caspase-3, -8 and -9 levels in

19

HepG2 cells.[114] IL-induced alterations in mitochondrial function have been linked to impact OxPhos and cause an overproduction of ROS. Recently Wright *et al.* proposed that Mim-based ILs can inhibit OxPhos, and that they can be reduced by the ETC to neutral radical species that undergo redox cycling to produce ROS, as well as induce apoptosis in isolated human hepatocytes and rat pancreatohepatic progenitor cells (B-13).[63]

1.6 Delocalised lipophilic cations

Delocalised lipophilic cations (DLCs) are cationic compounds that have their positive charge delocalised across extended aromatic π-systems.[117] Some examples of DLCs are displayed in **Figure 5**. As aromatic ILs, such as MIM and Quin, also contain a positive charge which is delocalised across the headgroup *via* resonance stabilisation they can therefore be considered as DLCs. This observation is important when considering the mechanism of IL-induced toxicity, as DLCs have well-characterised cellular actions and are known to accumulate in mitochondria.
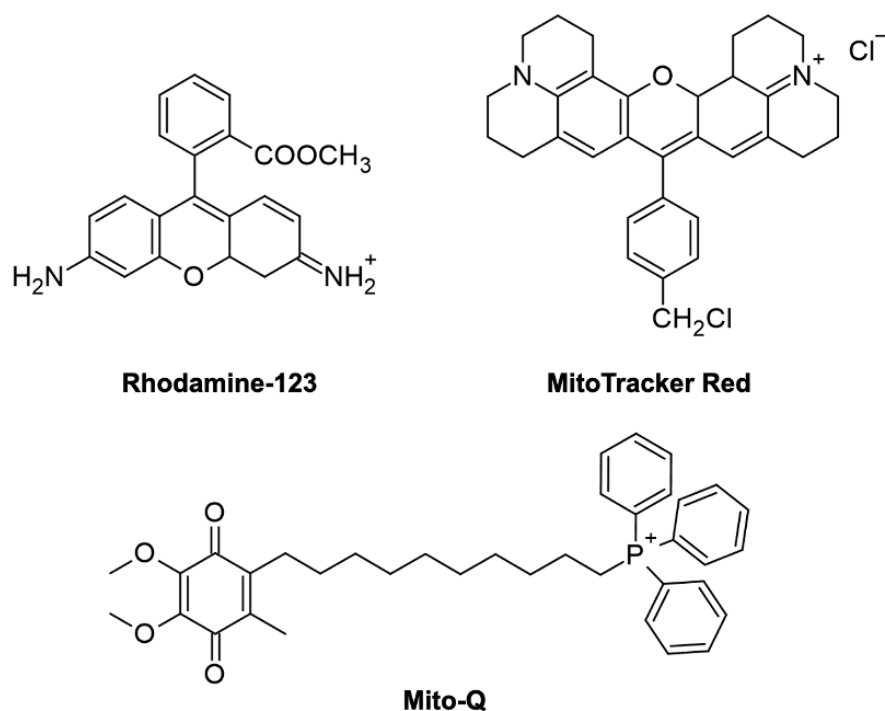
Figure 5 Chemical structures of common DLCs including rhodamine-123 (stain for live cells and detects a mitochondrial potential), Mitotraker Red (mitochondrial stain used in fluorescence microscopy) and Mito-Q (clinically approved antioxidant which prevents oxidative damage to the mitochondria).

Due to their lipohilic nature DLCs readily permeate through phospholipid bilayers and their positive charge attracts them to the negatively charges mitochndiral matrix. As a consequence, DLCs rapidly accumulate in mitochodnria when added to cells *in vitro* and *in vivo*. Key factors which influence the uptake of DLCs into mitochondria include their lipophilicity, size and the degree of positive charge delocalisation, thus affecting the electrostatic interaction with the negative $\Delta\Psi_M$.[118]

1.6.1 Accumulation of DLCs within mitochondria

Mitochondrial accumulation of DLCs is driven by the electrostatic interactions between the positively charged ion and the $\Delta\Psi_M$.[118-120] The accumulation of DLCs driven by the negative $\Delta\Psi_M$ is described according to the Nernst equation:

$$E = \frac{RT}{nF} \times ln\frac{X_{in}}{X_{out}}$$

where R is the universal gas constant (8.314 J mol^{-1} K^{-1}), T is the temperature in Kelvin, n is the number of electrons, and F is Faraday's constant (9.649 x 10^{-4} C mol^{-1}). The concentrations of the ion on both sides of the charged membrane are labelled as X_{in} and X_{out}.

The Nernst equation predicts a 10-fold accumulation per ~60 mV in $\Delta\Psi$.[121] Therefore, there is a 100-1000 fold increase in the concentration of DLCs in the mitochondria compared to the extracellular medium.[122] For example, MitoQ$_{10}$ has been shown to accumulate 10-20 fold within the cell driven by the $\Delta\Psi_p$ and then further accumulates ~150-200 fold within mitochondria driven by the $\Delta\Psi_M$.[123]

1.6.2 DLCs as mitochondrial targeting agents

DLCs readily pass through cellular membranes, such as the plasma membrane and the IMM.[117,124,125] As mentioned in **Section 1.6.1** DLCs are extensively taken up by mitochondria and are therefore widely used in mitochondrial research.[114,126,127] DLCs are therefore used as selective mitochondria stains for microscopy (eg MitoTracker dyes) and to selectively deliver drugs to the mitochondria.[119] Conjugation of mitochondrially-targeted anticancer agents to triphenylphosphonium (TPP) cations has been extensively used to direct these drugs to mitochondria.[119,128-130] The mitochondrial-specific delivery of TPPs to the IMM has been achieved through the addition of a long alkyl tail onto the TPP cation. For example, the therapeutically approved antioxidant Mito-Q (Error! Reference source not found.) consists of a TPP cation linked via a decyl chain to an antioxidant ubiquinol moiety.[128] When delivered *in vitro* or *in vivo*, Mito-Q accumulates in mitochondria and localises in the IMM, where the ubiquinol moiety embeds in the hydrophobic core of the IMM and protects it from lipid peroxidation.[123]
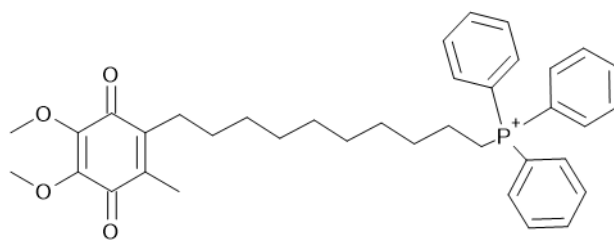
Mito-Q

Figure 6 The chemical structure of Mito-Q.

In addition, a study by Dong *et al.* conjugated a TPP cation with a mitochondrially targeted analog of vitamine E succinate (MitoVES). VE analogs are known to induce cell apoptosis by targeting Complex II in the ETC.[131] MitoVES, which consists of a 11-carbon linker between tocopheryl succinate and the TPP cation, stongly induced apoptosis (more than 90%) in cancer cells compared to the unmodified counterpart and other conjugates. MitoVES maintained selectivity towards cancerous cells as it did not induce apoptosis in non-cancerous cells and presented lower IC_{50} values in cancerous cells. Greater mitochondrial localisation of MitoVES was demonstrated by confocal microscopy compared to its unmodified counterpart.[132] A study by Millard *et al.* investigated Mito-Chlor, a triphenylphosphonium cation conjugated to the nitrogen mustard chlorambucil, as nitrogen mustards are currently used in chemotherapeutics as they damage DNA but have limited safety and efficacy. The IC_{50} value for Mito-Chlor was the lowest (7 µM) compared to the non conjugated chlorambucil (100 µM). In addition, a study of 10 other cancer cell lines were performed to compare the cytotoxicity of the non conjugated chlorambucil compared to Mito-Chlor and in all cases Mito-Chlor had a higher potency. Next Millard *et al.* found Mito-Chlor extensively accumulated in mitochondria and caused mitochondrial DNA damage and induced cell death. Lastly, in an *in vivo* study Mito-Chlor was revealed to possess greater tumor suppression efficiency compared to the non conjugated chlorambucil.[133] Hence aromatic ILs, which are a class of DLC, are

23

suspected to accumulate in the IMM of cancer cell mitochondria by permeabilising the membrane and inducing mitochondrial dysfunction ultimately leading to cell death.

1.7 Project aims

The overall aim of this thesis is based on the hypothesis that aromatic ILs are a class of DLCs and are therefore expected to accumulate in the IMM of mitochondria and induce cell death by permeabilising the membrane and inducing mitochondrial dysfunction.

The specific aims of this thesis are:

1. To undertake a mechanistic study and determine whether aromatic long chain ILs are able to permeabilise the IMM and induce mitochondrial dysfunction.

2. To design and synthesise a SAR study on a series of substituted quinolinium and pyridinium-based ILs.

3. To assess the effect of ILs on cytotoxicity against HeLa cells and provide new SAR information regarding substituent effects on ILs cytotoxicity.

To achieve these aims Chapter 2 describes the design, synthesis and biological evaluation of a series of aromatic and aliphatic containing cationic headgroup ILs substituted with butyl (C_4-ILs) or decyl (C_{10}-ILs) alkyl chains on the cationic headgroups (Library 1). In order to investigate the influence of their structure on cytotoxicity and mitochondrial actions, and hence determine the mechanism by which aromatic long chain ILs induce cell death.

Chapter 3 describes the design, synthesis and characterisation of quinolinium and pyridinium-based ILs. Including the quaternisation chemistry used to prepare ILs for a SAR study.

Chapter 4 describes the biological investigation of the ILs synthesised in Chapter 3, including the MTS cell viability assay and preliminary mechanistic studies of substituent effects on cytotoxicity using tBLMs.

Chapter 5 presents the conclusions and suggestions for future work, and the chemistry and biology experimental procedures are presented in Chapter 6.

Chapter 2 - Investigation of aromatic long chain ionic liquids which permeabilise the inner mitochondrial membrane and induce mitochondrial dysfunction

2.1 Introduction

As discussed in **Chapter 1**, the cellular mechanism/s by which ILs induce cytotoxicity is currently unclear, and the current body of evidence suggests ILs exert cytotoxicity by disrupting cellular membranes and/or inducing mitochondrial dysfunction. The lack of clarity regarding the precise cytotoxic mechanisms of ILs is an impediment in the design of safe ILs for industrial applications, or cytotoxic ILs as potential anticancer agents, hence there is currently a need to identify the cellular targets by which ILs induce cell death.[17,91,104]

ILs that possess an aromatic headgroup substituted with a long *N*-alkyl chain are the most cytotoxic ILs, and these ILs bear structural similarity to lipophilic cations such as the triphenylphosphonium-based drug MitoQ. This is important, as MitoQ is known to accumulate in mitochondria in response to the PMF and localise in the IMM due to its lipophilicity. Thus, it is possible that aromatic, long chain ILs may also accumulate in mitochondria and localise in the IMM, and induce cell death by disrupting the integrity of the IMM.

In this chapter, a library of ILs comprised of aromatic and aliphatic cationic headgroups substituted with butyl (C_4-ILs) or decyl (C_{10}-ILs) chains were prepared to investigate the influence of their structure on cytotoxicity and mitochondrial actions, and hence to provide insights into the mechanism/s by which ILs induce cell death. The mechanistic insights may be used to rationally design either safe or cytotoxic ILs which is a vital step in their development and application as potential anticancer agents.

2.2 Ionic liquid library 1 design

In this chapter a library of ILs were prepared to investigate the impact of different cations on cytotoxicity and mitochondrial actions (**Figure 7**). ILs substituted with butyl (C_4-ILs) or decyl (C_{10}-ILs) alkyl chains on the cationic headgroups were included as alkyl chain length has a strong influence on IL cytotoxicity[15,16,55] and their capacity to permeabilise lipid bilayers.[94,96] ILs with aromatic (methylimidazolium, pyridinium and quinolinium) and aliphatic (trimethylammonium) headgroups were included to investigate the effect of aromaticity on activity. It was anticipated that delocalisation of the cationic charge across the aromatic headgroup would increase the lipophilicity of aromatic ILs and therefore promote mitochondrial uptake. The anionic component of **[C_{10}Mim][Br]** was exchanged with CF_3SO_3 and BF_4 anions to investigate the influence of the anion on cytotoxicity. These anions were selected for their similarities in ionic strength.

[C_nMIM]   **[C_nPy]**   **[C_nTMA]**   **[C_nQuin]**
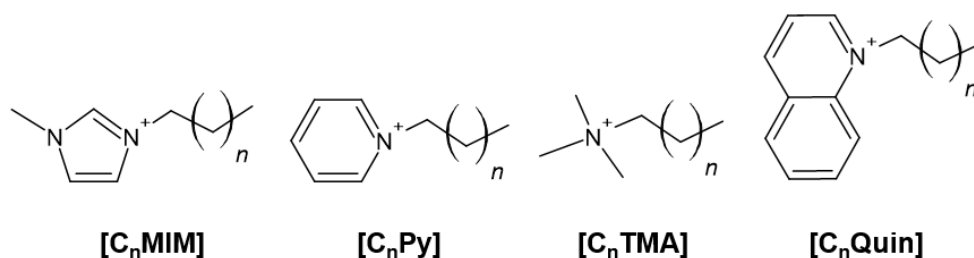
Figure 7 Chemical structures of aromatic and aliphatic ILs studied, n=2 or 8

2.2.1 Preparation of ionic liquids

ILs **[C_4MIM][Br]**, **[C_4Py][Br]**, **[C_4TMA][Br]** and **[C_{10}TMA][Br]** were commercially available and purchased from commercial suppliers. ILs **[C_{10}MIM][Br]**, **[C_{10}Py][Br]**, **[C_4Quin][Br]** and **[C_{10}Quin][Br]** were not commercially available, and were synthesised in a single step by reacting the appropriate heterocyclic headgroup with the appropriate 1-alkyl bromide using the Menshutkin reaction, outlined in **Chapter 5.2.3**. First described in 1890,[134] the Menshutkin reaction involves the quaternisation of a tertiary amine with an alkyl halide to

form a quaternary ammonium salt. The reaction proceeds *via* a S_N2 mechanism, where the alpha carbon of 1-bromoalkane is susceptible to the nucleophilic attack by the quinoline nitrogen atom, leading to a transition state. Subsequently, the bromine acts as a leaving group and the nitrogen of the quinoline becomes quaternised, forming a quaternary salt with a bromine anion (**Scheme 1**).
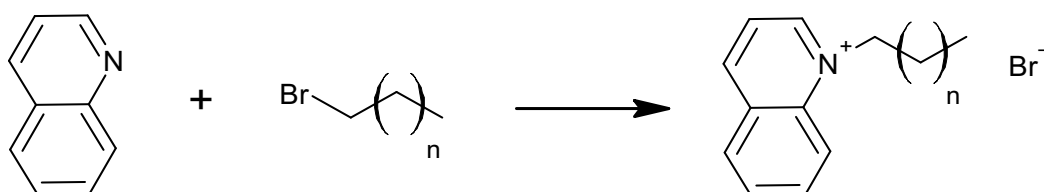
Scheme 1 An example of the reaction scheme, ILs were prepared by the neat quaternisation reaction between the appropriate heterocyclic headgroup and the appropriate bromoalkane (1-bromobutane or 1-bromodecane). Reagents and conditions: neat, 140 °C, 24 h, 48-96 %. n= C_2 or C_8.

To perform the reactions, each heterocycle was reacted with 1 molar equivalence of either 1-bromobutane or 1-bromodecane for 24 hours at 140 °C. After complete consumption of the heterocycle as monitored by TLC, the reaction mixture was cooled to room temperature. The crude products were then purified by trituration with hexane and re-precipitation from chloroform / diethyl ether. This procedure was able to be carried out for oily products, as the dense oil products sunk and allowed the solvents to be decanted from the product. The resulting products were thoroughly dried in a vacuum oven to afford pure products with yields of 48-96 %.

[C₁₀MIM][Br], **[C₁₀Py][Br]**, **[C₄Quin][Br]** and **[C₁₀Quin][Br]** were characterised by NMR spectroscopy and high resolution mass spectrometry (HRMS) techniques. The ^{1}H and ^{13}C NMR of **[C₁₀MIM][Br]**, as an example, are shown in **Figure 8** (^{1}H and ^{13}C NMR spectra

of the remaining ILs are shown in **Chapter 6**, the appendix). The successful quaternisation of the imidazolium headgroup was confirmed by the triplet at 4.30 ppm (**Figure 8A**), which arises from the CH_2 group adjacent to the quaternary nitrogen atom. This is further highlighted by the signal at 50.45 ppm in the ^{13}C NMR which also represents the CH_2 carbon adjacent to the quaternary nitrogen atom (**Figure 8B**). This peak is shifted downfield from the other alkyl chain length carbon signals (b-f) resulting from the strong deshielding effect by the neighbouring positively charged nitrogen atom. Additional evidence supporting the successful synthesis of **[C$_{10}$MIM][Br]** was obtained from HRMS. In positive mode, the HRMS detected a species with a m/z of 223.2177 which corresponds to the calculated m/z of **[C$_{10}$MIM]** as 223.2163.

Compound purity was confirmed by absolute quantitative ^1H NMR (qNMR) which involves dissolving the internal standard (IS) 1,3,5-trioxane in deuterated DMSO (DMSO-d$_6$), then adding the sample **[C$_{10}$MIM][Br]** to it and recording a ^1H NMR spectra. Purity (w/w %) was determined by calculating the proportionality between the average integration of one proton from the IS and the IL tested. So to further support the formation and purity of **[C$_{10}$MIM][Br]** qNMR was used and was found to have a 99.3 % purity.
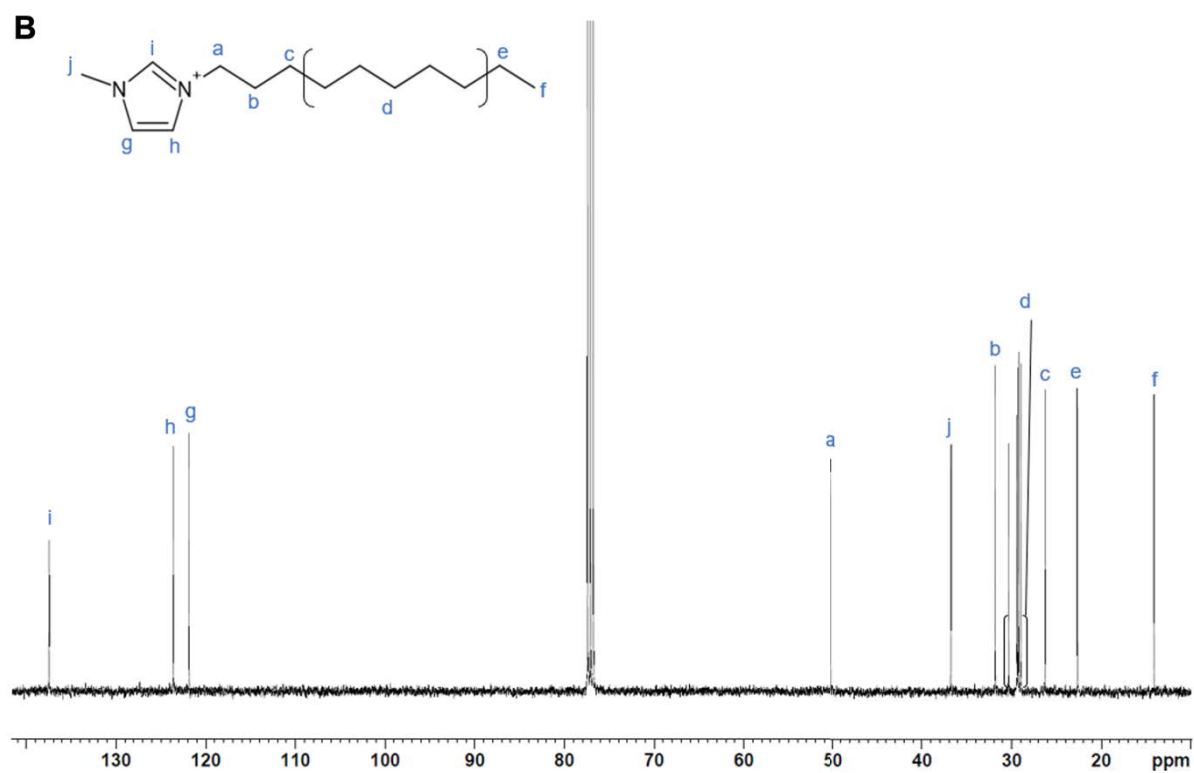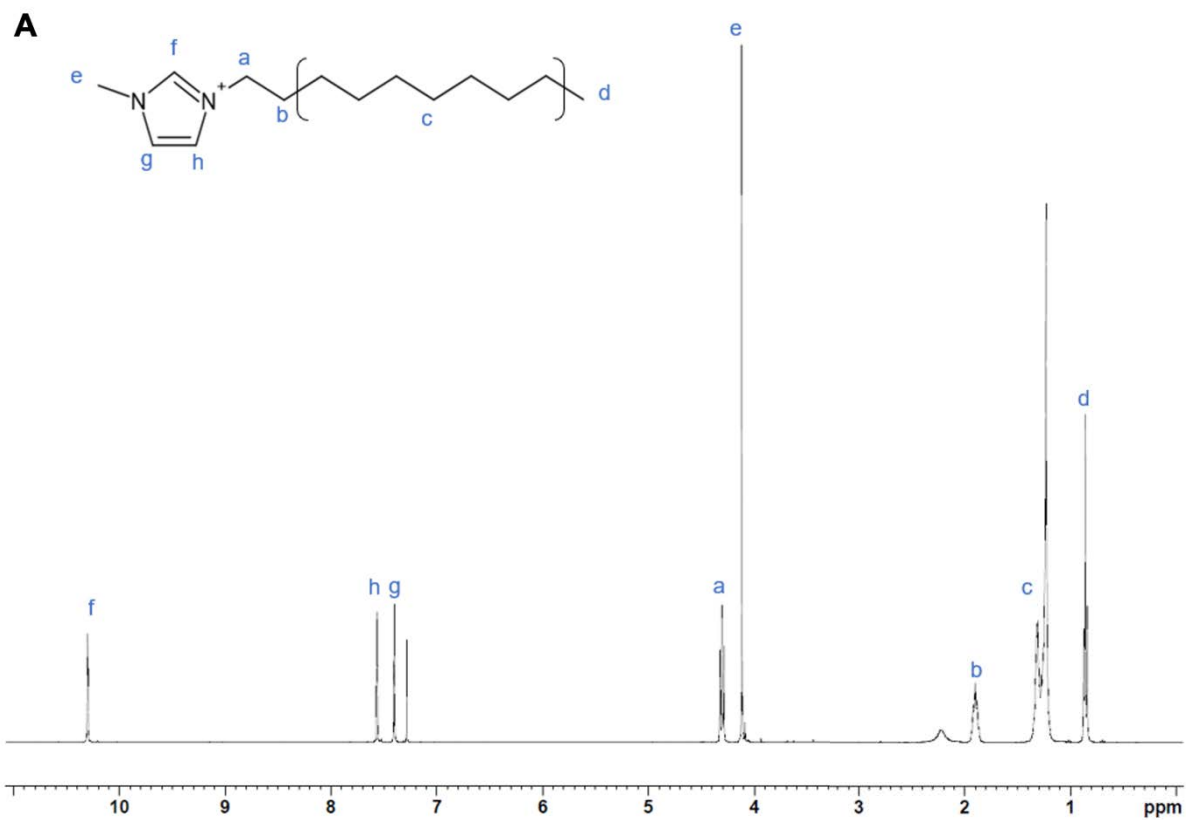
Figure 8 A) ^{1}H NMR spectrum of **[C$_{10}$MIM][Br]**, B) ^{13}C NMR of **[C$_{10}$MIM][Br]**.

2.2.2 Synthesis of [C₁₀MIM][BF₄] and [C₁₀MIM][CF₃SO₃]

[C₁₀MIM][BF₄] and [C₁₀MIM][CF₃SO₃] were prepared by a metathesis reaction between [C₁₀MIM][Br] and a saturated solution of sodium tetrafluoroborate (NaBF₄) and sodium trifluoromethansulfonate (CF₃NaO₃S) respectively. The precipitate was collected by vacuum filtration and washed then dried under vacuum yielding pure product with high yields of 92-95%, full experimental details in **Section 5.2.3**.

2.3 Effects of ILs on the viability of HeLa cells
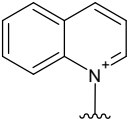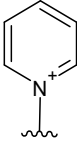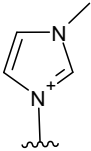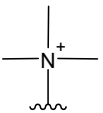
The capacity of the ILs to reduce the cell viability of HeLa cervical cancer cells and lung epithelial BEAS-2B cells was assessed using the 3-(4,5-dimethylthiazol-2-yl)-5-(3-carboxymethoxyphenyl)-2-(4-sulfophenyl)-2H-tetrazolium (MTS) cell viability assay. The MTS assay is a colorimetric method used to determine the number of viable cells in culture following the treatment with a test compound. Viable cells are able to metabolise the MTS dye to a dark red formazan product whilst non-viable cells are not able to metabolise MTS. Hence, the magnitude of absorbance at 490 nm is directly proportional to the number of viable cells remaining in the culture and allows the number of viable cells to be determine spectrophotometrically. The ILs were tested at varying concentrations from 0.01 – 100 µM and produced dose-dependent reductions in cell viability, and the dose-response curves (see **Figure 9** and appendix) were used to calculate IC₅₀ concentrations (**Table 3**).
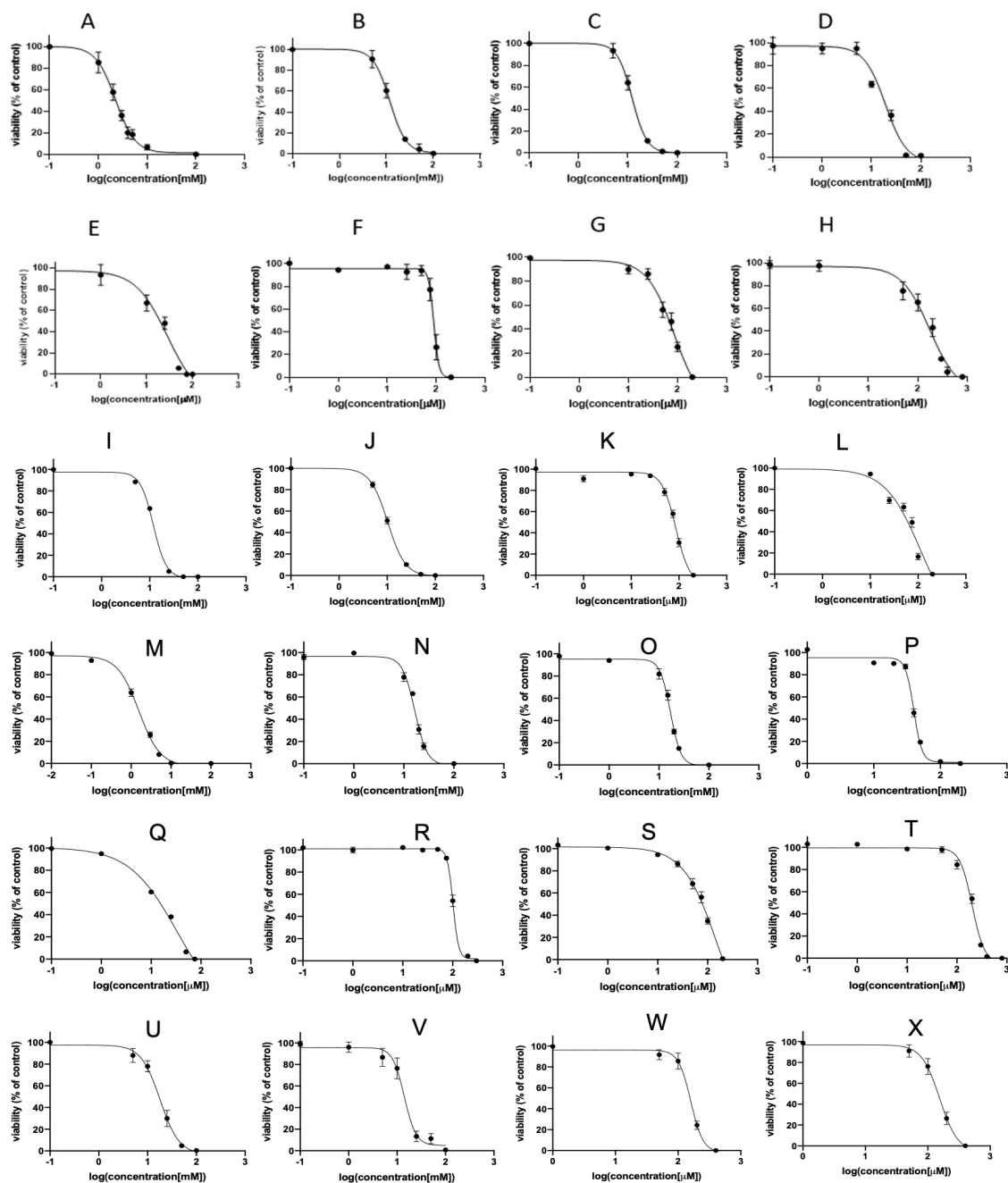
Figure 9 Dose-response curves showing the effect of ILs on the cell viability after 48 h treatment. In HeLa cells A) **[C₄Quin][Br]**, B) **[C₄Py][Br]**, C) **[C₄MIM][Br]**, D) **[C₄TMA][Br]**, E) **[C₁₀Quin][Br]**, F) **[C₁₀Py][Br]**, G) **[C₁₀MIM [Br]**, H) **[C₁₀TMA][Br]**, I) **[C₄MIM][BF₄]**, J) **[C₄MIM][CF₃SO₃]**, K) **[C₁₀MIM][BF₄]** and L) **[C₁₀MIM][CF₃SO₃]**. In BEAS-2B cells, M) **[C₄Quin][Br]**, N) **[C₄Py][Br]**, O) **[C₄MIM][Br]**, P) **[C₄TMA][Br]**, Q) **[C₁₀Quin][Br]**, R) **[C₁₀Py][Br]**, S) **[C₁₀MIM][Br]**, T) **[C₁₀TMA][Br]**, U) **[C₄MIM][BF₄]**, V)

[C₄MIM][CF₃SO₃], W) **[C₁₀MIM][BF₄]** and X) **[C₁₀MIM][CF₃SO₃]**. Data represents the mean ± SEM of 3 independent experiments.

Table 3 Cell viability IC$_{50}$ concentrations of ILs against HeLa and BEAS-2B cell lines.

Ionic liquid	Headgroup structure	HeLa IC$_{50}$ (mM)	BEAS-2B IC$_{50}$ (mM)
[C₄Quin] [Br]		2.24 ± 0.06	1.64 ± 0.22
[C₁₀Quin] [Br]		0.0268 ± 0.0003	0.03284 ± 0.00346
[C₄Py] [Br]		13.31 ± 1.18	15.70 ± 1.40
[C₁₀Py] [Br]		0.0888 ± 0.0003	0.10261 ± 0.00502
[C₄ MIM] [Br]		13.88 ± 1.84	16.98 ± 0.86
[C₄ MIM][BF₄]		11.80 ± 0.36	18.37 ± 1.42
[C₄ MIM][CF₃SO₃]		10.47 ± 0.28	14.05 ± 0.68
[C₁₀MIM] [Br]		0.0848 ± 0.0006	0.11230 ± 0.00675
[C₁₀MIM] [BF₄]		0.0875 ± 0.0097	0.0909 ± 0.00143
[C₁₀MIM] [CF₃SO₃]		0.0849 ± 0.0021	0.0894 ± 0.00121
[C₄TMA] [Br]		11.43 ± 1.23	39.93 ± 0.99
[C₁₀TMA] [Br]		0.197 ± 0.0073	0.20197 ± 0.00903

The general trends in IL cytotoxicity are consistent with previous reports which found that *N*-alkyl chain length was a major determinant of activity, [16,61,85,135,136] where cytotoxicity positively correlates with the length of the *N*-alkyl chain.[60,85,96,98,100] This is demonstrated in **Table 3**, where short chain C₄-ILs had IC$_{50}$ concentrations in the millimolar range while those with longer chains C₁₀-ILs were in the micromolar range, regardless of headgroup structure or cell line.

Headgroup aromaticity appeared to be an important factor determining cytotoxicity within the decyl-substituted series. Thus, **[C₁₀TMA][Br]** reduced the viability of both HeLa and BEAS-2B cells with IC$_{50}$ concentrations of ~200 μM, while the aromatic ILs **[C₁₀MIM][Br]** and **[C₁₀Py][Br]** were 2 fold more potent (IC$_{50}$ concentrations of ~100 μM, P < 0.05). This is consistent with previous reports which have shown the IL containing an aliphatic piperidinium headgroup is less cytotoxic than the aromatic pyridinium headgroup studied, this is due to aliphatic ILs lack of aromaticity and their relative polar nature.[96] The quinolinium-based IL **[C₁₀Quin][Br]** was the most potent in the series and reduced the viability of both cells lines IC$_{50}$ concentrations of ~30 μM, which suggests that larger cationic headgroups promote cytotoxicity. Interestingly, the nature of the cationic headgroup did not have a significant impact on the cytotoxicity of the short chain C$_4$-ILs **[C₄MIM][Br]**, **[C₄Py][Br]** and **[C₄TMA][Br]**, with these ILs reducing the viability of HeLa cells with IC$_{50}$ concentrations of ~12 mM, although **[C₄Quin][Br]** was 2.24 ± 0.06 mM.

To determine whether the anion has an influence on cytotoxicity, the anionic component of [C₄MIM][Br] and [C₁₀MIM][Br] was exchanged with trifluoromethanesulfonate (CF₃SO₃⁻) and tetrafluoroborate (BF₄⁻) anions. The IC$_{50}$ concentrations for the [C₄MIM] and [C₁₀MIM] ILs were similar in both cell lines, regardless of the anion (P > 0.05), despite differences in the lipophilicity of the anions (**Table 3**), showing that the cytotoxicity of these compounds is unaffected by the nature of the anion. This is supported by several studies which show that the cytotoxicity of imidazolium ILs are not affected by the anionic component.[55,137-140]

As mentioned in **Section 1.6.1**, the accumulation of ILs in mitochondria are driven by the electrostatic interactions between the positively charged ion and the negative charge of the

$\Delta\Psi_M$.[118-120] As cancer cell mitochondria are hyperpolarised compared to non-cancerous cells mitochondria, it is hypothesised this would allow for the preferential accumulation of ILs in cancer cell mitochondria similar to DLCs discussed in **Section 1.6.2**. Hence, ILs were tested in human lung epithelial BEAS-2B cells to evaluate their potential selectivity towards cancerous HeLa cells using the MTS cell viability assay (**Table 3**). In general, the IC_{50} concentrations were higher is BEAS-2B cells relative to HeLa cells. For example, aromatic C_{10}-ILs **[C$_{10}$Quin][Br]**, **[C$_{10}$MIM][Br]** and **[C$_{10}$Py][Br]** reduced the cell viability in HeLa cells with MTS IC_{50} concentrations of 26.8 ± 0.30 μM, 88.8 ± 0.30 μM and 84.8 ± 0.60 μM respectively, whilst in BEAS-2B cells they reduced cell viability to a lesser extent with their respective IC_{50} values of 32.8 ± 0.35 μM, 102.6 ± 0.50 μM and 112.3 ± 0.68 μM (**Table 3**). Similarly, in the C_4-IL [C$_4$ MIM][Br] was more cytotoxic towards HeLa cells than BEAS-2B cells. These data show that the HeLa cancer cell line was more susceptible to IL cytotoxicity than the non-cancerous BEAS-2B cells and are in good agreement with a previous study which found a range of ILs, **[C$_1$MIM][Cl]**, **[C$_4$MIM][Cl]**, triethylammonium sulphate and triethylammonium phosphate were less cytotoxic towards non-cancerous HEK (human embryonic kidney) cells compared to T98G brain cancer cells. [11]

2.4 Effects of ILs on the permeability of DOPC lipid bilayers

Disruption of the cellular membranes is suggested to contribute to IL cytotoxicity. Studies have shown ILs exert cytotoxicity by incorporating into and disrupting cellular membranes. The capacity of ILs in this chapter to disrupt membrane integrity was assessed using tethered bilayer lipid membranes (tBLMs). This system is comprised of a lipid bilayer tethered to a thin film gold electrode (**Figure 10**), to which tethering moieties are anchored via benzyl disulfide groups. As tethers incorporate into one leaflet, a lipid bilayer is formed, which tethers the bilayer to the metal surface. Combined with the tethers are spacer molecules which

provide a framework for the tethering molecules.[141] The tethering molecules are amphiphilic and are interspersed with polar short-chained spacer molecules which are located between the metal surface and the lipid bilayer, this creates an aqueous reservoir allowing for ions to cross the membrane.[142] Permeabilisation of the lipid bilayer is detected as an increase in membrane conductance, as measured by electrical impedance spectroscopy,[142] in response to the addition of a membrane disrupting compound. For this study tBLMs were assembled with 1,2-dioleoyl-sn-glycero-3-phosphocholine (DOPC), which is the major phospholipid component of the IMM.[143] Thus, these bilayer membrane models allow evaluating the ability of ILs to permeabilise the lipid bilayer, as larger membrane conductance values are the result of greater membrane disruption.
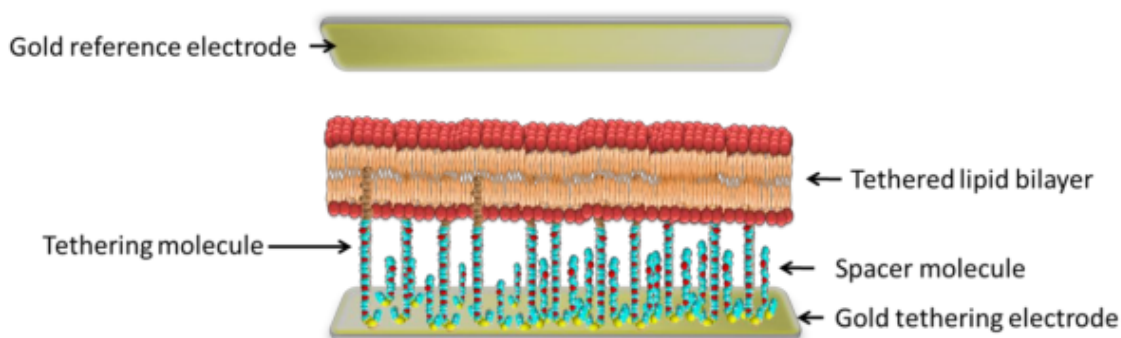
Figure 10 A tBLMs setup consisting of a gold metal electrode and tethered moieties anchored via benzyl disulfide groups.[141] (This image has been reproduced from Cranfield, Methods Mol Biol, 2015, 1232, 45-53)

For these studies, tBLMs were treated with the ILs at a concentration of 200 μM, as this concentration produced the most stable changes in membrane conductance. ILs were added to tBLMs to determine their effect on ionic conductance and assess their capacity to permeabilise lipid bilayers. As shown in **Figure 11**, the addition of C_{10}-ILs significantly increased lipid bilayer conductance. **[C₁₀MIM][Br]** and **[C₁₀Py][Br]** increased conductance 7-fold, whilst **[C₁₀Quin][Br]** produced the greatest increase with a 33-fold increase. The aliphatic

[C$_{10}$TMA][Br] had the least increase of the C$_{10}$-ILs with a 2.5 fold increase in conductance. In contrast the short chain C$_4$-ILs did not have a significant effect on bilayer conductance.
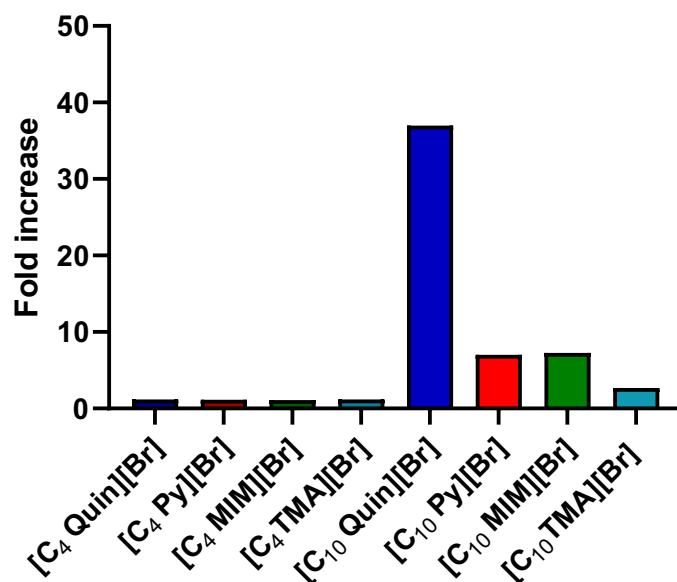
Figure 11 Effects of ILs (200 µM) on the conductance of DOPC lipid bilayers tethered to gold electrodes, as measured by electrical impedance spectroscopy. Data normalised to membrane conductance prior to IL treatment at pH = 7. Data represents the mean ± SEM of 2 independent experiments.

Importantly, the trends in membrane effects reflect with the cell viability IC$_{50}$ data (**Table 3**). Thus, the C$_4$-ILs which killed HeLa and BEAS-2B cells with relatively high IC$_{50}$ concentrations failed to increase the conductance of DOPC bilayers. In contrast, the C$_{10}$-ILs produce marked increases in membrane conductance and had MTS IC$_{50}$ concentrations in the micromolar range. This suggests ILs cytotoxic effects are related to their ability to permeabilise lipid bilayers. These findings are in agreement with previous findings which have demonstrated membrane effects are a major determinant in IL cytotoxicity, where increasing the length of the *N*-alkyl chain length led to greater membrane disruption and cytotoxicity.[94,97-100,144]

Within the C_{10}-IL series **[C₁₀Quin][Br]** produced the greatest increase in membrane conductance, which may arise due to its larger headgroup size and greater hydrophobicity compared to its counterparts. The next most active were **[C₁₀Mim][Br]** and **[C₁₀Py][Br]** and lastly the aliphatic **[C₁₀TMA][Br]**. These findings are in good agreement with a previous report by Kaur *et al.* who studied the effect of six ionic liquids containing benzimidazolium, imidazolium, pyrrolidinium, piperidinium, ammonium, and morpholinium based ILs substituted with a dodecyl alkyl chain in POPC bilayers. Permeability of the POPC bilayer was found to have a strong dependence on ionic liquid headgroup structure, where benzimidazolium and imidazolium ILs which contain larger and more hydrophobic headgroups produced the greatest effect and IL with an ammonium headgroup disrupted POPC bilayers to a lesser extent.[96] To further support that the cytotoxicity of ILs is related to their capacity to permeabilise lipid bilayers, the correlation between the MTS IC_{50} concentrations of the C_{10}-ILs and their tBLMs effects was investigated. To carry this out, a simple linear regression plot was constructed using the log $1/IC_{50}$ and log 1/fold increase which is customary in QSAR analysis,[145] this produced the plot shown in **Figure 12** with an r^2 value of 0.9956. This shows a correlation between the MTS IC_{50} concentrations and the increase in membrane conductance produce by the C_{10}-ILs and suggests that the cytotoxicity of the C_{10}-ILs is associated with their capacity to disrupt cellular membranes. C_4-ILs were not subjected to the same linear regression plot as they failed to induce disruption of DOPC bilayers and consequently an increase in membrane conductance.
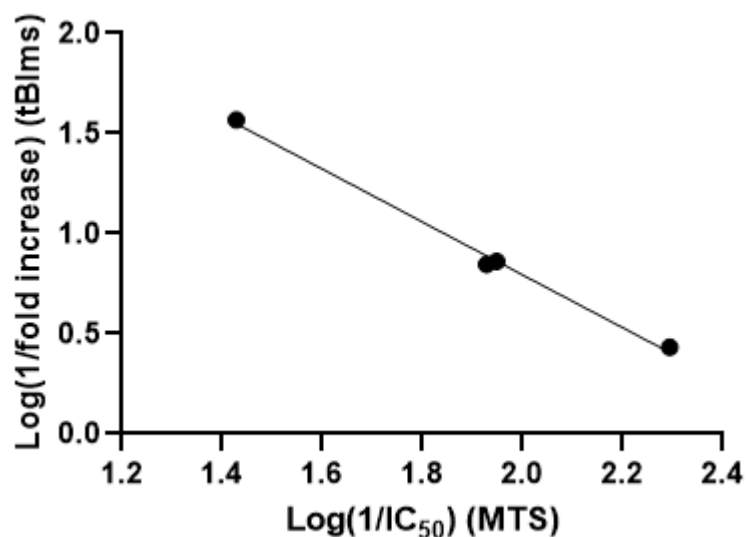
Figure 12 Correlation plot of tBLMs conductance Log(1/fold increase) against MTS Log(1/IC_{50}) for C_{10}-ILs.

2.5 Intracellular tracking of fluorescent quinolonium-based IL using confocal microscopy

The next question that arises is which cellular membrane is targeted by C_{10}-ILs to induce cell death. It was anticipated that C_{10}-ILs would target the IMM as other lipophilic cations such as MitoQ are known to accumulate at this membrane, and mitochondria are sites of critical cellular process, as well as regulators of cell death. Since the quinolinium-based ILs are fluorescent, it was envisioned that these ILs together with MitoTracker deep red ($\lambda_{ex}/\lambda_{em}$ 644/665 nm) and Hoechst ($\lambda_{ex}/\lambda_{em}$ 350/461 nm) could be used to follow subcellular localisation by confocal microscopy. Since MitoTracker deep red staining requires polarised mitochondria for effective staining, it was decided to use **[C₄Quin][Br]** as this short chain IL has less capacity to permeabilise and depolarise the IMM. Unfortunately, the excitation and emission profile of **[C₄Quin][Br]** was not available in the optical setup, and an analogue of **[C₄Quin][Br]** with optical properties suitable for confocal microscopy was prepared.

39

The addition of electron donating and withdrawing substituents on the aromatic ring can shift the absorbance band wavelength to either a higher or lower wavelength. Therefore, the electron donating alkyl group CH_3 was added on the C2 position of the quinolinium cation forming **[C₄MeQuin][I]**. **[C₄MeQuin][I]** was synthesised by the procedure detailed in **Section 2.2.1** and full experimental details are provides in **Section 5.2.2**. The optical properties of **[C₄MeQuin][I]** were studied by fluorescence spectroscopy (**Figure 13**). It was found that **[C₄MeQuin][I]** has an excitation band at ~430-520 nm and emission of ~520-700 nm, hence was capable to be imaged using a 458 nm laser and a 500-550 nm bandpass filter on the confocal microscope.
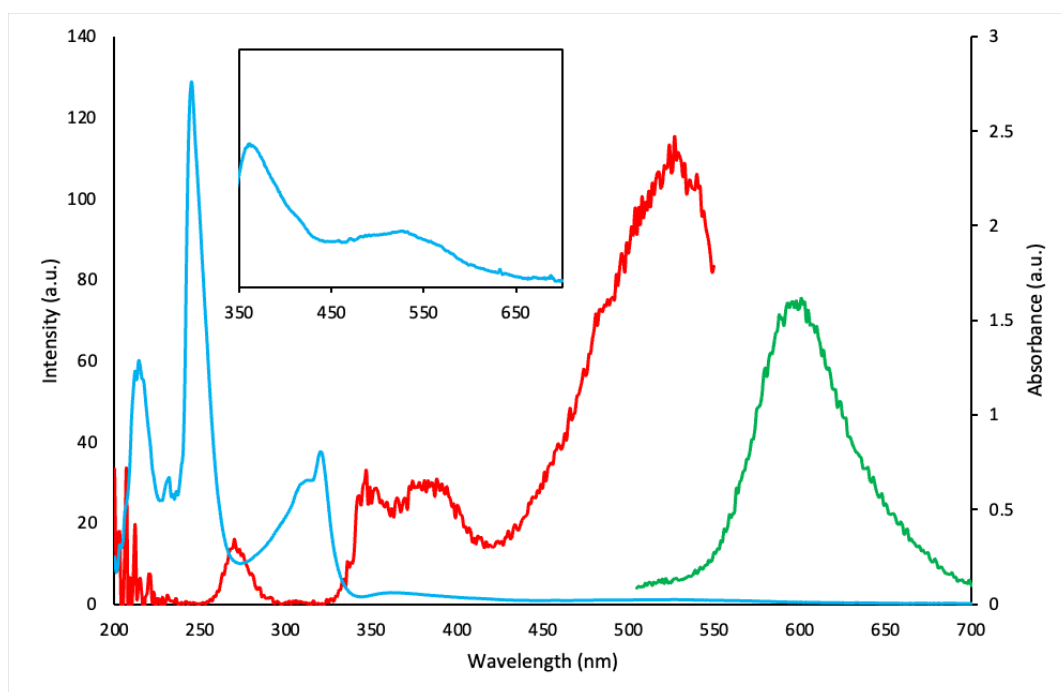
Figure 13 Optical absorbance (blue), excitation (red) and emission from 488 nm excitation (green) spectra for **[C₄MeQuin][I]** in acetonitrile. Insert shows absorbance between 350-700 nm for clarity.
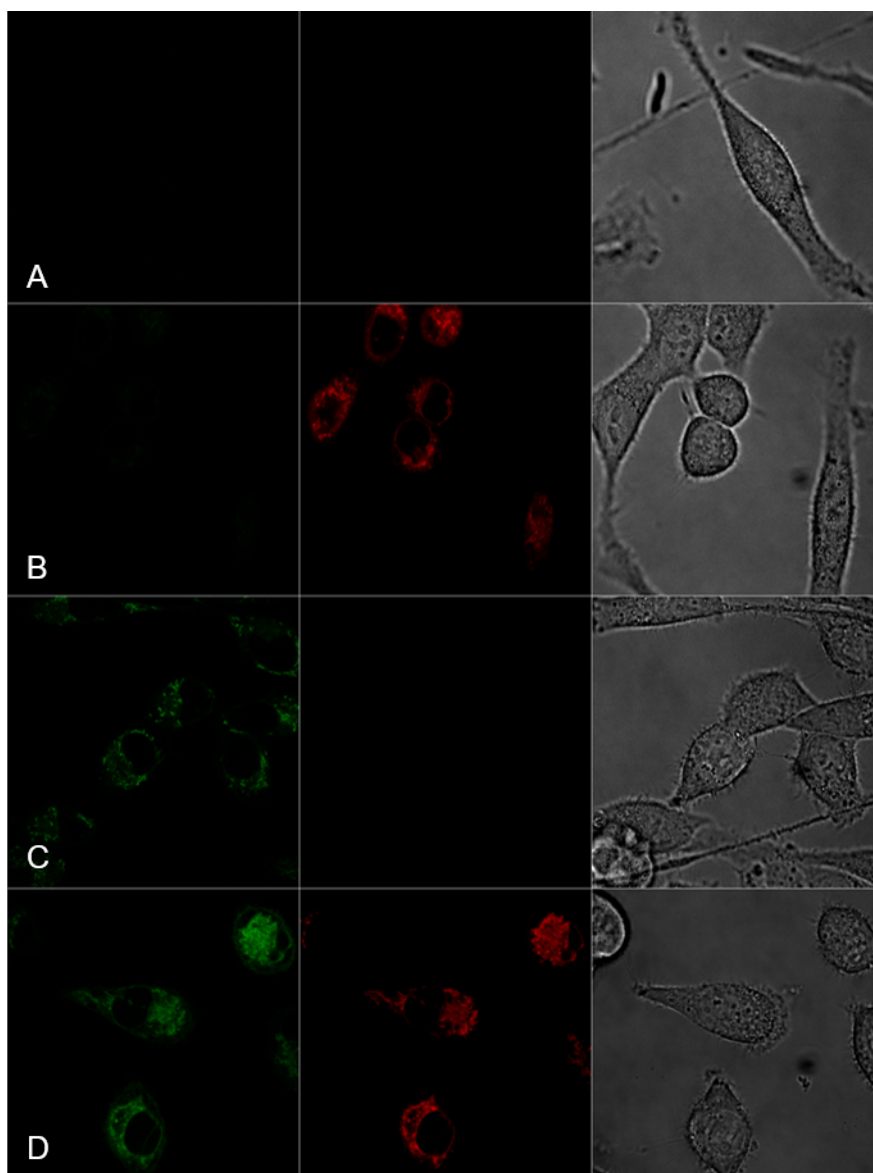
Figure 14 Single colour controls to demonstrate no bleed through between channels. (A) Cells only, (B) Red channel MitoTracker Deep Red (200 nM, λ_{ex}= 644 nm), (C) Green channel **[C₄MeQuin][I]** (500nM, λ_{ex}= 488 nm) and (D) MitoTracker Deep Red and **[C₄MeQuin][I]**.

Single colour controls (**Figure 14**) were acquired to confirm channel specificity of **[C₄MeQuin][I]** and MitoTracker Deep Red to the green and red channels respectively. **Figure 14A** shows an image collected of unstained cells. The lack of fluorescence shows the cells themselves did not cause any fluorescence that might interfere with the fluorophores. **Figure 14B** shows an image of cells treated with MitoTracker deep red only. No bleed through of

fluorescence into the green channel (column one) was observed. Similarly, **Figure 14C** showed no fluorescence cross over in the red channel (column two) after treatment of cells with **[C₄MeQuin][I]**. This confirms the fluorescence produced is channel specific and there was no bleed through between channels of **[C₄MeQuin][I]** and MitoTracker Deep Red.

2.5.1 Colocalisation analysis

A colocalisation study was preformed to confirm localisation of **[C₄MeQuin][I]** within HeLa mitochondria using MitoTracker deep red and the neculear stain Hoechst. The confocal microscopy reveals that **[C₄MeQuin][I]** exhibited high levels of colocalisation with MitoTracker Deep Red. This is clearly evident with the green fluorescence of **[C₄MeQuin][I]** in the green channel overlapping with the red fluorescence of MitoTracker Deep Red in the red channel (**Figure 15**). Hence, a colocalisation analysis was conducted to determine the Pearson's correlation coefficient between the green and red channels. A Pearson's correlation (PC) coefficient of 0.94 in HeLa cells was determined which further confirms the localisation of **[C₄MeQuin][I]** within mitochondria. These findings are consistent with previously reported studies which have shown the subcellular localisation of DLCs in mitochondria using confocal fluorescence microscopy with MitoTracker red.[146-148] The high PC values in all studies establishes mitochondrial specificity and the combination of these findings further supports the accumulation of ILs in mitochondria as they are structurally similar to DLCs with a delocalised charge across the headgroup which is known to bw essential for their accumulation in mitochondria.
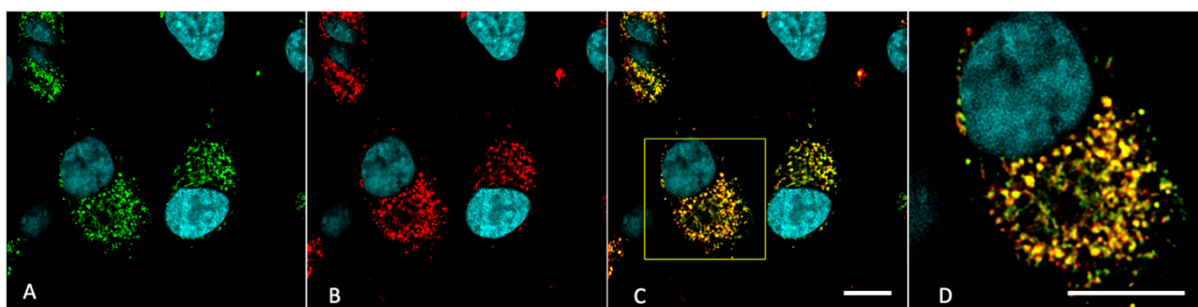
Figure 15 Confocal fluorescence microscopy of **[C₄MeQuin][I]** in HeLa cells reveals mitochondrial specificity. A maximum intensity projection of the labelled cell volume. (A) Green channel **[C₄MeQuin][I]** (500nM, λ_{ex}= 488 nm) (B) Red channel MitoTracker Deep Red (200 nM, λ_{ex}= 644 nm). (C) Merged *channels. (D) Magnified view of boxed region in (C). Blue* channel in all cases: Hoechst nuclear stain (4 μM, $\lambda_{ex}/\lambda_{em}$ 350/461 nm). Scale Bar (10 μm).

Some studies have suggested that ILs might target the cell nucleus, so colocalisation of **[C₄MeQuin][I]** with Hoechst nuclear stain was also assessed. The study produced a PC of less than 0.02, which suggests **[C₄MeQuin][I]** does not localise in the nucleus and thus further indicates selective accumulation of ILs in mitochondria.

2.6 Effects of ILs on mitochondrial function in HeLa cells

The fluorescent microscopy images and association between the MTS IC$_{50}$ and tBLM data suggest that the C$_{10}$-ILs in this study exert their cytotoxic actions at the IMM. The IMM being the target of C$_{10}$-ILs is reasonable given that mitochondria play critical roles in cell function and death, and the integrity of the IMM influences these functions.[149] The primary role of mitochondria is to convert nutrients to ATP through OxPhos. Drugs that disrupt OxPhos and ATP production (mitochondrial uncouplers) can induce cell death and are currently being explored as anticancer agents,[150] and several studies have suggested that imidazolium-based ILs affect OxPhos.[66,104,151]

43

A series of experiments were therefore undertaken to understand how the ILs in this study affected mitochondrial function in HeLa cells. For these studies HeLa cells were treated with the ILs at their MTS IC_{50} concentrations (**Table 3**) for short time periods to capture the early cellular effects that likely contribute to cell death.

2.6.1 Mitochondrial respiration

Mitochondrial and metabolic function can be measured using extracellular flux analysis, which allows a real time measurement of mitochondrial and glycolytic activity. The Agilent Seahorse XF Mito Stress Test measures these key functions by directly measuring the oxygen consumption rate (OCR) and extracellular acidification rate (ECAR) of cells over a short period of time.[152] OCR is a measure of oxidative phosphorylation (as molecular oxygen is consumed by complex IV in the ETC), whilst ECAR corresponds to glycolytic activity within the cell. First the basal OCR in HeLa cells were measured using the seahorse assay, after which the cells were treated with ILs to assess their effects on OCR and evaluate their capacity to inhibit OxPhos. Next, oligomycin was added, an ATP synthase inhibitor which decreases the flow of electrons through the ETC. The resultant decrease in OCR represents mitochondrial respiration linked to ATP production and indicates the amount of mitochondrial ATP produced to meet cell demands. Subsequently, the addition of FCCP, a protonophore which aids in proton movement across the IMM, imitates physiological energy demand by stimulating the ETC to operate at maximum capacity, and as a result increases OCR levels to reflect maximal respiration. Spare respiratory capacity, the difference between the maximal respiration and post-treatment OCR levels, are an indicator of mitochondria's ability to respond to increased respiratory requirement during cell stress. Lastly, the addition of rotenone and Antimycin A, inhibitors of Complexes I and III respectively, shut down mitochondrial respiration.
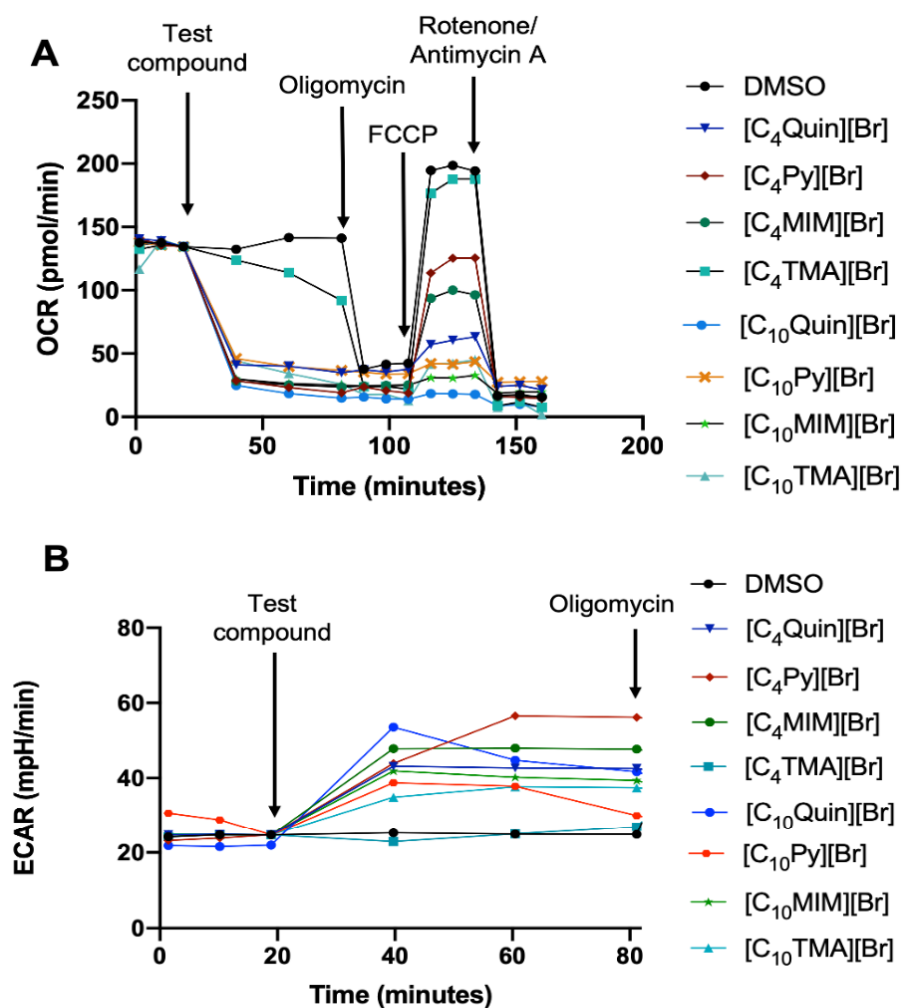
Figure 16 (A) The effect of ILs on oxygen consumption rate (OCR) in HeLa cells. HeLa cells were treated with the ILs at their IC_{50} concentrations, followed by sequential addition of oligomycin (1 μM), FCCP (2 μM) and then rotenone/antimycin A (1 μM). (B) ECAR of HeLa cells following the treatment of ILs. Data represents the average value of 2 wells from the same experiment.

As shown in **Figure 16A**, the addition of ILs to HeLa cells produced a rapid decrease in cellular OCR, which indicates that the ILs inhibit OxPhos at their MTS IC_{50} concentrations. The decrease in OCR was associated with an increase in ECAR (**Figure 16B**), which is proportional to glycolysis. Only the short chain aliphatic IL **[C4TMA][Br]** failed to effectively

decrease OCR and increase ECAR. These data suggest in general ILs inhibit OxPhos and the cells shift from OxPhos to glycolysis to generate ATP.[153] These findings are consistent with Wright *et al*, who pre-treat cells with methylimidazolium-based ILs and found them to decrease OCR levels and increase ECAR in B-13 hepatocytes with potency dependent on alkyl chain length and concentration.[151]
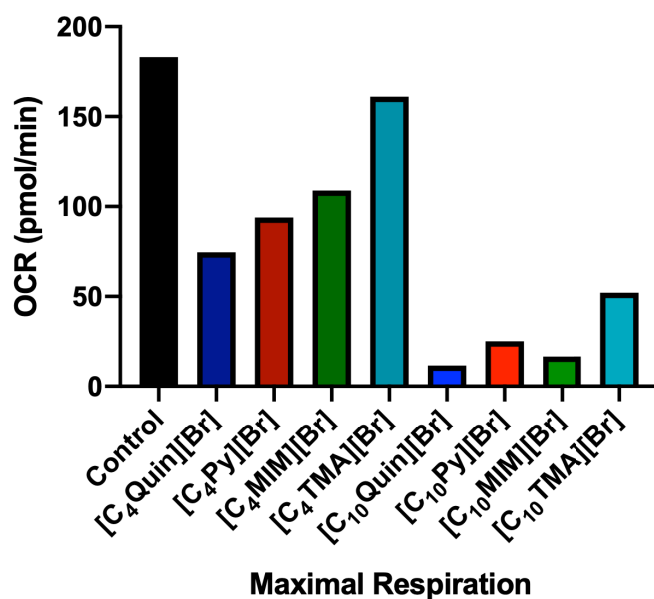
Figure 17 Determination of OCR associated with maximal respiration in HeLa cells following the treatment of ILs. Data represents the average value of 2 wells from the same experiment.

Maximal respiration, which is measured after the addition of FCCP, reflects the functional capacity of the ETC. With the exception of **[C₄TMA][Br]**, the ILs reduced maximal respiration compared to control (**Figure 17**), which is a strong indicator that these ILs induce mitochondrial dysfunction.[154,155] In cells treated with aromatic C_{10}-ILs **[C₁₀Quin][Br]**, **[C₁₀Mim][Br]** and **[C₁₀Py][Br]** but not **[C₁₀TMA][Br]** and the C_4-ILs, maximal respiratory capacities were below post-treatment levels, indicating these cells did not have any spare respiratory capacity. This is significant as spare respiratory capacity is another indicator of mitochondria's ability to respond to increased respiratory requirement during cell stress, where low capacities indicate an inability of the mitochondria to provide the increased need for ATP

during stress.[70,155,156] Combined, the Seahorse data shows that ILs affect OxPhos at their MTS IC_{50} concentrations, and that only the aromatic C_{10}-ILs reduce spare respiratory capacity, and induce mitochondrial dysfunction. In contrats HeLa cells treated with the C_4-ILs and **[C$_{10}$TMA][Br]** did have spare respiratory capacity which suggests these ILs exert cytotoxicity to cells by a different mechanism.

2.6.2 Depolarisation of the IMM

The integrity of the IMM is critical to maintaining the mitochondrial membrane potential and ATP synthesis via OxPhos. Given the results from the fluorescence microscopy, tBLM and Seahorse studies, it was suspected that inhibition of OxPhos may result from IL-mediated permeabilisation of the IMM and collapse of the proton gradient across this membrane. To assess this, the ability of ILs to depolarise the IMM in HeLa cell mitochondria were measured using the JC-1 assay. JC-1 is a redox active lipophilic cationic dye that selectively accumulates within mitochondria and forms aggregates that fluoresce red in the electronegative environment of polarised mitochondria. In response to depolarisation of the IMM, JC-1 leaves mitochondria and disaggregates to monomers that fluoresces green. Thus changes in JC-1 red:green fluorescence ratio can be used to detect changes in IMM depolarisation.
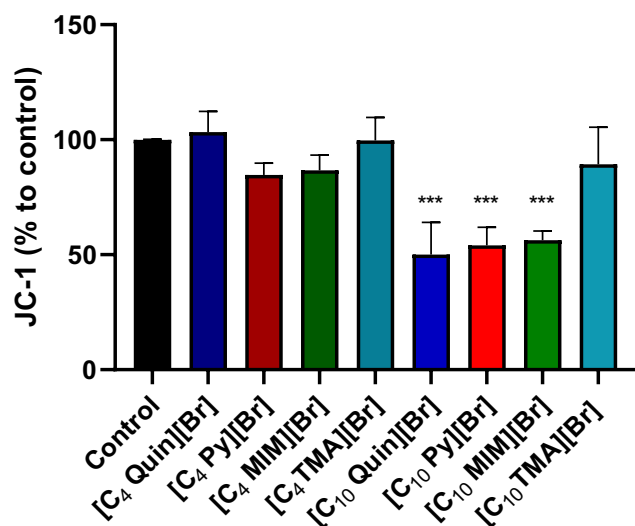
Figure 18 JC-1 red: green fluorescence percentage in HeLa cells treated for 1 hr at the MTS IC$_{50}$ concentration. Data represents the mean ± SEM of 3 independent experiments. Different from DMSO treated control: (***) P < 0.0001.

As shown in **Figure 18** aromatic C$_{10}$-ILs **[C$_{10}$Quin][Br]**, **[C$_{10}$Py][Br]** and **[C$_{10}$Mim][Br]** caused a shift in the JC-1 red:green fluorescence ratio to 50-56% of control after 1 hour treatments, which indicates that these long chain aromatic ILs rapidly collapse the IMM proton gradient. In contrast, the aliphatic C$_{10}$-IL **[C$_{10}$TMA][Br]** and all C$_4$-ILs had no activity in JC-1 assays, which suggests that these ILs do not affect the IMM polarisation. Overall, these findings suggest that the combination of a long alkyl chain and aromatic head group is critical for the ability of these ionic liquids to depolarise the mitochondrial membrane.

2.6.3 Effects of ILs on intracellular ATP levels

IL-mediated inhibition of OxPhos (Seahorse assay) and depolarisation of the IMM (JC-1 assay) is expected to lower ATP levels, thus intracellular ATP levels were measured in HeLa cells treated with the ILs at their MTS IC$_{50}$ concentrations. Since reduced intracellular ATP can reflect a loss of cell viability rather than inhibition of OxPhos, the time taken for the ILs to

48

impact cell viability was first assessed using the MTS assay. HeLa cells were treated with the ILs at their IC$_{50}$ concentrations and MTS cell viability was measured up to 4 hours. As no significant decrease in cell viability was observed over these short treatment periods (**Table 4**), ATP levels were monitored over 4 hours.

Table 4 MTS cell viability percentages at 4 hr treatment corresponding to ATP data in **Figure 19**.

Compound	MTS cell viability percentage (%)
[C$_4$Quin][Br]	93 ± 2.7
[C$_4$Py][Br]	99 ± 1.6
[C$_4$Mim][Br]	96 ± 2.8
[C$_4$TMA][Br]	96 ± 2.8
[C$_{10}$Quin][Br]	93 ± 0.98
[C$_{10}$Py][Br]	97 ± 0.47
[C$_{10}$Mim][Br]	97 ± 1.8
[C$_{10}$TMA][Br]	95 ± 1.2

As can be seen in **Figure 19B**, the aromatic C$_{10}$-ILs **[C$_{10}$Quin][Br]**, **[C$_{10}$Mim][Br]** and **[C$_{10}$Py][Br]** significantly decreased ATP levels in HeLa cells at their MTS cell viability IC$_{50}$ concentrations. **[C$_{10}$Quin][Br]** had the greatest effect, reducing intracellular ATP to 47 ± 0.72 % of control at 4 hours, while **[C$_{10}$Mim][Br]** and **[C$_{10}$Py][Br]** produce a similar decreases of ~68 %. In contrast, the aliphatic C$_{10}$-IL **[C$_{10}$TMA][Br]** and all C$_4$-ILs did not significantly decrease ATP production (**Figure 19A**). Li *et al.*[104] recently showed that [C$_8$MIM][Cl] lowers ATP levels in PC12 cells. These findings combined with the above findings suggests ILs with long alkyl chains and aromatic head groups are able to reduce intracellular ATP levels.
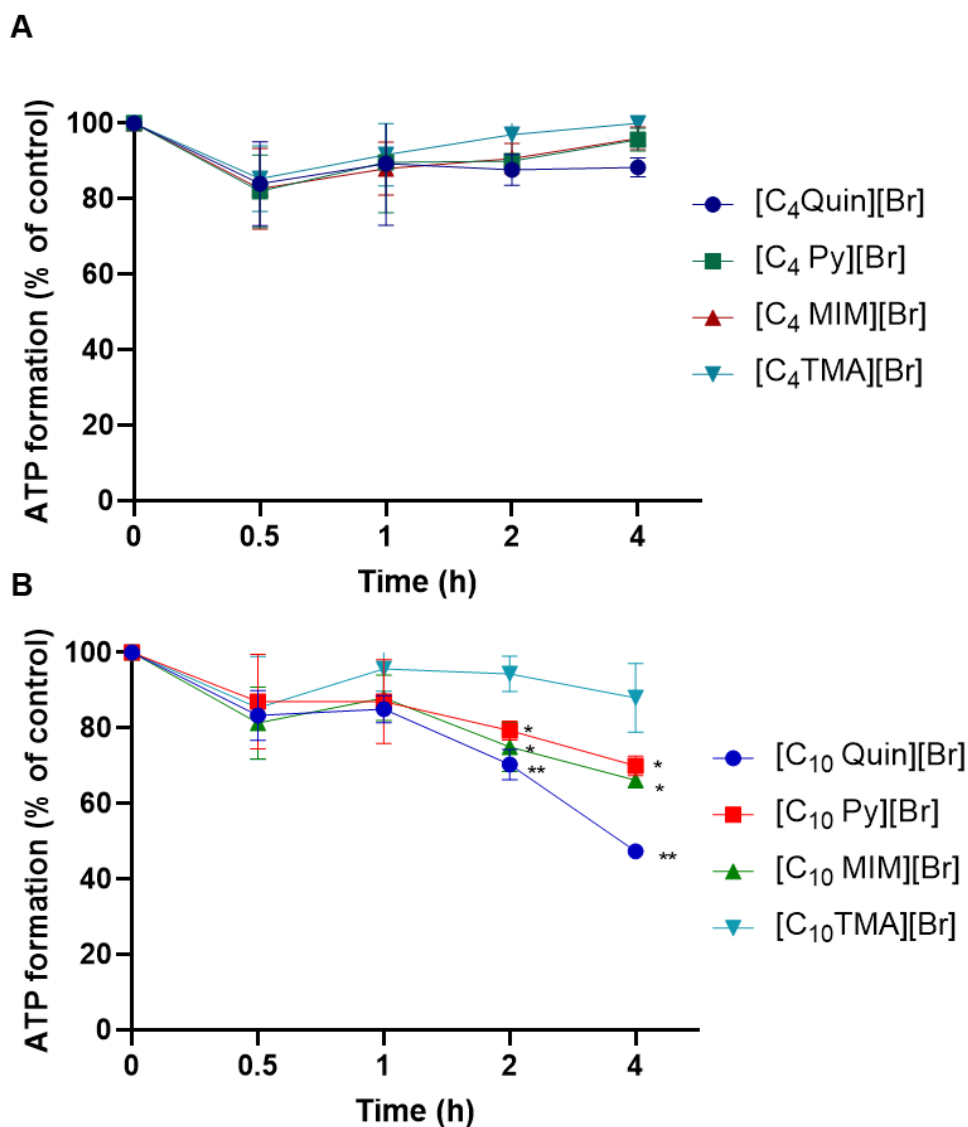
Figure 19 (A) Total intracellular ATP levels in HeLa cells following treatment with C_4-ILs at their MTS IC_{50} concentrations. (B) Total intracellular ATP levels in HeLa cells following treatment with C_{10}-ILs at their MTS IC_{50} concentrations. ATP levels are expressed as percentage of time-matched DMSO control. All data represents the mean ± SEM of 3 independent experiments. Different from DMSO-treated control: (*) $P < 0.05$, (**) $P < 0.01$ (***), $P < 0.001$.

Considered together with the JC-1 data, it can be concluded that of the ILs studied, only the aromatic C_{10}-ILs depolarise the IMM at their MTS IC_{50} concentrations to such an extent that is detected in the JC-1 assays and leads to impaired ATP production. This aligns with the Seahorse analysis which showed that HeLa cells treated with aromatic C_{10}-ILs lacked spare respiratory capacity, and the tBLM data which showed these ILs have the largest effect in membrane conductance. Considering that in the mitochondrial assays **[C$_{10}$Quin][Br]**, **[C$_{10}$Mim][Br]** and **[C$_{10}$Py][Br]** were tested at 25-90 μM, while **[C$_{10}$TMA][Br]** (200 μM) and C_4-ILs (2-15 mM) were tested at much higher concentrations, it is clear that the aromatic C_{10}-ILs have a much greater capacity to affect mitochondrial respiration. The relatively lipophilic nature of the aromatic C_{10}-ILs, which results from their larger alkyl chains and delocalised positive charge, likely accounts for the capacity of these ILs to accumulate in, and permeabilise, the IMM. This is further supported as several studies have found IL cytotoxicity is influenced by their lipophilicity.[58,85]

2.6.4 ROS production

Reactive Oxygen Species (ROS) are radicals, molecules or ions which have a single unpaired electron in their outermost shell of electrons. This property makes ROS highly reactive. The major species of ROS include superoxide ($O_2^{\bullet-}$), hydrogen peroxide (H_2O_2), and hydroxyl radical ($^{\bullet}OH$).[157] ROS are generated during normal cellular metabolism and mitochondrial functioning and are important in maintaining homeostasis. The overproduction of ROS is correlated with an increase in mitochondrial dysfunction, and overproduction of ROS can ultimately lead to cell death.[158, 127] Thus the capacity of the ILs to induce ROS formation was assessed. Indeed, several studies have shown that aromatic ILs cause an overproduction of ROS that leads to cell death.[17,104,114,126,127,151,159] The precise mechanism for IL-mediated ROS production is currently being investigated. Recently Wright *et al.* proposed

that Mim-based ILs can be reduced by the ETC to neutral radical species that undergo redox cycling to produce ROS.[151] Efficient ROS production was only induced by Mim-based ILs with long chains ($\geq C_6$), which the authors hypothesised was due to partitioning of these more lipophilic ILs in the IMM where the ETC is located. Alternatively, the pore forming agent alamethicin has been shown to induce ROS formation in isolated mitochondria by permeabilising the IMM, and it is possible that the ILs in this study could increase ROS by this mechanism.[160]

The capacity of ILs to induce ROS production was assessed in HeLa cells treated with the ILs at their MTS IC_{50} concentrations using the DCFDA assay. A kinetic experiment was used to determine the time point in which ILs induce ROS formation within the cells. The kinetic experiment was conducted every 30 mins over an 8-hr time period as cells would be affected after prolonged exposure without CO_2. This kinetic experiment produced a gradual increase in ROS over the initial 8 hrs (**Figure 20**).
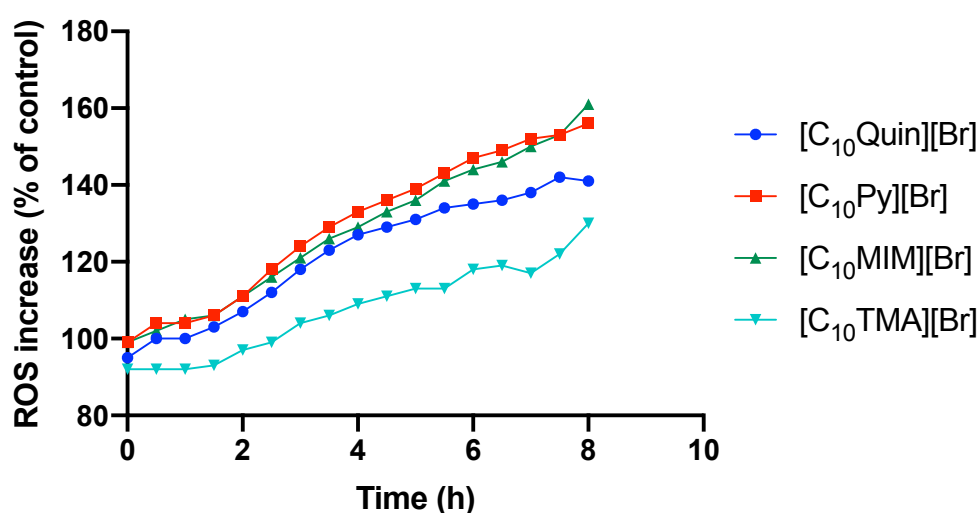
Figure 20 Percentage of control values for ROS increase over initial 8 hr when treated with C_{10}-ILs.

Subsequent ROS experiments were only measured at 6 hours of treatment as reasonably high ROS production was observed at this time point with. Consistent with previous findings,[151] the imidazolum based IL **[C$_{10}$Mim][Br]** increased intracellular ROS levels to ~140% of control (**Figure 21**). The remaining aromatic C$_{10}$-ILs **[C$_{10}$Quin][Br]** and **[C$_{10}$Py][Br]** also produced similar increases in ROS. This is due to ILs with greater lipophilicity having an increased ability to partition into the IMM.[151] In contrast, the aliphatic C$_{10}$-IL **[C$_{10}$TMA][Br]** and C$_4$-ILs **[C$_4$TMA][Br]**, **[C$_4$Mim][Br]** and **[C$_4$Py][Br]** did not induce ROS formation. The inactivity of these more polar ILs may result from their decreased capacity to accumulate in and depolarise the IMM, or in the case of the aliphatic ILs, an inability to efficiently produce ROS through the redox cycling mechanism proposed by Wright *et al*.[151] Interestingly **[C$_4$Quin][Br]** increased ROS to similar levels as the aromatic C$_{10}$-ILs. This is likely due to the larger quinolinium headgroup which renders **[C$_4$Quin][Br]** sufficiently lipophilic to accumulate in the IMM.
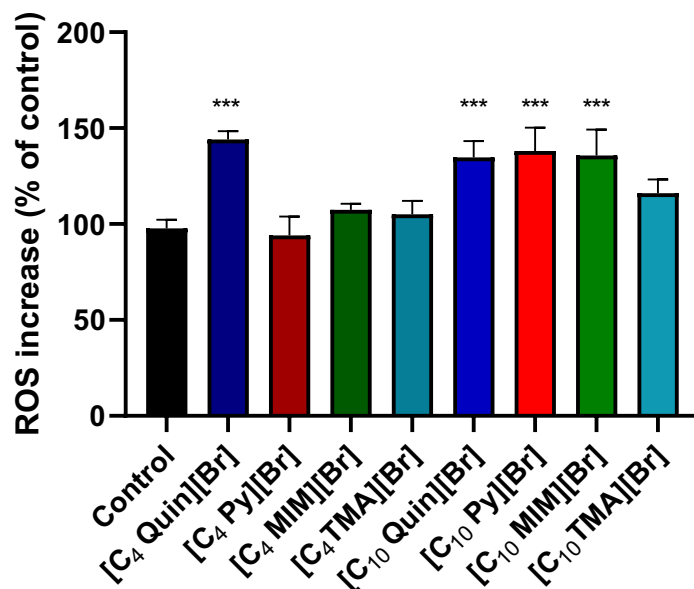
Figure 21 ROS production in HeLa cells treatment with ILs at their MTS IC_{50} concentrations (6 h). All data represents the mean ± SEM of 3 independent experiments. Different from DMSO-treated control: (***), $P < 0.001$.

2.7 Summary of findings

Taken together, the data presented shows that ILs containing aromatic cationic headgroups substituted with decyl tails target the IMM in HeLa cells and induce mitochondrial dysfunction at concentrations relevant to their cytotoxicity. These observed effects caused by ILs occur in HeLa cells treated at their MTS IC_{50} concentrations over short time periods, which suggests these effects may be early cellular events that result in cell death. In support of this, increased ROS is a known trigger of cell death, and dissipation of the proton gradient across the IMM and uncoupling of OxPhos by protonophores can induce cell death. Indeed, the use of mitochondrial uncouplers as clinical anticancer agents is currently being explored.[150] Given that numerous studies have suggested that ILs exert their cytotoxic actions by targeting either cell membranes or inducing mitochondrial dysfunction, our findings provide an important

insight into the mitochondrial actions of ILs. Which is long chain aromatic ILs specifically target the IMM due to the lipophilic nature of their cations.

Short chain (C_4) and aliphatic ILs also appear to affect mitochondrial function in Seahorse assays, albeit at much higher concentrations and to lesser extents than the aromatic C_{10}-ILs, however measurable effects on $\Delta\Psi_M$ in JC-1 assays, ATP production and ROS levels were not seen (with the exception of **[C$_4$Quin][Br]**). These data therefore suggest that short chain and/or aliphatic ILs were unsuccessful in producing cellular effects consistent with mitochondrial dysfunction. Hence, these ILs do not target the IMM in HeLa cell mitochondria and kill cells through a different mechanism, which also corresponds to a drop in cytotoxicity (IC_{50} concentrations in the millimolar range, compared to micromolar range for aromatic long chain ILs). The reduced activity of the aliphatic and short chain ILs likely results from the inability of these ILs to efficiently accumulate into and permeabilise the IMM. An exception is **[C$_4$Quin][Br]**, which increased ROS but did not affect JC-1 red:green ratios or ATP levels in HeLa cells. One possible explanation is that due to its larger headgroup **[C$_4$Quin][Br]** is sufficiently lipophilic to accumulate in the IMM where it produces ROS through redox cycling but lacks a sufficiently long alkyl chain to permeabilise and depolarise the IMM, and inhibit ATP production.

The mechanism proposed in this thesis can be used to explain some aspects of the SAR governing IL cytotoxicity, as structural features that increase the capacity of ILs to disrupt mitochondrial function should also be expected to promote cytotoxicity. To target the IMM and induce cell death, ILs must be sufficiently lipophilic to diffuse through the plasma membrane, and an alkyl chain long enough to disrupt the integrity of the IMM. Consistent with this, SAR studies have shown that increased alkyl chain length is a major determinant of IL

cytotoxicity.[15,16,55,58,61,66,83-86] Aromatic ILs are in general more cytotoxic than their aliphatic counterparts,[57] which can be explained by delocalisation of the cationic charge that renders aromatic ILs more lipophilic than aliphatic ILs. Headgroup aromaticity has less impact on the cytotoxicity of short chain ILs, which may result because these ILs kill cells by a different mechanism. Finally, there are conflicting reports regarding the influence of the anion, although it appears the nature of the anion has the least impact on the cytotoxicity of aromatic ILs with long alkyl chains.[57] This too can be rationalised by the proposed mechanism as it is only the cation that plays a role in the mitochondrial effects.

2.8 Conclusions

ILs share physiochemical properties with lipophilic cations and were therefore anticipated to target the IMM to induce cell death. Using fluorescence microscopy it was shown that a quinolinium-based IL is rapidly taken up into HeLa cells mitochondria. The capacity of a series of ILs to reduce viability and induce mitochondrial dysfunction in HeLa cells was assessed. ILs bearing aromatic headgroups substituted with decyl chains were the most effective at inducing cell death and permeabilising lipid bilayers. When tested at their MTS IC_{50} concentrations, long chain aromatic ILs produced a variety of cellular effects consistent with permeabilisation of the IMM. These effects are associated with cell death, and therefore indicate long chain aromatic ILs kill cells by targeting the IMM. ILs with short chains or aliphatic headgroups failed to produce these effects which suggests these ILs produce cytotoxicity by an alternate mechanism. These findings provide new mechanistic insights into IL cytotoxicity and may assist in the design of task-specific ILs for safe industrial application or as anticancer agents.

Chapter 3 - Structure-activity relationship studies: effects of headgroup substitution on IL cytotoxicity

3.1 Background

In addition to understanding the mechanisms by which ILs produce cytotoxic effects, a clearly defined structure-activity relationship (SAR) governing IL cytotoxicity will also assist in the development of safe ILs for industrial applications or cytotoxic ILs as potential anticancer agents. As discussed in **Section 1.4** of this thesis, it has been consistently shown that the length of the alkyl side chain on the headgroup of ILs is a major determinant of cytotoxicity, cytotoxicity increases as the alkyl chain length increases.[15,16,55,58,61,66,83-86] The effects of other structural elements on IL cytotoxicity are less well defined. It is likely that the anion has little to no impact on cytotoxicity, although this has not been consistently observed across studies.[17,89,90] Headgroup aromaticity appears to play an important role in IL cytotoxicity, as several studies have shown that ILs containing aromatic headgroups are significantly more cytotoxic than aliphatic counterparts.[11,17,88] Interestingly, the effect of aromatic headgroup substitution on cytotoxicity has not been widely explored and only one study has addressed this issue. The study assessed the cytotoxicity of pyridinium based ILs substituted with methyl groups at the 2, 3 and 4 position on the headgroup (**Figure 22**) and found that these ILs were equipotent to one another in MCF-7 cells.[57]

1-octyl-2-methylpyridinium cation

1-octyl-3-methylpyridinium cation

1-octyl-4-methylpyridinium cation
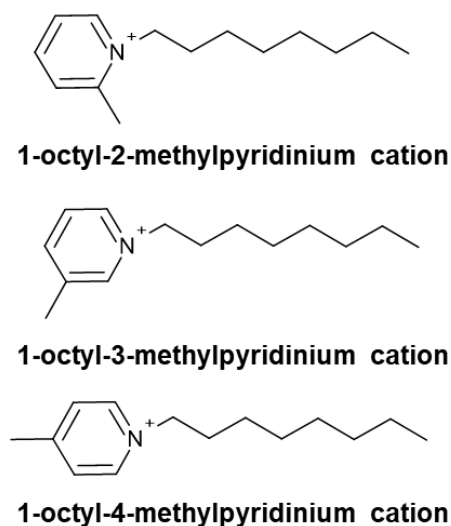
Figure 22 Substituted pyridinium based ILs with methyl groups at the 2, 3 and 4 position.

The lack of research into headgroup substitution is surprising given that aromatic substitution is widely explored in drug discovery research and is known to significantly affect drug activity by modifying the lipophilicity and electronic properties of drug and/or introducing new drug-target binding interactions.[161,162] Hence, the primary aim of this chapter was to examine the effects of headgroup substitution on IL cytotoxicity. To achieve this, a series of pyridinium- and quinolinium-based ILs with systematically varied headgroup substituents were prepared and their capacity to reduce the viability of HeLa cells was assessed *in vitro* using the MTS assay.

3.2 Optimisation of quinolinium-based IL *N*-alkyl chain length

Prior to designing a library of substituted quinolinium-based ILs for SAR studies, the optimal chain length for cytotoxicity was first determined. Hence, a series of quinolinium-based ILs containing *N*-alkyl chain lengths from C_{12} to C_{22} were prepared (**Figure 23**).
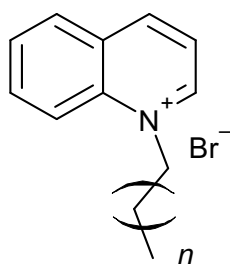
12: n = 10
13: n = 12
14: n = 14
15: n = 16
16: n = 18
17: n = 20

Figure 23 Chemical structure of quinolinium with varying *N*-alkyl chain lengths.

3.2.1 Synthesis of quinolinium ILs

ILs **12-17** were prepared following the procedure outlined in **Section 2.2.1**. Quinoline (**18**) was heated at 140 °C with the appropriate alkyl bromide for 24-72 hours (**Scheme 2**) and the crude solid was purified by trituration with hexane then re-precipitation from chloroform/diethyl ether to yield **12-17** in yields of 57-87%.

The reaction times required to prepare **12-17** were found to increase as alkyl chain length increased. For example, during the synthesis of **12** complete consumption of the alkyl bromide (1-bromododecane) starting material occurred in 24 hours, while for **17**, ~40 % of the alkyl bromide (1-bromodocosane) was remaining after 3 days of continuous reaction. This is in agreement with previous studies that have shown reduced rates of quaternisation associated with increasing length of alkyl chains. For example, Madaan *et al.* found the reaction times for the quaternisation of substituted pyridines increased as the chain length of the alkyl group increased.[163] As a result, the longer chain (≥ C16) reactions required significantly longer reaction times for the formation of ILs.
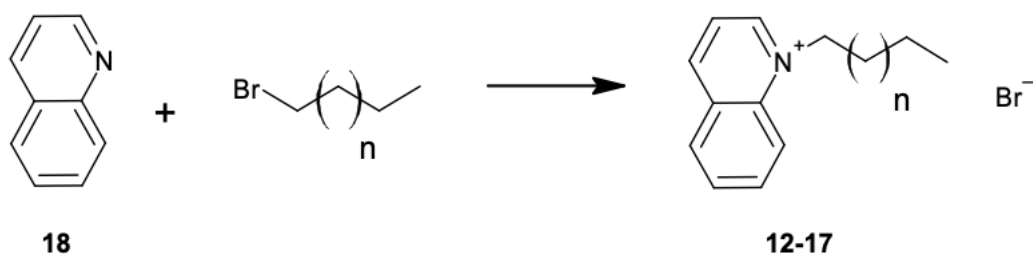
Scheme 2 Synthesis conditions of ILs **12-17** were prepared using similar conditions. Reagents and conditions: neat, 140 °C, 24-72 h, 57-87 %. n= C_9-C_{19}.

ILs **12-17** were characterised by NMR spectroscopy and HRMS techniques as described in **Section 2.2.1** (see experimental **Section 5.3** and appendix for full characterisation data and copies of ^{1}H and ^{13}C NMR spectra). The purities of **12-17** were determined by QNMR and were found to be between 95.7 and 100.0 %, which is sufficient for *in vitro* evaluation.

3.2.2 Effects of 12-17 on HeLa cell viability

The cytotoxicity of ILs **12-17** were assessed against HeLa cells using the MTS cell viability assay. ILs **12-17** were tested at varying concentrations ranging from 0.1 – 100 μM, with the exception of ILs **16** and **17** which were not sufficiently soluble to test over the full concentration range to allow determination of IC_{50} concentrations. Full dose-response curves were collected for **12-15** (**Figure 24**), and from these curves IC_{50} concentrations were calculated (**Table 5**).
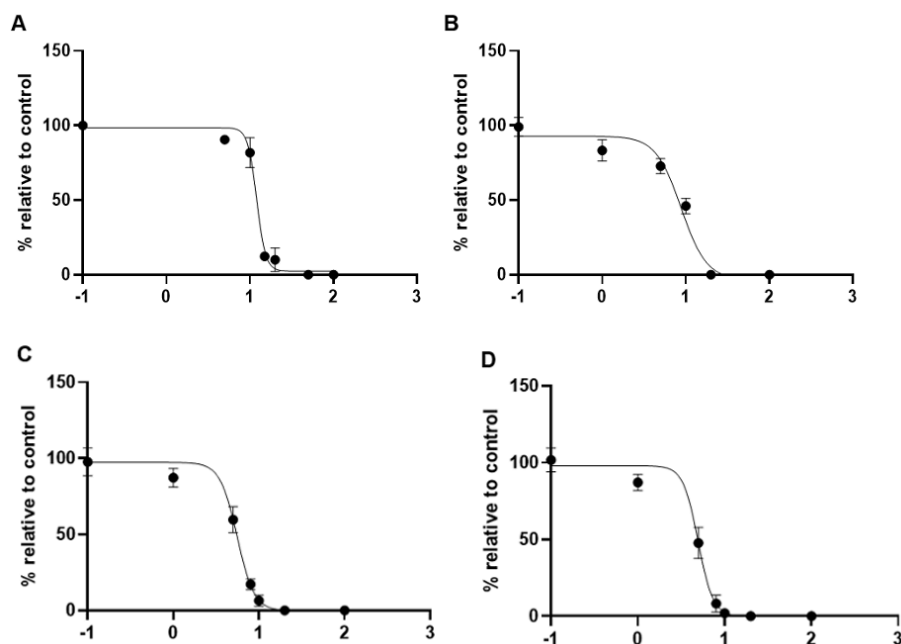
Figure 24 Dose-response curves showing the effect of ILs on the cell viability of HeLa cells after 48 h treatment. A) **12**, B) **13**, C) **14** and D) **15**. Data represents the mean ± SEM of 3 independent experiments.

ILs **12**-**15** caused a reduction in HeLa cell viability with IC_{50} concentrations ranging from 5.00 ± 0.15 μM to 12.99 ± 0.81 μM (**Table 5**). **12** and **13** exhibited IC_{50} concentrations of 12.99 ± 0.81 and 7.68 ± 0.89 μM respectively, whilst ILs **14** and **15** equally decreased cell viability with similar IC_{50} concentrations of ~ 5 μM. The IC_{50} data shows the cytotoxicity of ILs increased as alkyl chain length increased, which is consistent with SAR discussed in **Chapter 2**. As **15** was sparingly soluble in DMSO and possessed an identical IC_{50} to **14** which was completely soluble, C_{16} alkyl chains were optimal and used in subsequent experiments in this thesis.

Table 5 Cell viability IC$_{50}$ concentrations of various alkyl chain length ILs against HeLa cells.
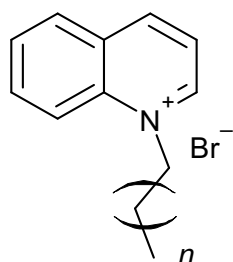
Compound	n	IC$_{50}$ (μM)
12	10	12.99 ± 0.81
13	12	7.68 ± 0.89
14	14	5.39 ± 0.22
15	16	5.00 ± 0.15
16	18	-
17	20	-

3.3 Synthesis and cytotoxicity of substituted quinolinium-based ILs

With the optimal chain length identified, the next step was to design a series of ILs that would facilitate an understanding of substituent effects on IL cytotoxicity. In the selection of substituents, the following parameters were considered:

- *Substituent hydrophobicity constant (π):* a measure of the hydrophobicity of a substituent relative to hydrogen. Substituents that are hydrophobic have positive values. Hydrophilic or polar substituents have a negative value.

- *Hammett substituent constant (σ)*: a measure of the electronic properties of an aromatic substituent relative to hydrogen. Electron donating substituents have a negative value and electron withdrawing substituents have a positive value.

3.3.1 Proposed substituted quinolinium library (Library 3)

In Library 3, quinolinium based ILs bearing substituents on the C-2 and C-3 positions were planned (**Figure 25**). These positions were chosen as it allowed access to the widest range of commercially available substituted quinolines. It was envisioned these ILs could be made in one step using the previously described quaternisation reaction (see **Section 2.2.1**) by reacting the appropriate substituted quinoline with the alkyl halide.
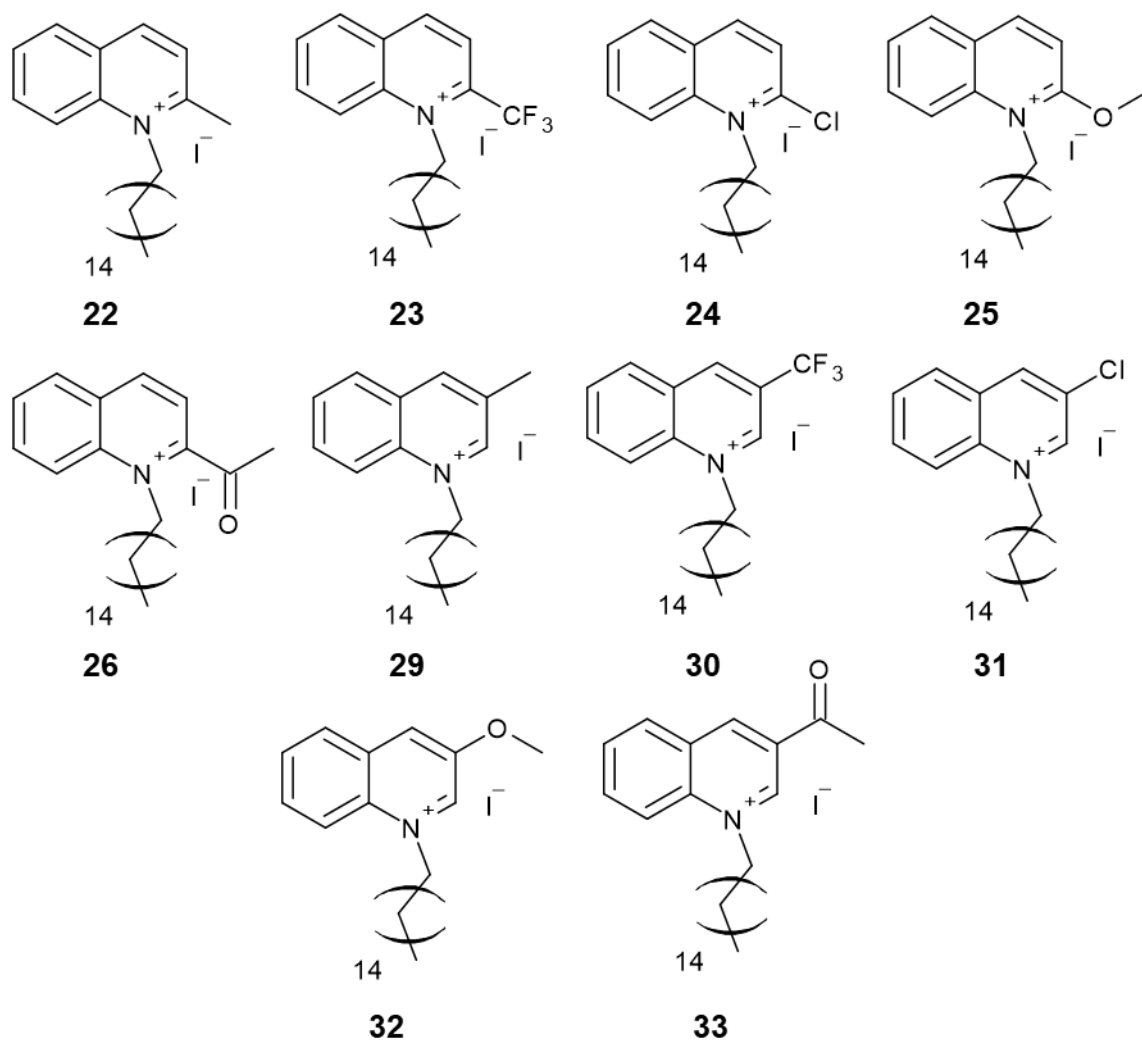
Figure 25 Substituted quinolinium ILs.

3.3.2 Synthesis of Library 3

To synthesise **22** quinaldine was reacted with 1-bromohexadecane using the same procedure used to prepare **12-17 (Scheme 2)**. NMR analysis of the reaction mixture after 48 hours indicated that no reaction had occurred and only the two starting materials were present in the reaction mixture. Extending the reaction time to 96 hours and increasing the temperature to 180 °C also failed to form the product **22**.

Due to the observed lack of reaction, 1-bromohexadecane was converted to 1-Iodohexadecane using the Finkelstein reaction. It was anticipated that quaternisation might

occur with 1-Iodohexadecane due to iodine being a better leaving group, which makes iodoalkanes more reactive than bromoalkanes.[164] The Finkelstein reaction is a nucleophilic substitution reaction which involves the exchange of one halogen atom to another and proceeds via an S_N2 mechanism. The nucleophile attacks the alpha carbon of the alkyl bromide to form a transition state. In the next step the bromine acts as a leaving group and the iodine from sodium iodide joins to form the iodoalkane product, the mechanism is shown in **Scheme 3**. This reaction goes to completion because sodium bromide is insoluble in the reaction solvent (acetone), and precipitation of NaBr from the reaction solution drives the equilibrium towards products.
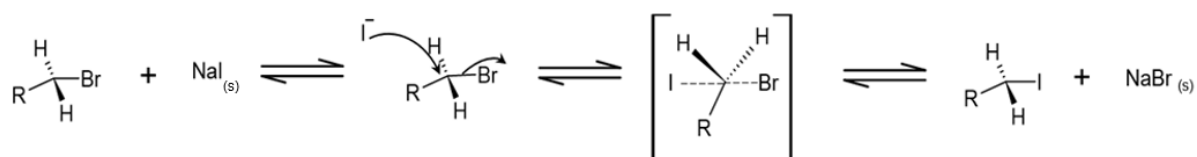
Scheme 3 General mechanism for the formation of an iodoalkane from bromoalkane using the Finkelstein reaction.

1-Iodohexadecane was readily prepared (see **Section 5.4** for details) and subsequently used in the quaternisation reaction with quinaldine. Under these conditions some product formation was observed, however the reaction failed to go to completion and **22** was isolated in a relatively poor yield of ~15 %.

22 was synthesised under neat reaction conditions and to improve yields the quaternisation reaction of **23** was attempted in acetonitrile, as polar solvents have been shown to improve the rate of heterocyclic quaternisation.[165] Unfortunately, reactions in acetonitrile resulted in the formation of multiple side products with little to no observable quaternisation, even under forcing conditions (220°C, 144 hours). The difficulties in synthesising ILs with

substituents in the C-2 position was attributed to steric effects, and therefore study of C-2 substituted quinoliniums was discontinued.

On the other hand, C-3 substituted ILs **29-32** were readily synthesised by reactions of the substituted quinolines with 1-Iodohexadecane in acetonitrile for 24-48 h (**Scheme 4**). Evaporation of the reaction solvent produced crude solids that were triturated with hexane and diethyl ether to afford the desired products. Only **33** was not able to be prepared. ^{1}H NMR analysis of the crude reaction product revealed the presence of a large number of impurities that could not be separated from the desired product.
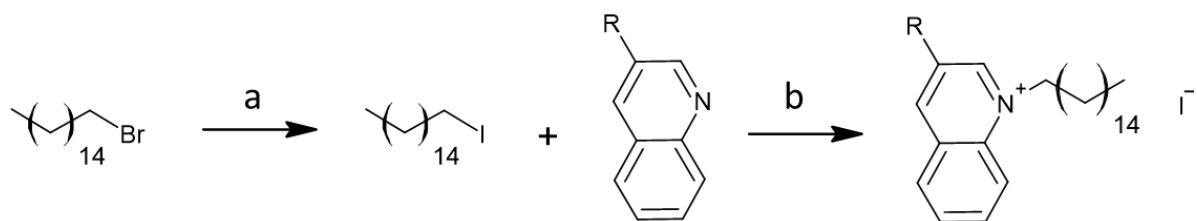
Scheme 4 Synthesis of **29-32**. Reagents and conditions: a) NaI, acetone, reflux, 3 h, 94 %, b) acetonitrile, 140 °C, 24-48 h, 13-85%.

ILs **29-32** were characterised by NMR spectroscopy and HRMS (see **Section 5.5**). The purities of **29-32** were determined by QNMR and were found to be between 97.1 and 99.6 %, which is sufficient for *in vitro* evaluation.

3.3.3 Effects of 29-32 on HeLa cell viability

The cytotoxicity of ILs **29-32** was assessed in HeLa cells using the MTS assay. The resultant dose response curves (**Figure 26**) were used to determine their IC_{50} concentrations (**Table 6**).
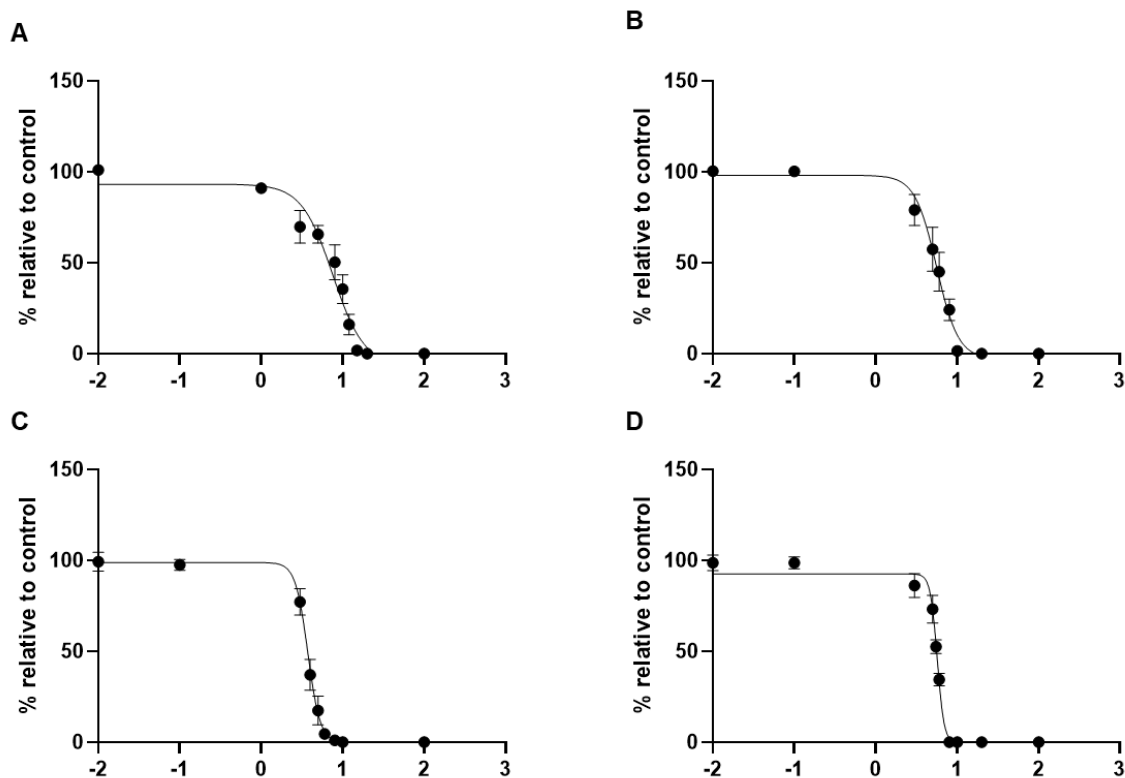
Figure 26 Dose-response curves showing the effect of substituted quinolinium-based ILs on the cell viability of HeLa cells after 48 h treatment. A) **29**, B) **30**, C) **31** and D) **32**. Data represents the mean ± SEM of 3 independent experiments.

The IC_{50} concentrations of ILs **29-32** ranged from 3.80 - 7.81 µM, which are not significantly different to the unsubstituted IL **14** (IC_{50} = 5.39 ± 0.22 µM). The similar cytotoxicity of these ILs indicates that the addition of substituents on the C-3 position of the quinolinium headgroup does not affect cytotoxicity. It should be noted however that only 4 substituents were included in this study due to the limited commercial availability of 3-substituted quinolines. As a result the full range of substitute properties could not be assessed, and this limits the strength of the SAR conclusions. For example, all substituents were relatively lipophilic (π values from -0.02 – 0.88) and therefore the impact of substituent polarity could not be thoroughly evaluated. For this reason a new IL library was envisioned.

Table 6 Chemical structure, aromatic substituent properties and cell viability IC_{50} concentrations of **29**-**32** against HeLa cells.
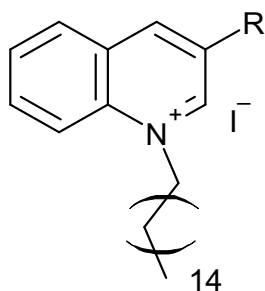
Compound	R	π	σ	IC_{50} (μM)
29	CH_3	0.56	-0.07	7.81 ± 0.97
30	CF_3	0.88	0.43	3.80 ± 0.04
31	Cl	0.71	0.37	5.58 ± 0.15
32	OCH_3	-0.02	0.12	5.59 ± 0.44

π: Hansch constant (hydrophobicity), σ**:** Hammet constant (electron-withdrawing capacity)[166,167]

3.4 Synthesis and cytotoxicity of substituted pyridinium-based ILs (Library 4)

The inability to synthesise C-2 substituted quinolines and the lack of commercially available C-3 substituted quinolines prevented a robust assessment of headgroup substituents on IL cytotoxicity. The pyridinium headgroup was subsequently explored as a wide range of pyridines bearing substituents in the C-3 position are commercially available. Thus, a library of 11 pyridyl-based ILs was planned (Library 4, **Figure 27**).
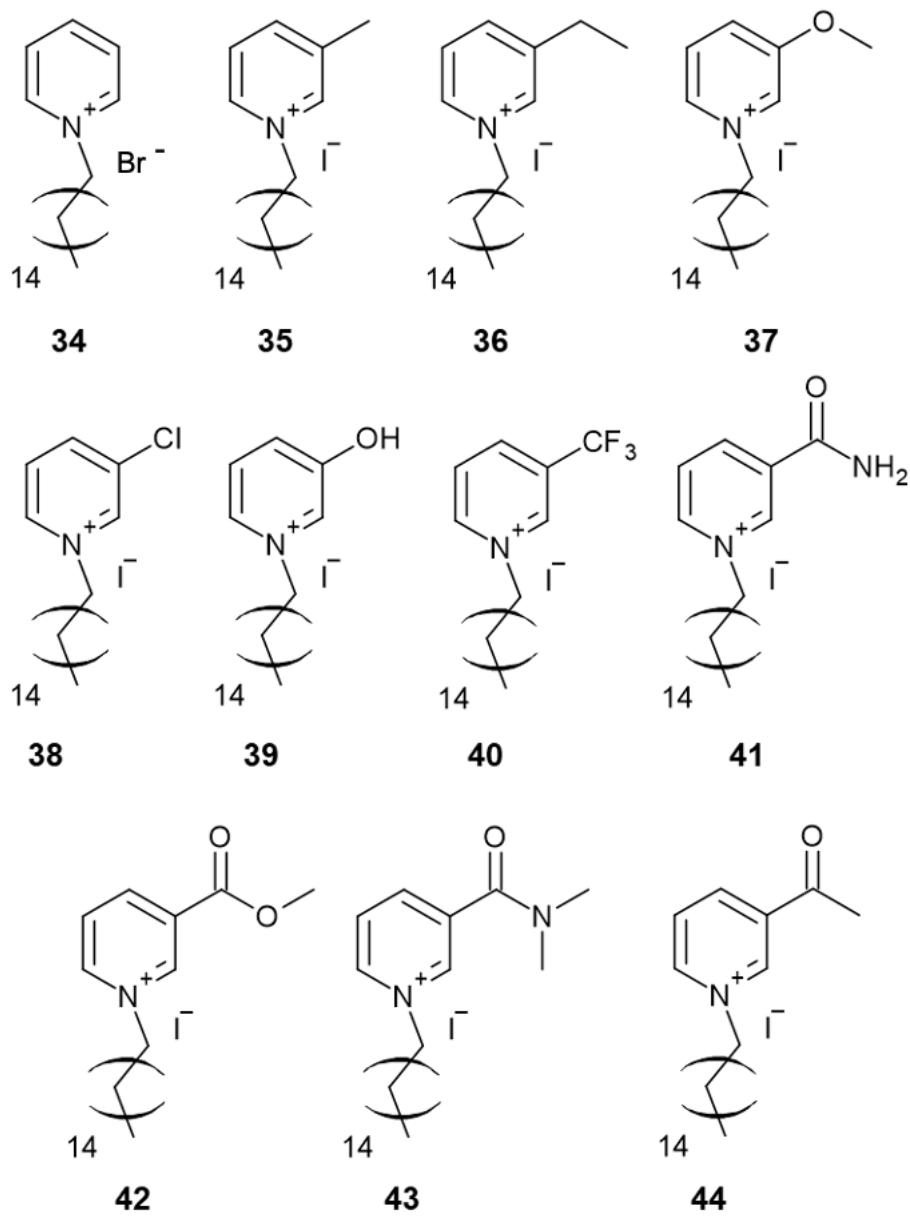
Figure 27 Chemical structures of substituted pyridinium based ILs studied.

3.4.1 Synthesis of 34

34 was synthesised by reflux of pyridine and 1-Bromohexadecane in acetonitrile for 24 hours, after which the crude solid was triturated with hexane and diethyl ether to afford pure product without further purification in a high yield of 86 % (**Scheme 5**).
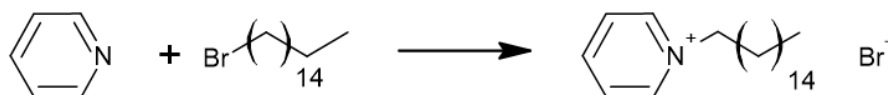
Scheme 5 Synthesis of **34**. Reagents and conditions: a) acetonitrile, 100 °C, 24 hr, 86 %.

3.4.2 Synthesis of 35-39 and 41-44

The general synthetic route for the synthesis of ILs **35-39** and **41-44** is depicted in **Scheme 6**. These quaternisation reactions with substituted pyridine headgroups successfully formed ILs **35-39** and **41-44** in moderate to high yields of 26-94 % after purification by trituration.

35: R = CH_3   **41**: R= CONH_2
36: R = CH_2CH_3   **42**: R= OCOCH_3
37: R = OCH_3   **43**: R = CON(CH_3)_2
38: R = Cl   **44**: R = COCH_3
39: R= OH
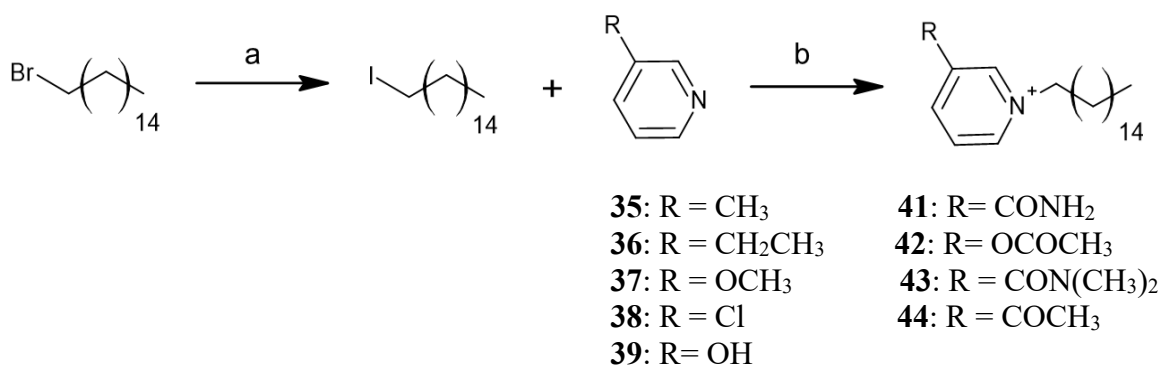
Scheme 6 Reagents and conditions: a) NaI, acetone, reflux, 3 h, 94 %, b) acetonitrile, reflux, 100 °C, 24 hr, 26-94 %.

Quaternisation of ILs **35-39** and **41-44** was confirmed by NMR spectroscopy and HRMS techniques. The purities of ILs **35-39** and **41-44** were determined to be 97.5- 102.4 % using QNMR.

3.4.3 Attempted synthesis of IL 40

The CF3-substituted IL **40** was attempted to be synthesised using the quaternisation method previously described. The ^{1}H NMR spectrum of the reaction product contained only three aromatic proton peaks instead of the expected four (**Figure 28**), which suggests a proton on the pyridinium-headgroup has been substituted for another functional group. The HRMS revealed a parent ion with a m/z of 388.2819 which is ~ 16 m/z higher than expected (372.5317). Combined, these data suggest that an aromatic proton may have been substituted by an OH group. The aromatic resonances appear as a singlet and two doublets, which is only possible if the OH group was added at the 4 or 6 positions. Based on the relative positions of doublets 'b' and 'c' with respect to the 'a' singlet, coupled with the significantly upfield shift of 'd' (which is usually observed > 4 ppm) it is most likely that the OH is on the C-6 position due to the increased electron density about the nitrogen (i.e. if the hydroxyl was on the 4 position, there would be a doublet with a higher chemical shift than singlet 'a'.
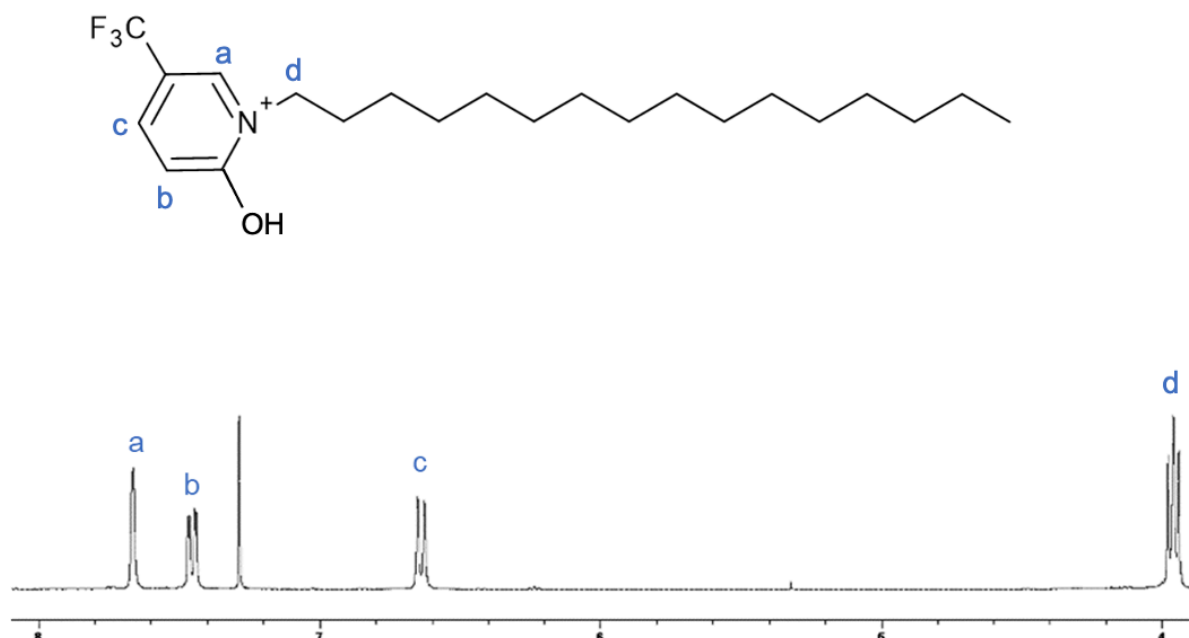
Figure 28 Low-field region of the ^{1}H NMR spectrum of the product isolated during the attempted synthesis of **40**.

The precise reaction mechanism that may have given rise to the suspected hydroxylated product is unknown, however it was possible that the OH group was derived from water in the reaction solvent. Thus, a second attempt to prepare **40** was undertaken, however this time the reaction was performed in a sealed pressure tube to minimise atmospheric moisture contamination. This method was successful as shown by the ^{1}H NMR spectrum of the reaction product (**Figure 29**). In this case, four aromatic environment signals were present between 8.0-10.2 ppm. Importantly, the peak arising from the CH_2 adjacent to the pyridyl-N atom (peak 'd' in **Figure 29**) appears at 5 ppm (as opposed to 4ppm in the first product), which is a similar chemical shift to those seen in the ^{1}H NMR spectra of **35-44**. The HRMS showed a molecular ion with m/z 372.5317 which matches the calculated mass of **40** (m/z 372.5305).
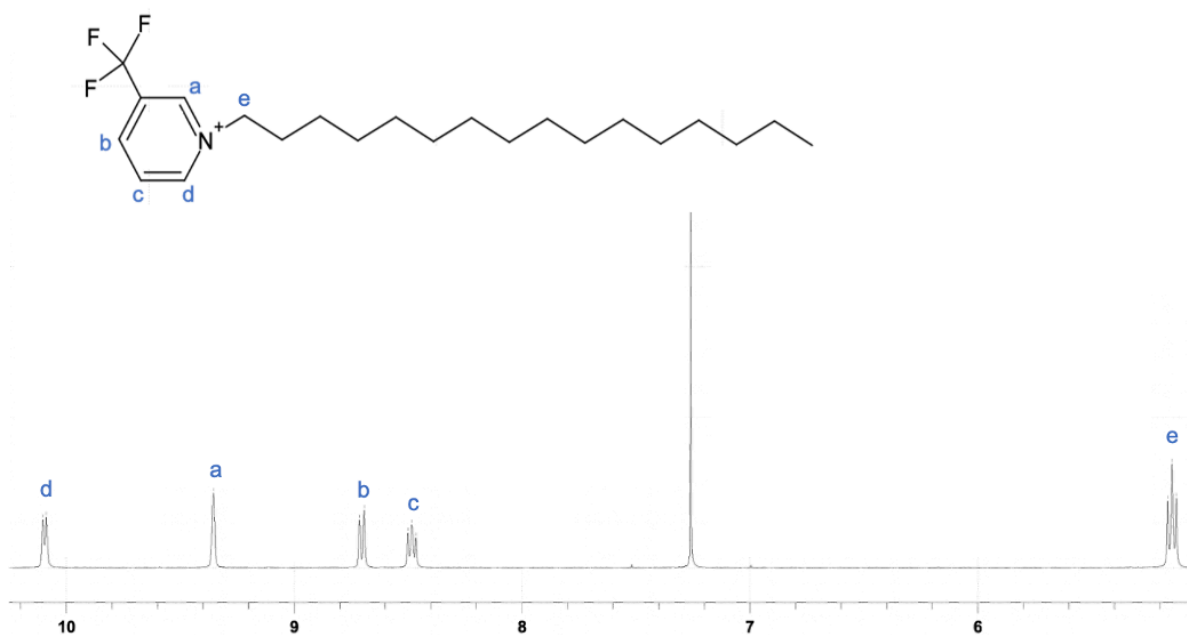
Figure 29 Low-field region of the ^{1}H NMR spectrum of **40**.

3.4.4 Effects of 34-44 on HeLa cell viability

The cytotoxic effects of C-3 substituted pyridinium-based ILs **34-44** were evaluated against HeLa cells using the MTS assay and their dose response curves and IC_{50} concentrations are presented in **Figure 30** and **Error! Reference source not found.**.
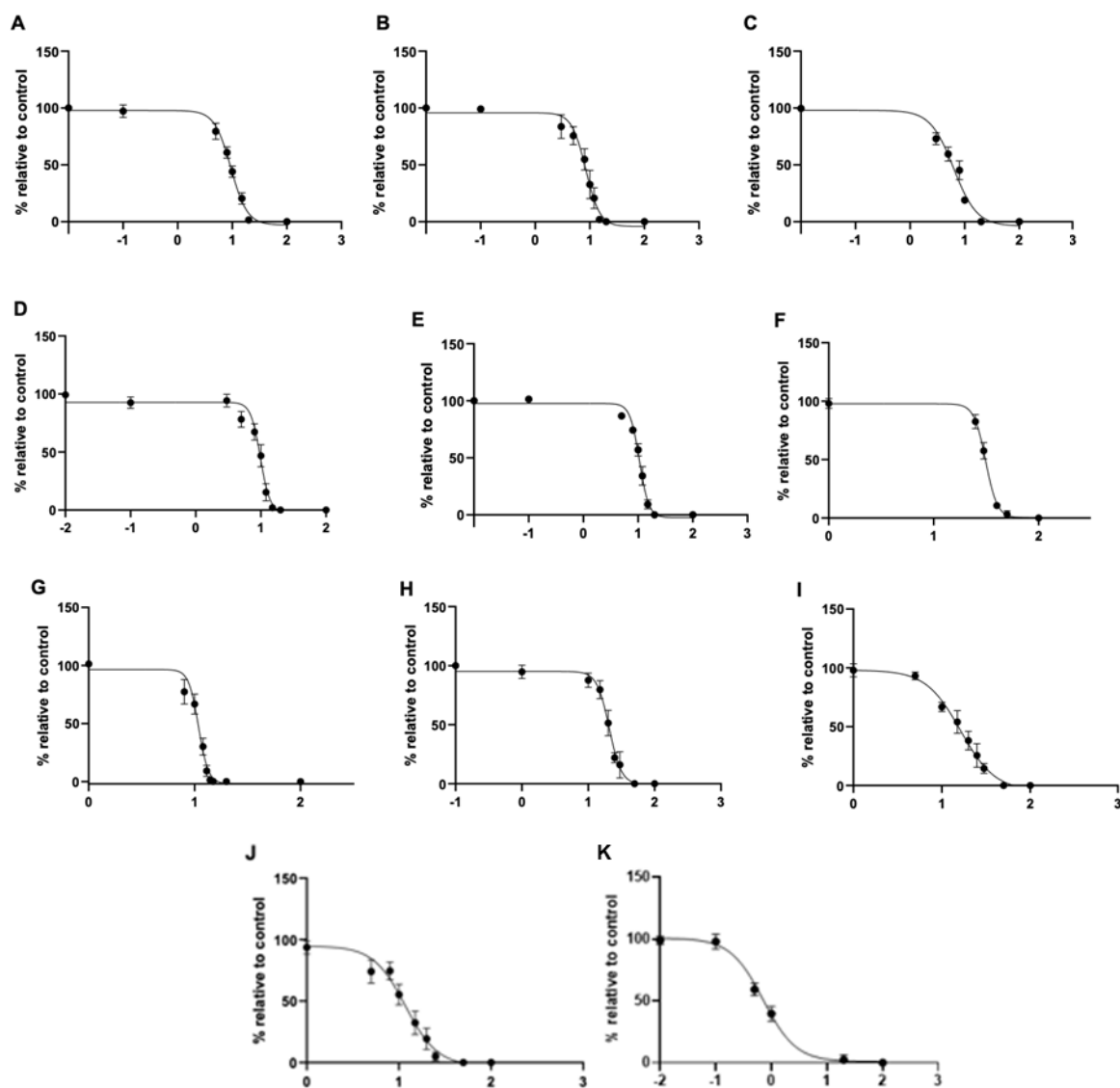

Figure 30 Dose-response curves showing the effect of substituted pyridinium based ILs on the cell viability of HeLa cells after 48 h treatment. A) **34**, B) **35**, C) **36**, D) **37**, E) **38**, F) **39**, G) **40**, H) **41**, I) **42**, J) **43** and K) **44**. Data represents the mean ± SEM of 3 independent experiments.

ILs **35-38, 40** and **42-43** reduced cell viability with a similar IC_{50} concentration as the unsubstituted analogue **34** (9.42 ± 0.18 µM), this suggests substituents properties have negligible effect on cytotoxicity. For example, ILs bearing either polar (-COOCH3, -OCH$_3$) or lipophilic (-CH$_3$, -CH$_2$CH$_3$) substitutes have similar IC_{50} concentrations as **34**, this suggests substituent polarity has no effect on cytotoxicity. In addition, when comparing compounds **35** (-CH$_3$) and **36** (-CH$_2$CH$_3$) with lipophilic substituents, which present the same value of σ (-0.07) and different values of π with an increase from 0.56 to 1.02 respectively (**Table 7**), the IC_{50} concentrations were not significantly different (8.35 ± 0.60 µM to 7.27 ± 0.52 µM respectively). This suggests substituent lipophilicity does not play a role in cytotoxicity. Furthermore, electronic properties of ILs also do not effect cytotoxicity. For example, compounds **36** (-CH$_2$CH$_3$) and **40** (-CF$_3$) are substituted with electron donating and withdrawing groups respectively, but have similar IC_{50} concentrations (**Table 7**). Similary IL **35** which contains an electron donating substituent -CH$_3$ had equipotent activity to **40** and both substituents are similar in size.

Interestingly, ILs **39 (**OH**)** and **41 (**CONH$_2$**)** possess hydrogen-bond donating substituents and were found to be 3 and 2-fold less cytotoxic that the other ILs in the series, with IC_{50} concentrations of 31.40 ± 1.42 µM and 21.34 ± 1.37 µM respectively. Combined, these data suggest that while substituent lipophilicity (π) and electronic properties (σ) do not affect IL cytotoxicity, the capacity of the substituent to participate in hydrogen bonds as a hydrogen bond donor does.

Table 7 Chemical structure, aromatic substituent properties and cell viability IC_{50} concentrations of **34-44** against HeLa cells.


Compound	R	π	σ	IC_{50} (μM)
34	H	0.00	0.00	9.42 ± 0.18
35	CH_3	0.56	-0.07	8.35 ± 0.60
36	CH_2CH_3	1.02	-0.07	7.27 ± 0.52
37	OCH_3	-0.02	0.12	9.40 ± 0.48
38	Cl	0.71	0.37	11.43 ± 0.32
39	OH	-0.67	0.12	31.40 ± 1.42
40	CF_3	0.88	0.43	10.87 ± 0.13
41	$CONH_2$	-0.98	0.19	21.34 ± 1.37
42	$COOCH_3$	-0.01	0.33	16.21 ± 0.80
43	$CON(CH_3)_2$	*n/a*	*n/a*	11.18 ± 1.15
44	$COCH_3$	-0.55	0.38	0.77 ± 0.06

π: Hansch constant (hydrophobicity), σ: Hammet constant (electron-withdrawing capacity)[166,167]

n/a = constant were not available for this substituent

3.4.5 Evaluation of hydrogen bond donor substituents on the permeability of DOPC lipid bilayers

To understand how the hydrogen bond donating capacity of a headgroup substituent may affect IL cytotoxicity, the effects of the ILs on membrane integrity was assessed.

Membrane effects were specifically investigated as the experimental data collected in **Chapter 2** suggested that aromatic long chain ILs target and permeabilise the IMM, which leads to mitochondrial dysfunction and cell death.

The capacity of the ILs to permeabilise lipid bilayers was assessed using tBLM produced from DOPC, as described in **Section 2.4**. For these studies the hydrogen bond donating ILs **39** and **41** were chosen. ILs **42, 43, 44** were chosen for comparison as these ILs bear substituents with similar steric properties to **39** and **41**, as well as the unsubstituted IL **34**.
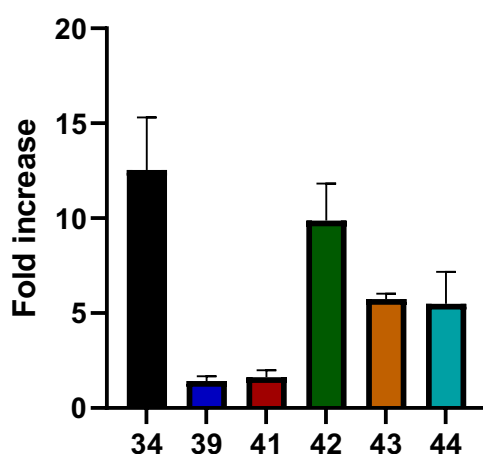
Figure 31 Addition of **34**, **39** and **41-44** at 20 μM increased conductance across a DOPC lipid bilayer tethered to a gold electrode, as measured by electrical impedance spectroscopy. Data normalised to membrane conductance prior to IL treatment at pH = 7. Data represents the mean ± SEM of 3 independent experiments.

As shown in **Figure 31** the most cytotoxic ILs in the series **(34,** and **42-44)** produced the greatest increases in bilayer conductance. In contrast, the ILs bearing hydrogen bond donating substituents **(39** and **41)** produced the smallest changes in bilayer conductance. These ILs were the least cytotoxic. Thus, the tBLM studies suggest that ILs **39** and **41** are less

cytotoxic because they have a diminished capacity to permeabilise lipid bilayers such as the IMM.
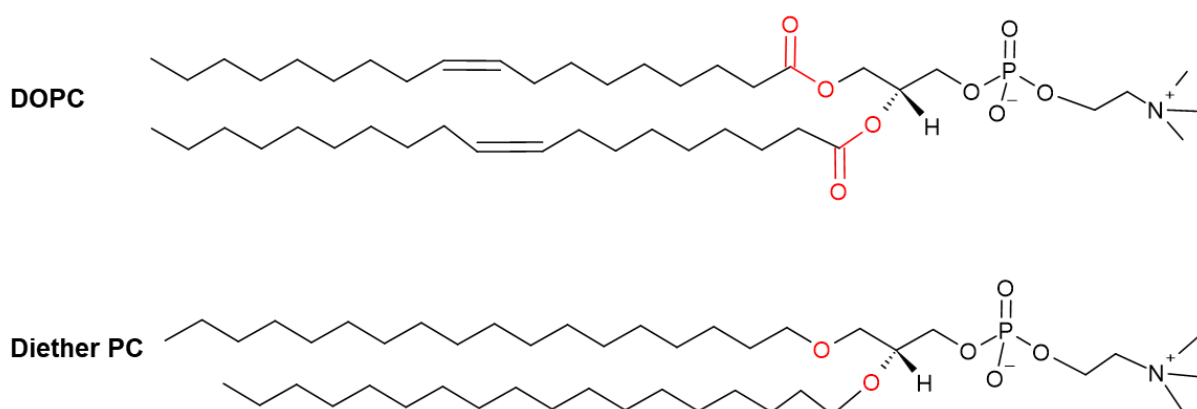
Figure 32 Chemical structures of DOPC and Diether PC lipids.

The next question that arises is how the hydrogen bond donating substituents on an IL headgroup limit their ability to permeabilise membranes. One possible explanation is that following insertion into the bilayer, **39** and **41** form hydrogen bonds with hydrogen bond acceptor groups on phospholipids in the bilayer, which improves lipid packing and minimises any effect of the ILs on membrane integrity. A potential hydrogen bond acceptor group in DOPC is the carbonyl oxygen atoms of the ester groups. To test if **39** and **41** interact with this group the tBLM experiment was repeated, however this time the bilayers were formed from Diether PC, which contains an ether linkage as opposed to the ester linkage in DOPC (**Figure 32**). If the carbonyl groups do participate in hydrogen bonds then the effects of **39** and **41** on Diether PC membranes should be similar to those produced by the other ILs in the series. As shown in **Figure 33**, the results obtained from tBLM studies with Diether PC bilayers were broadly similar to those found when using DOPC. Importantly, **39** and **41** were the least active in both DOPC and Diether PC tBLMs. These results suggest **39** and **41** do not interact *via* hydrogen bonding with the C=O group in DOPC but does not rule out their potential interaction

with alternate hydrogen bond acceptors in DOPC such as the phosphate group. Indeed, the phosphate carries a full negative change and is therefore a stronger hydrogen bond acceptor.
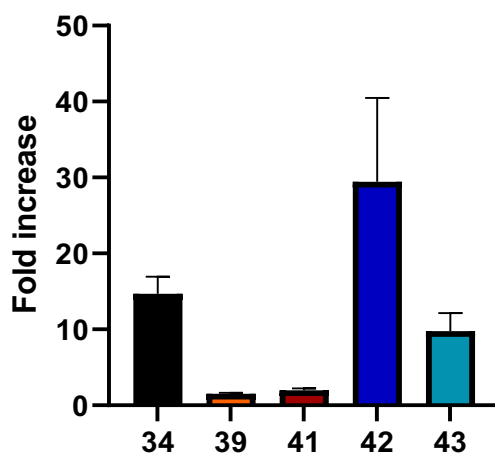
Figure 33 Addition of **34**, **39** and **41**-**43** at 20 µM increased conductance across a Diether PC lipid bilayer tethered to a gold electrode, as measured by electrical impedance spectroscopy. Data normalised to membrane conductance prior to IL treatment at pH = 7. Data represents the mean ± SEM of 3 independent experiments.

3.5 Conclusion

A series of quinolinium and pyridinium based ILs were designed and synthesised to investigate the influence of headgroup substitution on cytotoxicity. ILs **12**-**17** containing C_{12} to C_{22} *N*-alkyl chain lengths were prepared through a quaternisation reaction between quinoline and alkyl bromides. The cytotoxicity of **12**-**17** was evaluated using the MTS cell viability assay. ILs bearing C_{20} and C_{22} *N*-alkyl chains were too insoluble for *in vitro* evaluation. The most potent of the series, **14,** effectively decreased the cell viability of HeLa cells with an IC_{50} of 5.39 ± 0.22 µM, indicating the optimal chain length to be C_{16}. A quinolinium-based series of ILs was next investigated. Synthesis of ILs substituted at the C-2 position was not successful due to steric hindrance, but a small series of C-3 substituted ILs (**29**-**32)** was prepared. These ILs had MTS IC_{50} concentrations similar to the unsubstituted analogue **14** which suggests that

substitution on the quinolinium headgroup does not significantly modify cytotoxicity. A wider range of pyridinium-based substituted ILs was prepared (**35-44**) using the reaction conditions employed to prepare ILs **29-32**. Comparison of these ILs to **34**, an unsubstituted IL, showed that substituent lipophilicity and electronic properties does not have a significant effect on cytotoxicity. ILs **39** and **41**, which contain hydrogen bond donor groups, did have decreased cytotoxicity and as well as a decreased capacity to permeabilise lipid bilayers. This is consistent with the mechanistic studies in **Chapter 2** that indicated the ILs induce cell death by targeting the IMM. Preliminary studies aimed at understanding the role of the hydrogen bond donating substituent in governing membrane effects were conducted, however no conclusive findings were made and further studies are required.

Chapter 4 - Conclusions and Future Directions

4.1 Conclusions

ILs have potential applications in a variety of different processes, however their apparent toxicity and the incomplete understanding of the underlying cellular mechanism/s compromises their widespread adoption. This thesis sought to address this problem by providing new insights into the mechanism/s by which ILs induce cell death and the structural features that promote cytotoxicity.

In **Chapter 2** the mechanism by which ILs induce cytotoxicity was investigated. The underlying hypothesis of this chapter was that ILs, particularly those with a delocalised positive charge and long *N*-alkyl chain, target the IMM to induce mitochondrial dysfunction and cell death. A library of ILs comprised of aromatic and aliphatic cationic headgroups substituted with butyl (C_4-ILs) or decyl (C_{10}-ILs) chains were prepared. The cytotoxicity of these ILs towards HeLa cells was assessed using the MTS assay. It was found that aromatic C_{10}-ILs were significantly more cytotoxic than their butyl or aliphatic counterparts. The cytotoxicity observed in MTS assays was found to correlate with their capacity to permeabilise tBLMs, which suggests cytotoxic ILs target membranes. To identify the target membrane the subcellular localisation of a fluorescent IL (**[C₄MeQuin][I]**) was tracked by fluorescence microscopy which showed the rapid accumulation of **[C₄MeQuin][I]** in mitochondria of HeLa cells. Next, the capacity of a series of C_4-ILs and C_{10}-ILs to induce mitochondrial dysfunction was assessed. When tested at the MTS IC_{50} concentrations, aromatic C_{10}-ILs produced a variety of cellular effects consistent with permeabilisation of the IMM. These effects include depolarisation of the IMM which then led to a reduction of ATP production, a decrease in OCR and the overproduction of ROS. These effects are associated with cell death, and therefore indicate aromatic C_{10}-ILs kill cells by targeting the IMM. ILs with short chains or aliphatic

headgroups failed to produce these effects which suggested these ILs produce cytotoxicity by an alternate mechanism.

In **Chapter 3**, a library of quinolinium and pyridinium based ILs were synthesised to investigate the influence of headgroup substitution on cytotoxicity. Firstly, ILs **12-17** containing C_{12} to C_{22} N-alkyl chain lengths were prepared through a quaternisation reaction between quinoline and alkyl bromides and their cytotoxicity was evaluated using the MTS cell viability assay. The most potent of the series, **14**, was found to effectively decrease the cell viability of HeLa cells with an IC_{50} of 5.39 ± 0.22 μM. Next, a series of substituted quinolinium-based ILs were synthesised. ILs substituted on the C-2 position were unable to be synthesised due to steric hindrance, hence ILs substituted on the C-3 position (**29-32**) were prepared. The MTS IC_{50} concentrations of **29-32** ranged from 3.80 ± 0.04 μM to 7.81 ± 0.97 μM, which is similar to the unsubstituted analogue **14** and suggests that headgroup substitution does not significantly affect cytotoxicity. The diversity of substituents included in the quinolinium series was limited and to develop a more robust SAR a pyridinium-based IL series (**35-44**) was prepared and assessed for cytotoxicity. From this series it was shown that substituent lipophilicity and electronic properties did not affect cytotoxicity whilst the hydrogen bond donating capacity of the substituent produced higher IC_{50} values. Thus, ILs **39** and **41**, which are substituted with -OH and -$CONH_2$, were shown to reduce HeLa cell viability with IC_{50} concentrations of 2-3 fold higher than other ILs in the series. The lower cytotoxicity of these ILs was attributed to their diminished capacity to disrupt and permeabilise lipid bilayers, as established in tBLM assays.

Combined, these studies provide new insights into the mechanism by which ILs induce toxicity and the SAR governing IL cytotoxicity. It is anticipated that these findings will assist

in the design of safe ILs that can be used as environmentally friendly alternatives to organic solvents in industrial processes and applications.

4.2 Future directions

Whilst this study has evaluated the cytotoxic properties of aromatic ILs, there are still some interesting aspects of cytotoxicity that remain unexplored. Firstly, further experiments are required to understand how hydrogen-bond donating substituents reduce the capacity of ILs to kill cells and disrupt lipid bilayers. The substituents are likely forming hydrogen bonds with phosphate groups in the lipid membrane, and molecular dynamics (MD) simulations could be used to provide some insights into the prevailing binding networks. Identification of the hydrogen bond acceptor from MD could then be confirmed by tBLM studies using structurally modified lipids. The reductions in cytotoxicity produced were relatively minor, and further reductions may be achieved through different substitution patterns (*ortho* or *para*), as well as di- or tri substitution. Access to some of these ILs will require new synthetic strategies as the corresponding substituted pyridines are not commercially available. Next, the mitochondrial actions of these ILs must be investigated to determine whether the trends observed in tBLM studies are also observed in mitochondrial assays such as JC-1.

Finally, the link between the mitochondrial effects observed in **Chapter 2** and cell death should be strengthened. The cell death pathway (apoptosis) induced by the ILs can be established through Annexin V/propidium iodide staining, which could be used to determine if ILs induce cell death through necrosis or apoptosis. To determine if ROS production is critical to cell death, co-treatment of cells with the IL and an antioxidant can be performed. Additionally, a larger variety of cell types should be used to provide a more robust evaluation of the cytotoxicity and selectivity of the ILs tested.

Chapter 5 - Experimental

5.1 Experimental procedures - Chemistry

Materials and general procedures

All chemical reagents, analytical grade solvents, **[C₄Py][Br]**, **[C₄MIM][Br]**, **[C₄TMA][Br]** and **[C₁₀TMA][Br]** were purchased from Sigma Aldrich (Castle Hill, NSW, Australia), Chem-Supply (Port Adelaide, SA, Australia) or Fluorochem (Derbyshire, United Kingdom). The purity of all test compounds was confirmed to be ≥ 95% by absolute quantitative ^{1}H nuclear magnetic resonance (qNMR) spectroscopy. Reactions were monitored by thin-layer chromatography (TLC) using silica gel 60 F254 plates. TLC plates were visualised with UV light and potassium permanganate TLC stain. ^{1}H and ^{13}C NMR spectra were acquired using an Agilent and/or Bruker 500 MHz spectrometer (500.13 MHz for ^{1}H and 125.76 MHz for ^{13}C) in deuterated chloroform (CDCl₃) unless otherwise specified. Melting point determination was preformed using Stuart automatic melting point. High- resolution mass spectroscopy (HRMS) was performed on an Agilent 6510 Accurate-Mass Q-TOF Mass Spectrometer equipped with an ESI source.

5.2 Ionic liquids

5.2.1 General Procedure for synthesis of Ionic liquids in Library 1

Where commercial analogues were unavailable, the desired compounds were synthesised by addition of the alkyl bromide (5 mmol) and appropriate heterocycle (Pyridine, Quinoline, Imidazole) (5 mmol) and heated at 140 °C for 24 hours. The reaction mixture was cooled to room temperature and the resulting crude products were purified by one of the following methods:

Method 1 – Crude solids were triturated with hexane. The solids were then dissolved in a minimum volume of chloroform, and diethyl ether was added dropwise until precipitation.

The resultant solid was then collected using vacuum filtration and used without further purification.

Method 2 – Crude oils were washed with hexane which was subsequently removed by decantation. The washed oil was then dissolved in a minimum volume of chloroform, and diethyl ether was added dropwise until the oil reformed. The ether layer was removed via decantation and the resultant oil was dried under reduced pressure.
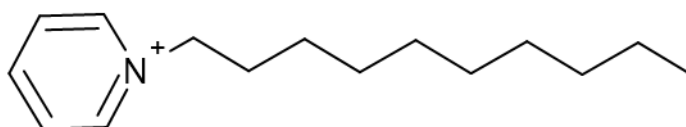
1-Decylpyridinium bromide ([C$_{10}$Py][Br]) was obtained as a yellow wax. Product formed by method 1. Yield = 90%. ^{1}H NMR (CDCl$_3$): δ 9.47 (d, J = 6 Hz, 2H), 8.51 (t, J = 8 Hz, 1H), 8.13 (t, J = 6.5 Hz, 2H), 5.03 (t, J = 7.5 Hz, 2H), 2.03 (pent, J = 8 Hz, 2H), 1.22-1.42 (m, 14H), 0.88 (t, J = 7.5 Hz, 3H). ^{13}C NMR (CDCl$_3$): δ 145.31, 144.99, 129.71, 128.56, 62.21, 31.90, 31.80, 29.44, 29.34, 29.21, 29.05, 26.07, 22.63, 14.09. HRMS (ESI) m/z [M]$^+$ calculated for C$_{15}$H$_{26}$N 220.2054; found 220.2061. Purity by Q-NMR = 96.3 %.
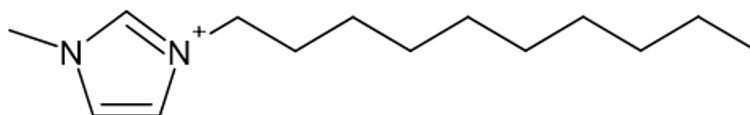
1-Decyl-3-methylimidazolium bromide ([C$_{10}$Mim][Br]) obtained as a colourless liquid. Product formed by method 1. Yield = 96 %. ^{1}H NMR (CDCl$_3$): δ 10.46 (s, 1H), 7.45 (t, J = 1.5 Hz, 1H), 7.32 (t, J = 2 Hz, 1H), 4.30 (t, J = 7.5 Hz, 2H), 4.12 (s, 3H), 1.86-1.94 (m, 2H), 1.18-1.37 (m, 14H), 0.86 (t, J = 7.5 Hz, 3H). ^{13}C NMR (CDCl$_3$): δ 137.36, 123.68, 121.51, 60.45, 36.75, 31.79, 30.29, 29.41, 29.33, 29.20, 28.96, 26.23, 22.61, 14.07. HRMS (ESI) *m/z* [M+H]$^+$ calculated for C$_{14}$H$_{27}$N 223.2163; found 223.2177. Purity by Q-NMR = 99.3 %.
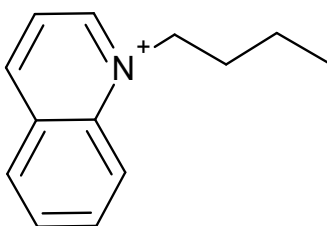
1-Butylquinolinium bromide ([C$_4$Quin][Br]) obtained as a brown solid. Product formed by method 2. Yield = 93 %. Mp = 159.3 °C. ^{1}H NMR (CDCl$_3$): δ 10.63 (d, J = 5.5 Hz, 1H), 9.00 (d, J = 8 Hz, 1H), 8.30-8.35 (m, 2H), 8.21 (t, J = 7.5 Hz, 2H), 7.97 (t, J = 8 Hz, 1H), 5.42 (t, J = 7.5 Hz, 2H), 2.10 (pentet, J = 8 Hz 2H), 1.57 (sext, J = 8 Hz, 2H), 1.01 (t, J = 7.5 Hz, 3H). ^{13}C NMR (CDCl$_3$): δ 150.48, 147.25, 137.67, 136.06, 131.18, 130.20, 129.71, 122.61, 118.40, 58.01, 32.26, 19.81, 13.63. HRMS (ESI) *m/z* [M]$^+$ calculated for C$_{13}$H$_{16}$BrN 186.1272; found 186.1280. Purity by Q-NMR = 95.1 %.
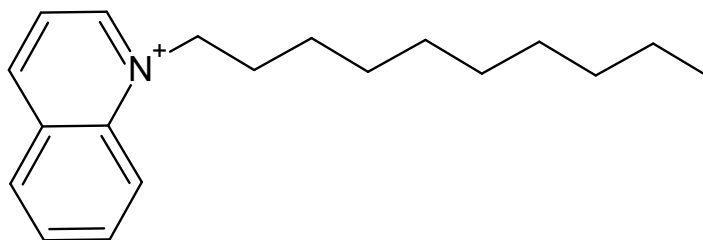
1-Decylquinolinium bromide ([C₁₀Quin][Br]) obtained as a brown solid. Product formed by method 2. Yield = 81 %. Mp = 53.4 °C. ^{1}H NMR (CDCl$_3$): δ 8.93 (dd, J =1.5, 4 Hz, 1H), 8.17 (d, J = 8.5 Hz, 1H), 8.12 (d, J = 8 Hz, 1H), 7.83 (d, J = 8 Hz, 1H), 7.73 (t, J = 8 Hz, 1H), 7.56 (t, J = 8 Hz, 1H), 7.41 (dd, J = 4.5, 8.5 Hz, 1H), 3.41 (t, J = 7 Hz, 2H), 1.85 (pent, J = 8 Hz, 2H), 1.20-1.34 (m, 14H), 0.88 (t, J = 7 Hz, 3H). ^{13}C NMR (CDCl$_3$): δ 150.59, 147.16, 137. 65, 135.94, 131.17, 130.15, 129.72, 122.72, 118.30, 58.25, 31.79, 30.41, 29.43, 29.33, 29.20, 29.15, 26.50, 22.62, 14.09. HRMS (ESI) *m/z* [M]$^+$ calculated for C$_{19}$H$_{28}$N 270.2211; found 270.2217. Purity by Q-NMR = 97.9 %.

5.2.2 Procedure for the synthesis of [C₄MeQuin][I]

Quinaldine (1 mmol) was heated with 1-Iodobutane (5 mmol) at 140 °C for 24 hours in a sealed pressure tube. The crude mixture was cooled to room temperature and the resulting solid was triturated with hexane and then diethyl ether to afford pure product.
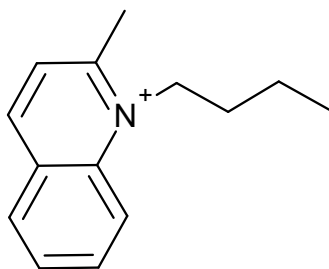
1-butyl-2-methylquinolinium iodide ([C₄MeQuin][I]) obtained as a black solid. Yield = 48 %. Mp = 156.9 °C. ^{1}H NMR (DMSO): δ 9.10 (d, J = 11 Hz, 1H), 8.58 (d, J = 10 Hz, 1H), 8.25-8.21 (m, 1H), 8.12 (d, J = 11 Hz, 1H), 7.99 (t, J = 9 Hz, 1H), 4.92 (t, J = 10 Hz, 2H), 3.12 (s, 3H), 1.89 (pentet, J = 10 Hz 2H), 1.59 (sext, J = 9 Hz, 2H), 0.99 (t, 9 Hz, 3H). ^{13}C NMR (CDCl₃): δ 161.06, 146.14, 138.75, 135.77, 131.09, 129.52, 128.73, 126.05, 119.42, 51.72, 30.47, 22.96, 19.77, 14.00. HRMS (ESI) m/z [M]$^+$ calculated for C₁₄H₁₈N 200.1428; found 200.1432. Purity by Q-NMR = 98.2 %.

5.2.3 Procedure for anion exchange

[C₁₀Mim][[BF₄] and **[C₁₀Mim][CH₃SO₃$^-$]** were prepared by a metathesis reaction between **[C₁₀Mim][Br]** and saturated solutions of sodium tetrafluoroborate (NaBF₄) and sodium trifluoromethanesulfonate (CF₃NaO₃S) respectively. The precipitate was collected with vacuum filtrations and washed then dried under vacuum.

5.3 General Procedure for synthesis of Ionic liquids with varying *N*-alkyl chain length of Quinolonium

The desired compounds were synthesised by addition of the appropriate 1-Bromoalkyl (5 mmol) and the commercially available quinoline heterocycle (5 mmol) and were heated at 140 °C for 24-96 hours. The crude solid was cooled to room temperature and triturated with hexane. The solids were then dissolved in a minimum volume of chloroform, and diethyl ether was added dropwise until precipitation formed. The resultant solid was then collected using

vacuum filtration and used without further purification.
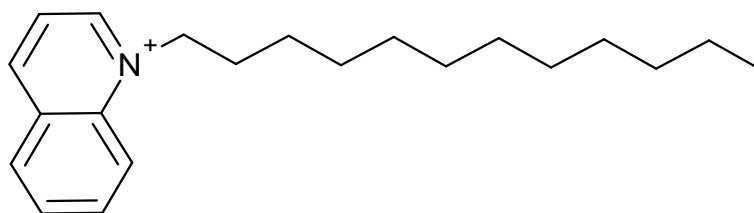
1-Dodecylquinolinium bromide (12) obtained as a brown solid. Yield = 65 %. Mp = 86.5 °C.

^{1}H NMR (CDCl$_3$): δ 10.52-10.53 (m, 1H), 9.06 (d, J =10.5 Hz, 1H), 8.32-8.36 (m, 2H), 8.18-8.23 (m, 2H), 7.97 (t, J = 9.5 Hz, 1H), 5.39 (t, J = 9.5 Hz, 2H), 2.10 (pent, J = 10 Hz, 2H), 1.51 (pent, J = 10 Hz, 2H), 1.22-1.35 (m, 16H), 0.86 (t, J = 9 Hz, 3H). ^{13}C NMR (CDCl$_3$): δ 150.73, 147.04, 137.68, 135.94, 131.14, 130.16, 130.01, 122.73, 118.28, 58.26, 31.88, 30.44, 29.57, 29.50, 29.36, 29.31, 29.17, 26.53, 22.67, 14.11. HRMS (ESI) m/z [M]$^+$ calculated for C$_{21}$H$_{32}$N 298.4849; found 298.4851. Purity by Q-NMR = 95.9 %.
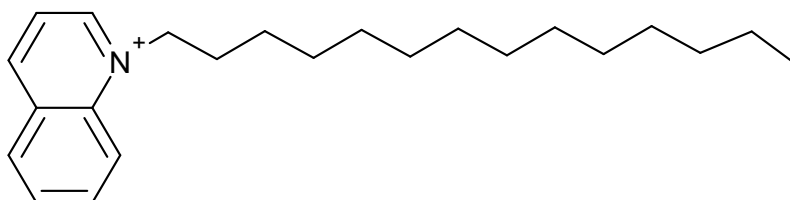
1-tetradecylquinolinium bromide (13) obtained as a brown solid. Yield = 87%. Mp = 107.1 °C. ^{1}H NMR (CDCl$_3$): δ 10.44 (d, J =6.5 Hz, 1H), 9.15 (d, J = 10 Hz, 1H), 8.38 (d, J = 11 Hz, 2H), 8.17-8.22 (m, 2H), 7.94 (t, J = 10 Hz, 1H), 5.38 (t, J = 10 Hz, 2H), 2.03-2.11 (m, 2H), 1.45-1.51 (m, 2H), 1.18-1.32 (m, 20H), 0.84 (t, J = 9 Hz, 3H). ^{13}C NMR (CDCl$_3$): δ 150.52, 147.24, 137.65, 135.99, 131.20, 130.16, 130.0, 129.71, 122.65, 118.32, 58.24, 31.89, 30.43, 29.64, 29.61, 29.57, 29.50, 29.35, 29.32, 29.17, 26.51, 22.66, 14.10. HRMS (ESI) m/z [M]$^+$ calculated for C$_{23}$H$_{36}$N 326.5381; found 326.5378. Purity by Q-NMR = 98.5 %.
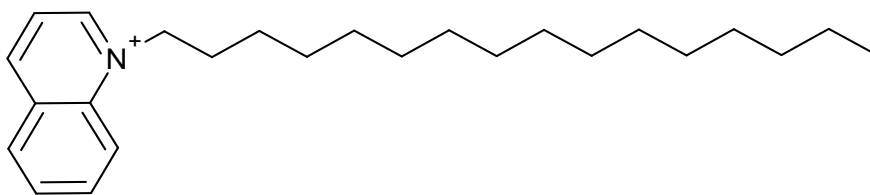
1-hexadecylquinolinium bromide (14) obtained as a purple solid. Yield = 70 %. Mp = 109.2 °C. ^{1}H NMR (CDCl$_3$): δ 10.40 (d, J =7 Hz, 1H), 9.18 (d, J = 10.5 Hz, 1H), 8.38 (d, J = 11 Hz, 2H), 8.15-8.21 (m, 2H), 7.93 (t, J = 9 Hz, 1H), 5.36 (t, J = 9.5 Hz, 2H), 2.06 (pent, J = 10 Hz, 2H), 1.46 (pent, J = 10 Hz, 2H), 1.17-1.29 (m, 24H), 0.82 (t, J = 8.5 Hz, 3H). ^{13}C NMR (CDCl$_3$): δ 150.40, 147.34, 137.64, 136.02, 131.23, 130.17, 130.02, 129.69, 122.60, 118.33, 58.23, 31.88, 30.42, 29.65, 29.62, 29.60, 29.56, 29.50, 29.35, 29.32, 29.16, 26.50, 22.65, 14.10. HRMS (ESI) m/z [M]$^+$ calculated for C$_{25}$H$_{40}$N 354.5913; found 354.5947. Purity by Q-NMR = 97.3 %.
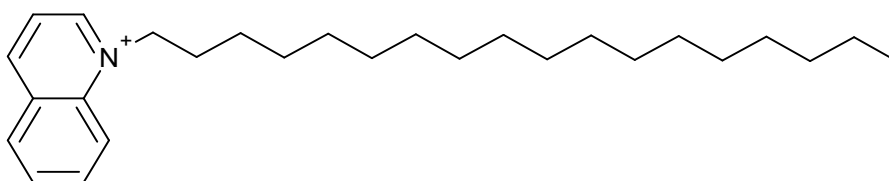
1-octadecylquinolinium bromide (15) obtained as a purple solid. Yield = 57 %. Mp = 113.8 °C. ^{1}H NMR (CDCl$_3$): δ 10.44 (d, J =7 Hz, 1H), 9.15 (d, J = 10.5 Hz, 1H), 8.37 (d, J = 10.5 Hz, 2H), 8.22-8.17 (m, 2H), 7.94 (t, J = 9.5 Hz, 1H), 5.38 (t, J = 9.5 Hz, 2H), 2.03-2.11(m, 2H), 1.43-1.51 (m, 2H), 1.18-1.32 (m, 28H), 0.84 (t, J = 8.5 Hz, 3H). ^{13}C NMR (CDCl$_3$): δ 150.52, 147.23, 137. 65, 135.97, 131.19, 130.15, 130.01, 129.71, 122.66, 118.33, 58.23, 31.90, 30.43, 29.68, 29.64, 29.62, 29.58, 29.51, 29.36, 29.34, 29.17, 26.51, 22.67, 14.11. HRMS (ESI) m/z [M]$^+$ calculated for C$_{27}$H$_{44}$N 382.6444; found 382.6460. Purity by Q-NMR = 95.7 %.
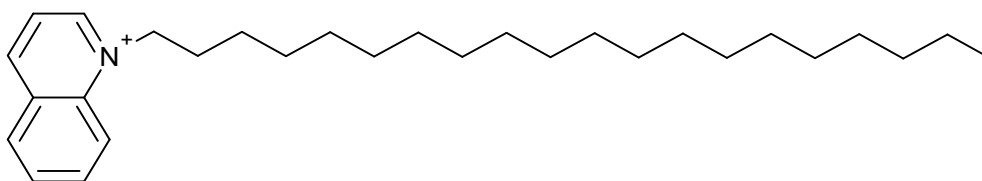
1-eicosylquinolinium bromide (16) obtained as a brown solid. Yield = 74 %. Mp = 114.6 °C.

^{1}H NMR (CDCl$_3$): δ 10.51 (d, J =6 Hz, 1H), 9.09 (d, J = 10.5 Hz, 1H), 8.33- 8.37 (m, 2H), 8.18- 8.22 (m, 2H), 7.96 (t, J= 9.5 Hz, 1H), 5.39 (t, J = 9.5 Hz, 2H), 2.09 (pent, J = 10 Hz, 2H), 1.46-1.53 (m, 2H), 1.21-1.34 (m, 32 H), 0.86 (t, J = 14 Hz, 3H). ^{13}C NMR (CDCl$_3$): δ 150.77, 147.01, 137.67, 135.90, 131.13, 130.13, 130.00, 122.75, 118.28, 58.24, 31.92, 30.45, 29.65, 29.64, 29.59, 29.52, 29.37, 29.36, 29.18, 26.53, 22.68, 14.12. HRMS (ESI) *m/z* [M]$^+$ calculated for C$_{29}$H$_{48}$N 410.6976; found 410.6971. Purity by Q-NMR = 99.2 %.
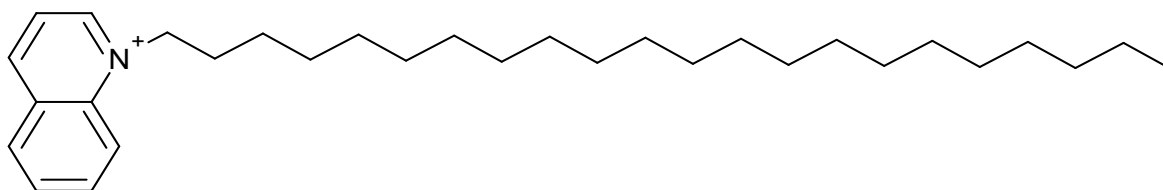
1-docosylquinolinium bromide (17) obtained as a brown solid. Yield = 57 %. Mp = 105 °C.

^{1}H NMR (CDCl$_3$): δ 10.49 (d, J =7 Hz, 1H), 8.13 (d, J = 10 Hz, 1H), 8.35- 8.39 (m, 2H), 8.17- 8.22 (m, 2H), 7.95 (t, J = 10 Hz, 1H), 5.39 (t, J = 9.5 Hz, 2H), 2.08 (pent, J = 10 Hz, 2H), 1.48 (pent, J = 10 Hz, 2H), 1.20- 1.33 (m, 36 H), 0.85 (t, J = 9 Hz, 3H). ^{13}C NMR (CDCl$_3$): δ 150.63, 147.14, 137. 67, 135.94, 131.16, 130.14, 130.00, 122.68, 118.32, 58.23, 31.91, 30.45, 29.70, 29.64, 29.59, 29.52, 29.37, 29.35, 29.18, 26.52, 22.68, 14.11. HRMS (ESI) *m/z* [M]$^+$ calculated for C$_{31}$H$_{52}$N 438.7507; found 438.7504. Purity by Q-NMR = 100.0 %.

5.4 Procedure for Finkelstein reaction

Sodium iodide (1.28 g, 8.52 mmol) was dissolved in 10 mL of dry acetone and the reaction mixture was stirred for 10 minutes. 1-Bromohexadecane (2 mL, 6.55 mmol) was then added dropwise and then the solution was refluxed for 3 hours. After the reaction mixture was allowed to cool to room temperature, diethyl ether (20 mL) was added, and the suspension was filtered. The solvent was removed under reduced pressure, the resulting oil solution was washed with 2% NaOH (2 × 15 mL), water (15 mL) and saturated sodium chloride (15 mL). The organic layers were combined and dried over MgSO4, and the solvent was removed under reduced pressure to afford pure product.
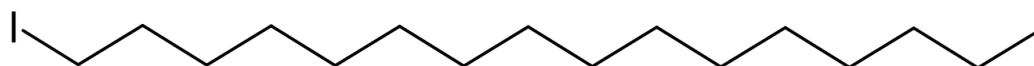
1-iodohexadecane (27) obtained as a white solid. Yield = 94 %. Mp = 22 °C. ^{1}H NMR (CDCl$_3$): δ 3.19 (t, J = 9 Hz, 2H), 1.82 (pent, J = 9 Hz, 2H), 1.26-1.40 (m, 26H), 0.88 (t, J = 9 Hz, 3H). ^{13}C NMR (CDCl$_3$): δ 34.51, 33.34, 32.21, 30.02, 29.93, 29.82, 29.75, 29.55, 29.14, 28.27, 27.26, 23.18, 14.54. HRMS (ESI) m/z [M]$^+$ calculated for C$_{16}$H$_{33}$I 352.3377; found 352.3375 Purity by Q-NMR = 98.5 %.

5.5 General Procedure for synthesis of Quinolonium Ionic liquids with sustituents

A solution of 1-Iodohexadecane (5 mmol) and the commercially available appropriate substituted quinoline heterocycles (5 mmol) in acetonitrile were heated at 140 °C for 24-96 hours in a screw cap pressure tube. The crude solid was cooled to room temperature and triturated with hexane. The solid was then dissolved in a minimum volume of chloroform, and diethyl ether was added dropwise until precipitation formed. The resultant solid was then collected using vacuum filtration and used without further purification.
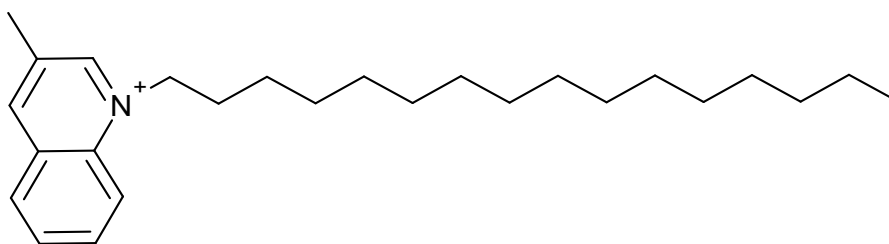
3-methyl-1-hexadecylquinolinium iodide (29) obtained as a yellow solid. Yield = 82 %. Mp

= 144.5 °C. ^{1}H NMR (CDCl$_3$): δ 10.33 (s, 1H), 8.75 (s, 1H), 8.25 (d, J = 11 Hz, 1H), 8.20 (d,

J = 10 Hz, 1H), 8.09- 8.13 (m, 1H), 7.90 (t, J = 9.5 Hz, 1H), 5.26 (t, J = 9.5 Hz, 2H), 2.82 (s,

3H), 2.10 (pent, J = 10 Hz, 2H), 1.51 (pent, J =10 Hz, 2H), 1.31- 1.39 (m, 2 H), 1.22-1.30 (m,

22 H), 0.86 (t, J = 9 Hz, 3H). ^{13}C NMR (CDCl$_3$): δ 150.81, 145.88, 136.12, 134.78, 133.39,

130.23, 130.00, 129.87, 117.92, 57.99, 31.92, 30.35, 29.69, 29.68, 29.66, 29.64, 26.61, 29.53,

29.38, 29.36, 29.16, 26.55, 22.69, 18.68, 14.13. HRMS (ESI) *m/z* [M]$^{+}$ calculated for C$_{26}$H$_{42}$N

368.6178; found 368.6164. Purity by Q-NMR = 97.9 %.

3-(trifluoromethyl)-1-hexadecylqinolinium iodide (30) obtained as an orange solid. Yield =

13 %. Mp = 130.7 °C. ^{1}H NMR (CDCl$_3$): δ 10.49 (s, 1H), 9.36 (s, 1H), 8.59 (d, J = 11 Hz, 1H),

8.53 (d, J = 10 Hz, 1H), 8.39- 8.43 (m, 1H), 8.12 (t, J = 9.5 Hz, 1H), 5.56 (t, J = 9.5 Hz, 2H),

2.14 (pent, J = 10 Hz, 2H), 1.53 (pent, J =10 Hz, 2H), 1.31- 1.38 (m, 2 H), 1.23-1.29 (m, 22

H), 0.87 (t, J = 9 Hz, 3H). ^{13}C NMR (CDCl$_3$): δ 146.49, 144.40, 139. 09, 138.76, 132.20,

131.71, 129.19, 125.19, 124.82, 122.71, 119.98, 119.33, 59.79, 31.93, 30.53, 29.70, 29.68,

29.64, 29.60, 29.52, 29.36, 29.14, 26.52, 22.70, 14.13. HRMS (ESI) *m/z* [M]$^{+}$ calculated for

C$_{26}$H$_{39}$N 422.5892; found 422.5880. Purity by Q-NMR = 99.8 %.

3-Chloro-1-hexadecylquinolonium iodide (31) obtained as a yellow solid. Yield = 54 %. Mp = 154.2 °C. ^{1}H NMR (CDCl$_3$): δ 10.40 (s, 1H), 9.06 (s, 1H), 8.42 (d, J = 11 Hz, 1H), 8.32 (d, J = 10 Hz, 1H), 8.19- 8.24 (m, 1H), 7.99 (t, J = 9.5 Hz, 1H), 5.40 (t, J = 9.5 Hz, 2H), 2.12 (pent, J = 10 Hz, 2H), 1.52 (pent, J =10 Hz, 2H), 1.31- 1.37 (m, 2 H), 1.23-1.30 (m, 22 H), 0.87 (t, J = 9 Hz, 3H). ^{13}C NMR (CDCl$_3$): δ 148.91, 145.09, 136.49, 136.16, 131.18, 130.38, 130.00, 129.12, 118.74, 58.93, 31.93, 30.40, 29.70, 29.60, 29.53, 29.37, 29.16, 26.53, 22.69, 14.13. HRMS (ESI) m/z [M]$^+$ calculated for C$_{25}$H$_{39}$N 389.0363; found 389.0399. Purity by Q-NMR = 99.6 %.
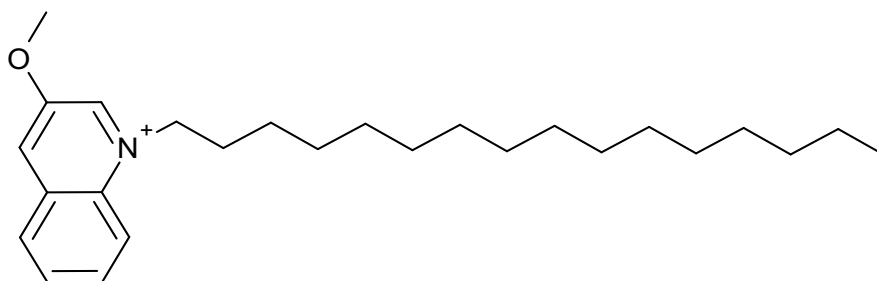
1-hexadecyl-3-methoxyquinolinium iodide (32) obtained as a yellow solid. Yield = 85 %. Mp = 102.3 °C. ^{1}H NMR (CDCl$_3$): δ 9.90 (d, J = 3.5 Hz, 1H), 8.71 (d, J = 3 Hz, 1H), 8.36 (d, J = 9.5 Hz, 1H), 8.21 (d, J = 11.5 Hz, 1H), 7.94-7.98 (m, 1H), 7.83 (t, J = 9.5 Hz, 1H), 5.33 (t, J = 9.5 Hz, 2H), 4.20 (s, 3H), 2.07 (pent, J = 10 Hz, 2H), 1.48 (pent, J = 10 Hz, 2H), 1.20-1.34 (m, 24H), 0.85 (t, J = 9 Hz, 3H), ^{13}C NMR (CDCl$_3$): δ 153.04, 141.16, 133.47, 132.92, 130.85, 130.30, 130.08, 126.74, 117.87, 58.95, 58.57, 31.91, 30.41, 29.67, 29.54, 29.62, 29.59, 29.53, 29.36, 29.34, 29.15, 26.41, 22.68, 14.12. HRMS (ESI) m/z [M]$^+$ calculated for C$_{26}$H$_{42}$NO 384.6172; found 384.6162. Purity by Q-NMR = 97.1 %.

5.6 Procedure for synthesis of Pyridinium Ionic liquids

A solution of 1-Bromohexadecane (5 mmol) and the pyridine heterocycle (5 mmol) in acetonitrile were refluxed for 24 hours. The reaction mixture was then cooled to room temperature and the resulting crude solid was triturated with hexane and diethyl ether. The resultant solid was then collected using vacuum filtration and used without further purification.
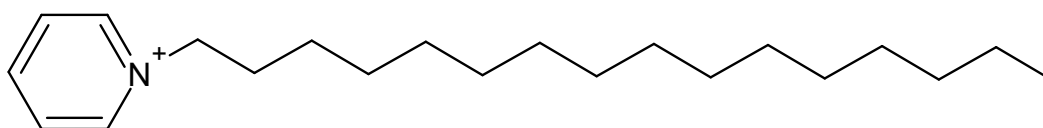
1-hexadecylpyridinium bromide (34) obtained as a white solid. Yield = 86 %. Mp = 105.1 °C. ^{1}H NMR (CDCl$_3$) δ 9.47 (d, J= 7 Hz, 2H), 8.51 (t, J= 9.5 Hz, 1H), 8.13 (t, J= 9 Hz, 2H), 5.00 (t, J= 9 Hz, 2H), 2.03 (quin, J= 9 Hz, 2H), 1.36-1.22 (m, 26H), 0.86 (t, J= 9 Hz, 3H). ^{13}C NMR (125.76 Hz) δ 145.14, 145.08, 128.43, 62.28, 32.03, 31.92, 29.69, 29.66, 29.60, 29.36, 29.07, 26.09, 22.69, 14.12; HRMS (ESI) m/z [M]$^+$ calculated for C$_{21}$H$_{38}$N 304.5326; found 304.5302. Purity by Q-NMR = 99.1 %.

5.7 General Procedure for the synthesis of substituted Pyridinium Ionic liquids

A solution of 1-Iodohexadecane (5 mmol) and the appropriate substituted pyridine heterocycle (5 mmol) in acetonitrile were refluxed for 24 hours. The reaction mixture was cooled to room temperature and the resulting crude products were purified by one of the following methods:

Method 1 –The crude solid were triturated with hexane and diethyl ether. The resultant solid was then collected using vacuum filtration and used without further purification.

Method 2 – The crude solid were triturated with hexane and ethyl acetate then the resulting solids was dissolved in a minimum volume of chloroform, and diethyl ether was added dropwise until precipitation formed. The solid was then collected using vacuum filtration
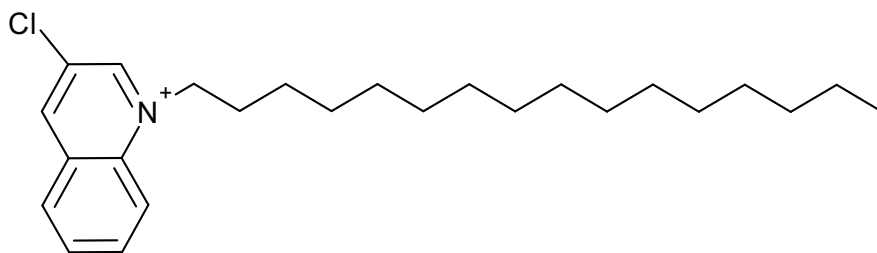
and used without further purification.

Method 3 – The crude solid were triturated with chloroform and the resultant solid was then collected using vacuum filtration and used without further purification.
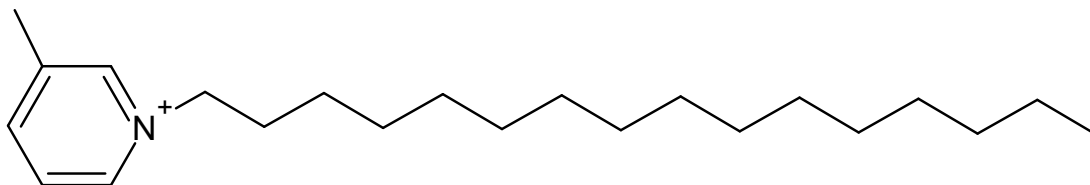
1-hexadecyl-3-methylpyridinium iodide (35) obtained as a purple solid. Yield = 94 %. Mp = 90.3 °C. Product purified by method 1. ^{1}H NMR (CDCl$_3$) δ 9.28 (s, 1H), 9.12 (d, J= 7.5 Hz, 1H), 8.27 (d, J= 10 Hz, 1H), 8.01 (t, J= 7.5 Hz, 1H), 4.88 (t, J= 9.5 Hz, 2H), 2.65 (s, 3H), 2.06-1.99 (m, 2H), 1.39-1.22 (m, 26H), 0.86 (t, J= 9 Hz, 3H). ^{13}C NMR (125.76 Hz) δ 145.83, 144.41, 142.01, 139.73, 127.83, 62.03, 31.92, 31.87, 29.70, 29.66, 29.61, 29.53, 29.36, 29.07, 26.08, 22.69, 18.84, 14.13; HRMS (ESI) m/z [M]$^+$ calculated for C$_{22}$H$_{40}$N 318.5592; found 318.5557. Purity by Q-NMR = 99.1 %.
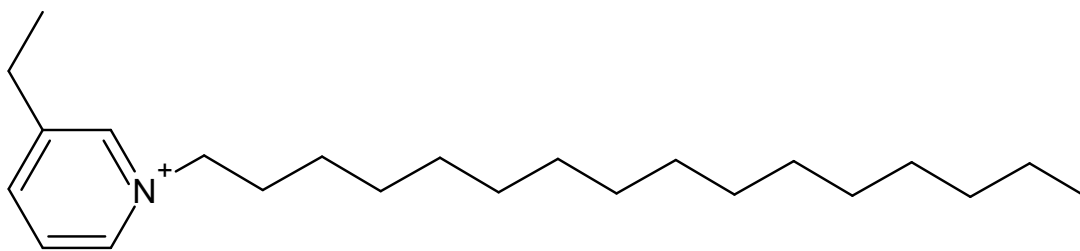
3-Ethyl-1-hexadecylpyridinium iodide (36) obtained as a brown solid. Yield = 82 %. Mp = 74.2 °C. Product purified by method 1. ^{1}H NMR (CDCl$_3$) δ 9.19 (s, 1H), 9.16 (d, *J*= 7.5 Hz, 1H), 8.27 (d, *J*= 10 Hz, 1H), 8.03 (t, *J*= 7.5 Hz, 1H), 4.93 (t, *J*= 9.5 Hz, 2H), 2.98 (q, *J*= 9.5 Hz, 2H), 2.04 (quin, *J*= 9.5 Hz, 2H), 1.40 (t, *J*= 9.5 Hz, 3H), 1.36-1.23 (m, 26H), 0.87 (t, *J*= 9 Hz, 3H). ^{13}C NMR (125.76 Hz) δ 145.51, 144.51, 143.82, 142.23, 128.01, 62.26, 31.97, 31.93, 29.70, 29.66, 29.61, 29.52, 29.36, 29.07, 26.12, 22.69, 14.41, 14.13; HRMS (ESI) *m/z* [M]$^+$ calculated for C$_{23}$H$_{42}$N 332.5857; found 332.5814. Purity by Q-NMR = 102.4 %.
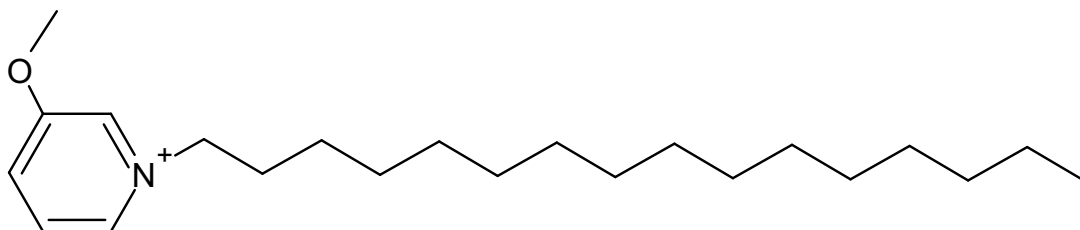
1-hexadecyl-3-methoxypyridinium iodide (37) obtained as a yellow solid. Yield = 74 %. Mp = 99.8 °C. Product purified by method 1. ^{1}H NMR (CDCl$_3$) δ 9.24 (s, 1H), 8.80-8.78 (m, 1H), 8.01-7.96 (m, 2H), 4.98 (t, *J*= 9.5 Hz, 2H), 4.18 (s, 3H), 2.03 (quin, *J*= 9 Hz, 2H), 1.40-1.22 (m, 26H), 0.86 (t, *J*= 9 Hz, 3H). ^{13}C NMR (125.76 Hz) δ 158.81, 137.11, 131.57, 131.49, 128.48, 62.44, 59.00, 32.08, 31.92, 29.70, 29.66, 29.61, 29.54, 29.38, 29.36, 29.10, 26.01, 22.69, 14.13; HRMS (ESI) *m/z* [M]$^+$ calculated for C$_{22}$H$_{40}$NO 334.5586; found 334.5570. Purity by Q-NMR = 100.8 %.
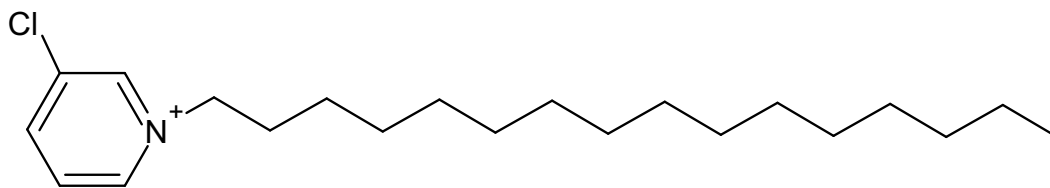
3-chloro-1-hexadecylpyridinium bromide (38) obtained as a gold solid. Yield = 64 %. Mp =

103.6 °C. Product purified by method 1. ^{1}H NMR (CDCl$_3$) δ 9.50 (d, J= 7.5 Hz, 1H), 9.35 (s,

1H), 8.50-8.47 (m, 1H), 8.26-8.22 (m, 1H), 5.01 (t, J= 9.5 Hz, 2H), 2.05 (quin, J= 9 Hz, 2H),

1.42-1.23 (m, 26H), 0.86 (t, J= 9Hz, 3H). ^{13}C NMR (125.76 Hz) δ 145.28, 143.91, 143.39,

135.85, 129.36, 62.76, 31.93, 31.76, 29.70, 29.66, 29.61, 29.52, 29.36, 29.06, 26.03, 22.69,

14.13; HRMS (ESI) m/z [M]$^+$ calculated for C$_{21}$H$_{37}$NCl 338.9773; found 338.9752. Purity by

Q-NMR = 100.4 %.
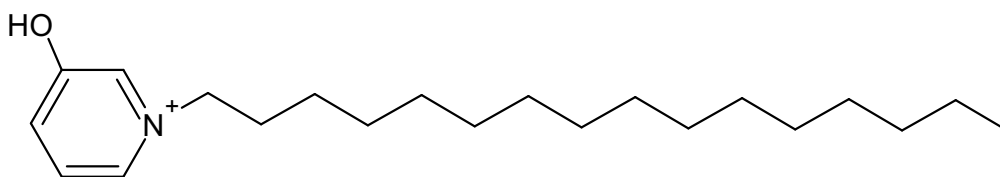
1-hexadecyl-3-hydroxypyridinium iodide (39) obtained as a white solid. Yield = 80 %. Mp

= 93 °C. Product purified by method 2. ^{1}H NMR (CDCl$_3$): δ 8.93 (s, 1H), 8.32 (d, J = 7.5 Hz,

1H), 8.24 (dd, J = 2, 11 Hz, 1H), 7.83 (dd, J = 12, 15.5 Hz, 1H), 4.62 (t, J = 9.5 Hz, 2H), 2.01

(pent, J = 10 Hz, 2H), 1.34-1.29 (m, 4H), 1.23-1.29 (m, 22 H), 0.86 (t, J = 9 Hz, 3H). ^{13}C NMR

(CDCl$_3$): δ 157.70, 134.85, 132. 71, 128.53, 62.65, 31.92, 31.52, 29.70, 29.66, 29.61, 29.51,

29.36, 29.00, 26.11, 22.69, 14.13. HRMS (ESI) m/z [M]$^+$ calculated for C$_{21}$H$_{38}$NO 320.5320;

found 320.5353. Purity by Q-NMR = 100.6 %.

3-(aminocarbonyl)-1-hexadecylpyridinium iodide (41) obtained as a yellow solid. Yield = 82 %. Mp = 70.2 °C. Product purified by method 3. ^{1}H NMR (DMSO) δ 9.47 (br. s, 1H), 9.19 (d, J= 7.5 Hz, 1H), 8.92 (d, J= 10 Hz, 1H), 8.53 (br. s, 1H), 8.28-8.25 (m, 1H), 8.16 (br. s, 1H), 4.64 (t, J= 9.5 Hz, 2H), 1.95-1.92 (m, 2H), 1.28-1.23 (m, 26H), 0.85 (t, J= 9 Hz, 3H). ^{13}C NMR (125.76 Hz, DMSO) δ 163.31, 146.81, 145.24, 143.72, 134.37, 128.33, 61.66, 31.75, 31.11, 29.51, 29.46, 29.38, 29.23, 29.16, 28.86, 25.87, 22.56, 14.43; HRMS (ESI) m/z [M]$^+$ calculated for $C_{22}H_{39}N_2O$ 347.5573; found 347.5561. Purity by Q-NMR = 101.3 %.
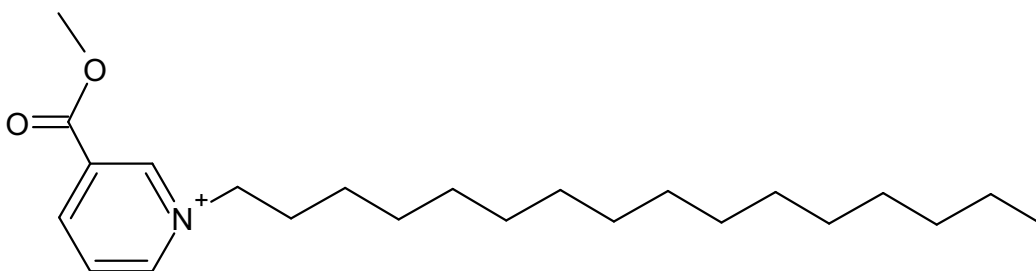
**3-(methoxycarbonyl)-1-hexadecylpyridinium iodide (42)** obtained as a yellow solid. Yield = 26 %. Mp = 70.2 °C. Product purified by method 1. ^{1}H NMR (CDCl$_3$): δ 9.87 (d, J =7.5 Hz, 1H), 9.43 (s, 1H), 8.96 (d, J = 10 Hz, 1H), 8.40 (t, J = 5 Hz, 1H), 5.06 (t, J =9.5 Hz, 2H), 4.05 (s, 3H), 2.08 (pent, J = 10 Hz, 2H), 1.32-1.42 (m, 4H), 1.22-1.31 (m, 22 H), 0.85 (t, J = 9 Hz, 3H). ^{13}C NMR (CDCl$_3$): δ 161.48, 148.69, 145.29, 145.06, 130.50, 129.27, 63.12, 54.02, 31.91, 31.68, 29.69, 29.65, 29.59, 29.51, 29.35, 29.05, 26.04, 22.68, 14.12. HRMS (ESI) m/z [M]$^+$ calculated for $C_{23}H_{40}NO_2$ 362.5687; found 362.5654. Purity by Q-NMR = 97.5 %.
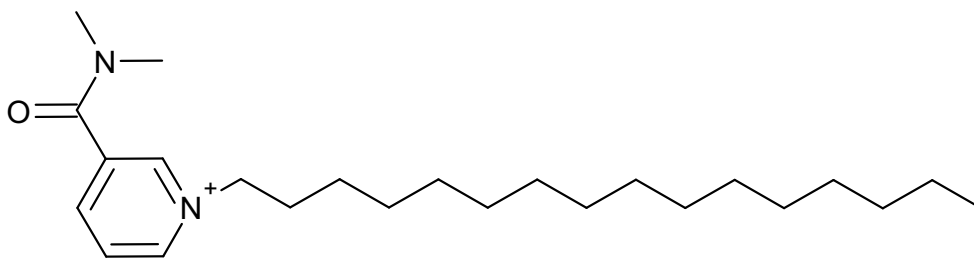
**3-[(dimethylamino)carbonyl]-1-hexadecylpyridinium iodide (43)** obtained as a yellow solid. Yield = 91 %. Mp = 83.4 °C. Product purified by method 1. ^{1}H NMR (CDCl$_3$) δ 9.36 (d, J = 7.5 Hz, 1H), 9.10 (s, 1H), 8.51 (t, J = 10 Hz, 1H), 8.21-8.24 (m, 1H), 4.96 (t, J = 9.5 Hz, 2H), 3.21 (s, 3H), 3.14 (s, 3H), 2.04 (quin, J = 10 Hz, 2H), 1.42-1.24 (m, 26H), 0.87 (t, J = 9 Hz, 3H). ^{13}C NMR (125.76 Hz) δ 145.14, 145.08, 128.43, 62.28, 32.03, 31.92, 29.69, 29.66, 29.60, 29.36, 29.07, 26.09, 22.69, 14.12; HRMS (ESI) m/z [M]$^+$ calculated for C$_{24}$H$_{43}$N$_2$O 375.6105; found 375.6124. Purity by Q-NMR = 100.7 %.

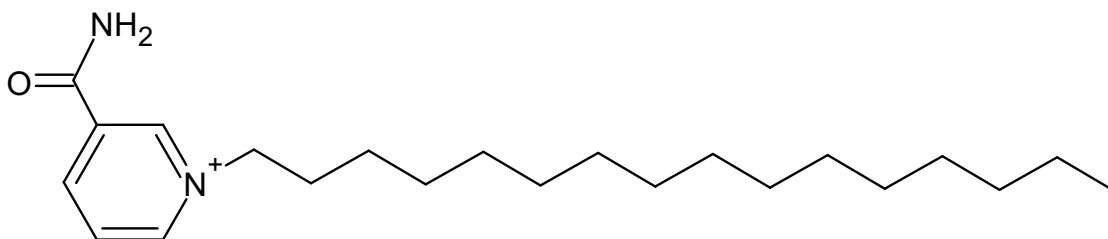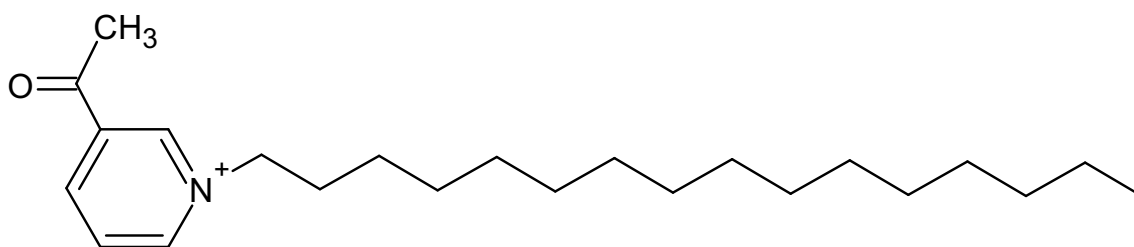**3-acetyl-1-hexadecylpyridinium iodide** obtained as a yellow solid. Yield = 53 %. Mp = 86.1 °C. Product purified by method 1. ^{1}H NMR (CDCl$_3$) δ 9.85 (s, 1H), 9.58 (d, J= 7.5 Hz, 1H), 9.02 (d, J= 10 Hz, 1H), 8.03 (t, J= 7.5 Hz, 1H), 5.09 (t, J= 9.5 Hz, 2H), 2.91 (s, 3H), 2.07 (quin, J= 10 Hz, 2H), 1.42-1.22 (m, 26H), 0.86 (t, J= 9 Hz, 3H). ^{13}C NMR (125.76 Hz) δ 192.63, 147.68, 145.03, 144.26, 135.66, 128.92, 62.73, 31.92, 29.70, 29.66, 29.61, 29.53, 29.37, 29.07, 28.50, 26.08, 22.69, 14.13; HRMS (ESI) m/z [M]$^+$ calculated for C$_{23}$H$_{40}$NO 346.5693; found 346.5680. Purity by Q-NMR = 99.3 %.
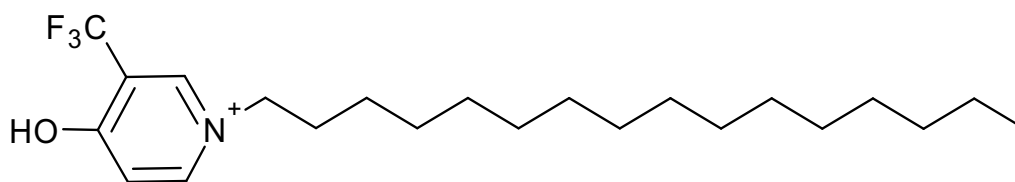
3-(trifluoromethyl)-1-hexadecylqinolinium iodide obtained as an orange solid. Yield = 13 %. Mp = 130.7 °C. Product purified by method 1. ^{1}H NMR (CDCl$_3$): δ 10.49 (s, 1H), 9.36 (s, 1H), 8.59 (d, J = 11 Hz, 1H), 8.53 (d, J = 10 Hz, 1H), 8.39- 8.43 (m, 1H), 8.12 (t, J = 9.5 Hz, 1H), 5.56 (t, J = 9.5 Hz, 2H), 2.14 (pent, J = 10 Hz, 2H), 1.53 (pent, J =10 Hz, 2H), 1.31- 1.38 (m, 2 H), 1.23-1.29 (m, 22 H), 0.87 (t, J = 9 Hz, 3H). ^{13}C NMR (CDCl$_3$): δ 146.49, 144.40, 139. 09, 138.76, 132.20, 131.71, 129.19, 125.19, 124.82, 122.71, 119.98, 119.33, 59.79, 31.93, 30.53, 29.70, 29.68, 29.64, 29.60, 29.52, 29.36, 29.14, 26.52, 22.70, 14.13. HRMS (ESI) *m/z* [M]$^+$ calculated for C$_{26}$H$_{39}$N 422.5892; found 422.5880. Purity by Q-NMR = 99.8 %.

5.8 Procedure for synthesis of 3-(trifluoromethyl)-1-hexadecylpyridinium iodide

A mixture of 1-Iodohexadecane (5 mmol) and 3-(trifluoromethyl)pyridine (5 mmol) in acetonitrile were heated at 100 °C for 24 hours in a screw top pressure tube. The reaction mixture was cooled to room temperature and the crude solid were triturated with hexane and diethyl ether. The resultant solid was then collected using vacuum filtration and used without further purification.
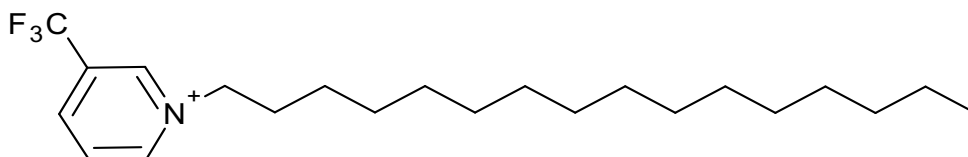
3-(trifluoromethyl)-1-hexadecylpyridinium iodide (40) obtained as a yellow solid. Yield = 75 %. Mp = 111.1 °C. ^{1}H NMR (CDCl$_3$) δ 10.10 (d, J= 7.5 Hz, 1H), 9.35 (s, 1H), 8.70 (d, J= 10 Hz, 1H), 8.48 (t, J= 9.5 Hz, 1H), 5.15 (t, J= 9.5 Hz, 2H), 2.11 (pent, J= 9.5 Hz, 2H), 1.47-1.24 (m, 26H), 0.87 (t, J= 9 Hz, 3H). ^{13}C NMR (125.76 Hz) δ 149.21, 142.19, 141.85, 131.16, 130.79, 130.02, 122.36, 119.63, 63.42, 31.92, 31.79, 29.70, 29.66, 29.60, 29.51, 29.26, 29.34, 29.03, 26.03, 22.69, 14.12; HRMS (ESI) m/z [M]$^+$ calculated for C$_{22}$H$_{37}$NF$_3$ 372.5305; found 372.5317. Purity by Q-NMR = 101.0 %.

5.9 Experimental procedures - Biology

General cell culture and cell-based assays

HeLa cervical cancer cells were provided by Professor Michael Murray from the University of Sydney and grown at 37 °C in a humidified atmosphere of 5% CO_2 in air in DMEM supplemented with 10% fetal bovine serum (Invitrogen, Life Technologies, Victoria, Australia). Confluent cells (80 – 90%) were harvested using Trypsin/EDTA after washing with PBS. Cells were treated with various concentrations of the test compounds in media (for C_4-ILs) or in media with 0.1% DMSO (for C_{10}-ILs); matched control cells were treated media only or media with 0.1% DMSO. Dulbecco's Modified Eagle Medium (DMEM), phosphate-buffered saline (PBS), DMSO and general biochemical were purchased from Sigma-Aldrich (Castle Hill, NSW, Australia). Fetal bovine serum (FBS) and trypsin/EDTA were purchased from Invitrogen, Life Technologies (Victoria, Australia).

Cell viability assay

The ability of ILs to decrease the cell viability in HeLa cervical cancer cells was assessed using the 3-(4,5-dimethylthiazol-2-yl)-5-(3-carboxymethoxyphenyl)-2-(4-sulfophenyl)-2H-tetrazolium (MTS) *in vitro* cytotoxicity assay. Cells (HeLa and BEAS-2B) were seeded in 96-well plates (5 x 10^3 cells per well) and allowed to adhere overnight. The cells were then treated with various concentrations of ILs for 48 h. Control cells were treated with DMEM supplemented with 10% FBS and 0.1% DMSO. The cell viability was determined using the CellTiter 96® AQueous One Solution Cell Proliferation Assay (Promega, USA) according to the manufacturer's recommendation. The IC_{50} dose response curves were defined as the test compound concentrations which prevented cell growth of more than 50% (relative to the vehicle control) and were constructed using non- linear regression analysis with Prism 8.4.2 (GraphPad Software, CA, USA).

Fluorescence microscopy

HeLa cells were seeded on a 24-well glass bottom plate (1 x 10^4 cells/well) and allowed to adhere overnight. Cells were treated with **[C4MeQuin][I]** (500 nM) and stained with Hoechst (5 μM) and mitotracker deep red (100 nm) and then incubated (37 °C, 20 min). The cells were then washed twice with media, then the cells were incubated with 4% paraformaldehyde/PBS to fix the cells (37 °C, 20 min). The cells were washed twice with PBS prior to examination of the cells on a Nikon A1 laser scanning confocal microscope with a 60X Plan Apo (NA 1.4) objective. Hoechst 33342 stained nuclei were detected using a 405 nm laser and a 400-450 nm bandpass filter. **[C4MeQuin][I]** labelled structures were detected with a 458 nm laser and a 500-550 nm bandpass filter. MitoTracker Deep Red labelled mitochondria were detected with a 640 nm laser and a 662-737 nm bandpass filter.

Tethered bilayer lipid membranes

Lipid bilayers were anchored across a gold electrode according to "T10" architecture[168,169]. This consists of 10% benzyl-disulfide (tetra-ethyleneglycol) n=2 C20-phytanyl "tethering" molecules interspersed with 90% benzyl-disulfide-tetra-ethyleneglycol-OH "spacer" molecules. Spacer and tether molcules are all coordinated onto a 2.1 mm^2 gold tethering electrode. To these first layer chemistries were added a second layer of mobile phase lipid molecules of 3 mM 1,2-dioleoyl-sn-glycero-3-phosphocholine (DOPC) (Avanti Polar Lipids Inc., Alabaster, USA) which was left to incubate with the tethering molecules for exactly 2 min before a rapid exchange of 3 x 400 μL 100 mM NaCl tris buffer induced the formation of a completed tBLM.

Electrical impedance spectroscopy

Swept frequency electrical impedance spectroscopy ranging from 0.1 Hz to 2000 Hz

was applied at 25 mV peak-to-peak, using a Tethapod^{TM} electrical impedance spectrometer (SDx Tethered Membranes Pty Ltd). Impedance and phase profiles were fitted to an equivalent circuit consisting of a constant phase element, representing the tethering gold electrode and reservoir region, in series with a resistor, to represent the impedance of the surrounding electrolyte solution, and a resistor/capacitor representing the lipid bilayer. Data fitting utilised a proprietary adaptation of a Levenberg–Marquardt fitting routine incorporated into the TethaQuickTM software (SDx Tethered Membranes Pty Ltd).

Mitochondrial membrane potential (JC-1) assay

HeLa cells were seeded in triplicate in black 96-well plates (1 x 10^4 cells/well) and allowed to adhere overnight. The cells were treated with ILs at their individual cell viability IC$_{50}$ values for 1 h, control cells received DMEM with 10% FBS and 0.1% DMSO. Cells were incubated with the JC-1 dye in media with 10% FBS (37°C, 20 min) and the JC-1 red: green ratio was measured on the teacan plate reader. (JC-1 Mitochondrial Membrane Potential Assay Kit; Cayman Chemical, Ann Arbor, MI).

ATP

ATP formation was assessed in HeLa cells which were seeded in triplicate in black 96-well plates (7.5 x 10^3 cells/well) and allowed to adhere overnight. Cells were treated with ILs at their respective cell viability IC$_{50}$ concentration at various time points (0-4 hr) in DMSO (final concentration of 0.1 %), control cells were treated with 0.1% DMSO alone. CellTiter-Glo solution was added to cells (RT, 30 min) and the luminescence was determined (CellTiter-Glo® luminescent cell viability assay, Promega; Annandale, NSW, Australia).

ROS

HeLa cells were seeded in triplicate in a 96-well black plate (2 x 10^4 cells/well) and allowed to adhere overnight. The following day cells were washed with 200 μL prewarmed PBS, then cells were incubated with 100 μL of DCFDA solution for 20 mins at 37 ºC. Next, cells were treated with ILs at their individual cell viability IC_{50} values for 6 h and H_2O_2 (200 μM, positive control) and ROS was measured on the teacan plate reader.

Seahorse

Mitochondrial function was measured by determining the OCR of cells with a Seahorse XF24 extracellular flux analyser (Seahorse Bioscience, MA, USA) according to the manufacturer's protocol. HeLa cells were seeded in a 24-well XF cell culture microplates (2.5×10^4 cells per well) and allowed to adhere overnight (37 °C, 5% CO_2). After 24 h, the culture media was replaced with buffered XF Base Medium supplemented with 2 mM L-glutamine, 10 mM glucose and 2 mM sodium pyruvate at pH=7.4. The cells were incubated at 37 °C without CO_2 for an hour, and then, the OCR was measured utilising an XF Cell Mito Stress Test Kit (Seahorse Bioscience, MA, USA). Test compounds (final concentration at MTS IC_{50}), oligomycin (final concentration 1 μM), carbonylcyanide m-chlorophenylhydrazone (FCCP-final concentration 2 μM) and rotenone/antimycin A (final concentration 0.5 μM) were added to the sensor cartridge, and the OCR was measured using a modified cycling program.

Statistical analysis

For *in vitro* assays, the data obtained was analysed using one-way analysis of variance (ANOVA) followed by Tukey's post hoc analysis. $P < 0.05$ were accepted as being statistically significant. All statistical analyses were performed using GraphPad Prism version 8.4.2

(GraphPad Software, CA, USA). The results are expressed as the means ± SEM unless otherwise specified.

A
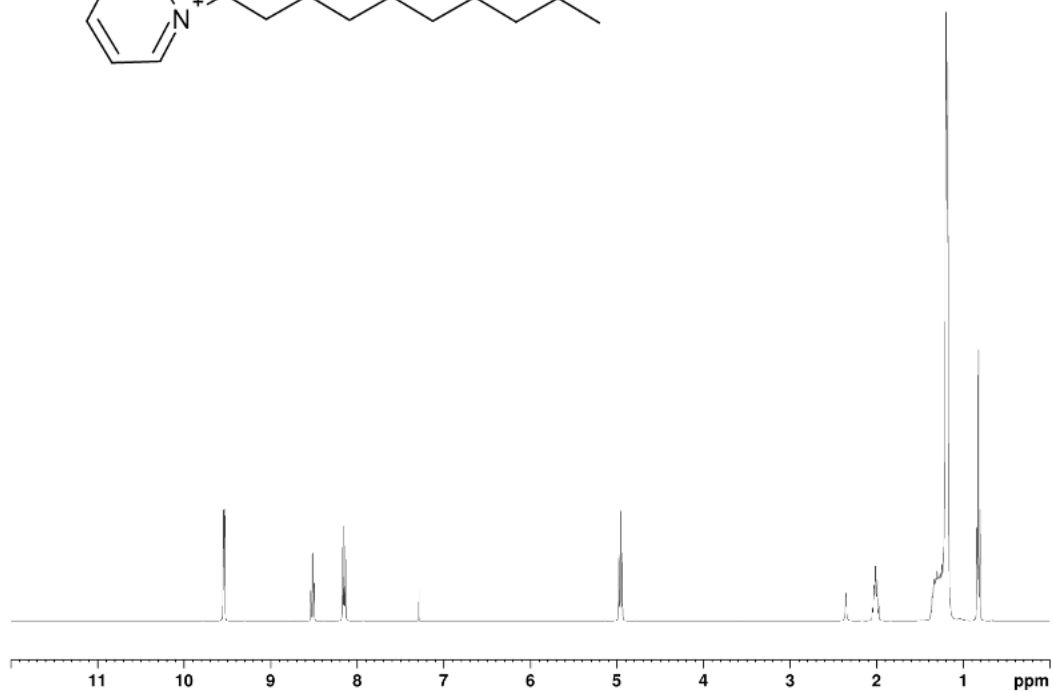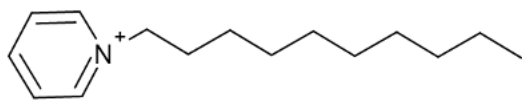
B
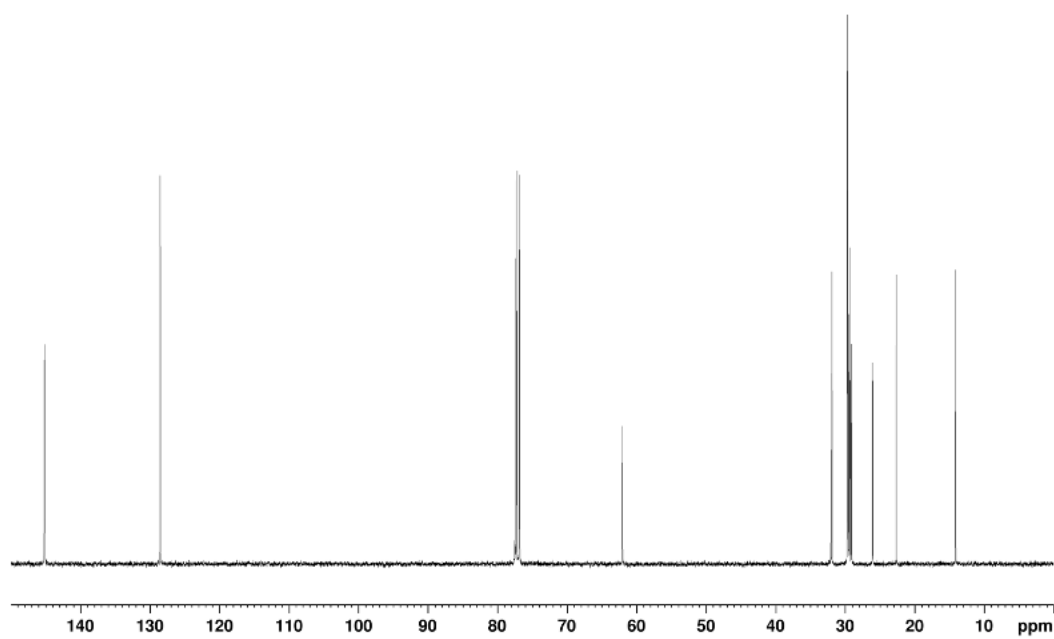
Figure 34 A)^{1}H NMR spectrum of **[C$_{10}$Py][Br]**, B)^{13}C NMR spectrum of **[C$_{10}$Py][Br]**.
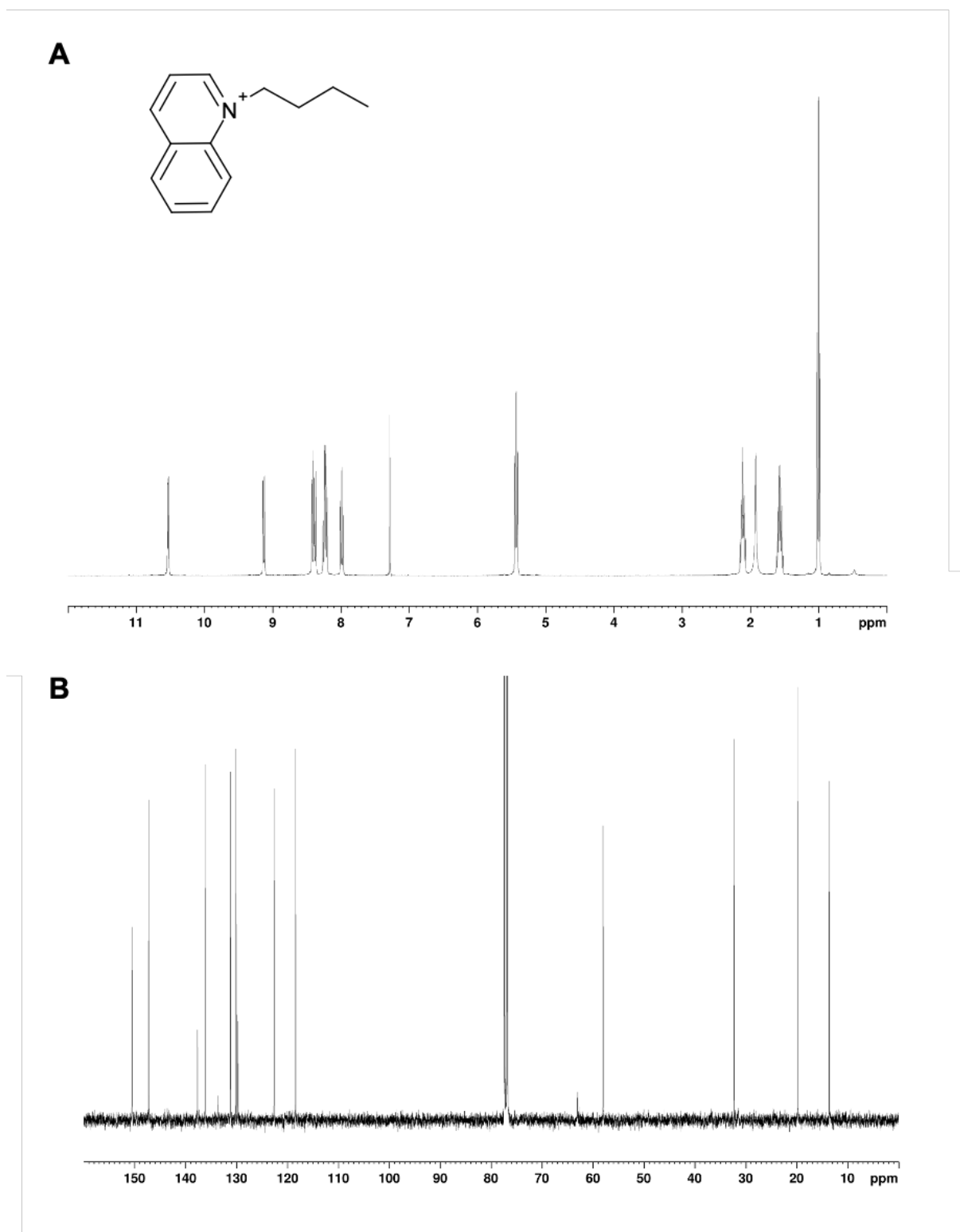
Figure 35 A) ^{1}H NMR spectrum of **[C₄Quin][Br]**, B) ^{13}C NMR of spectrum of **[C₄Quin][Br]**
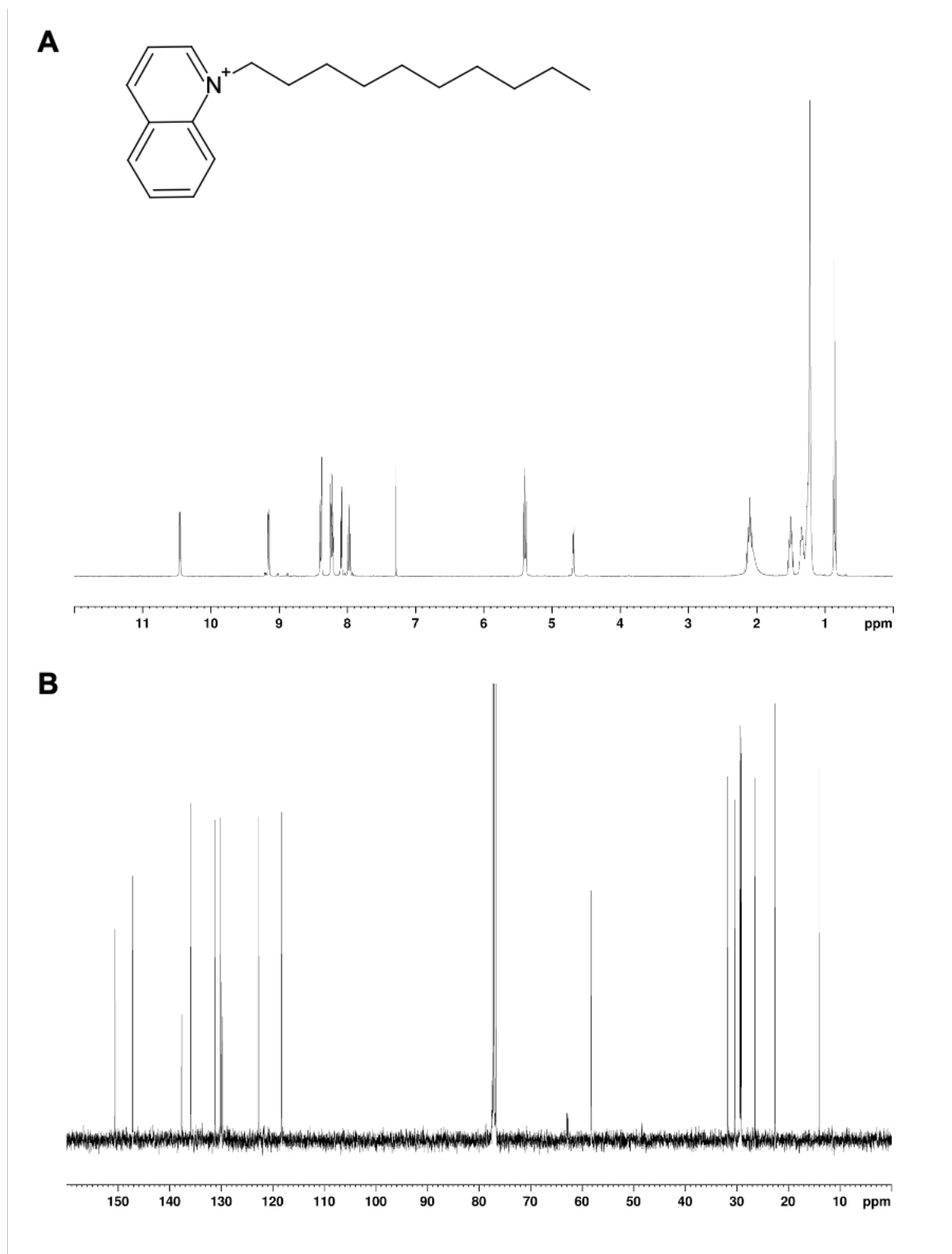
Figure 36 A)^{1}H NMR spectrum of **[C$_{10}$Quin][Br]**, B)^{13}C NMR of spectrum of **[C$_{10}$Quin][Br]**.
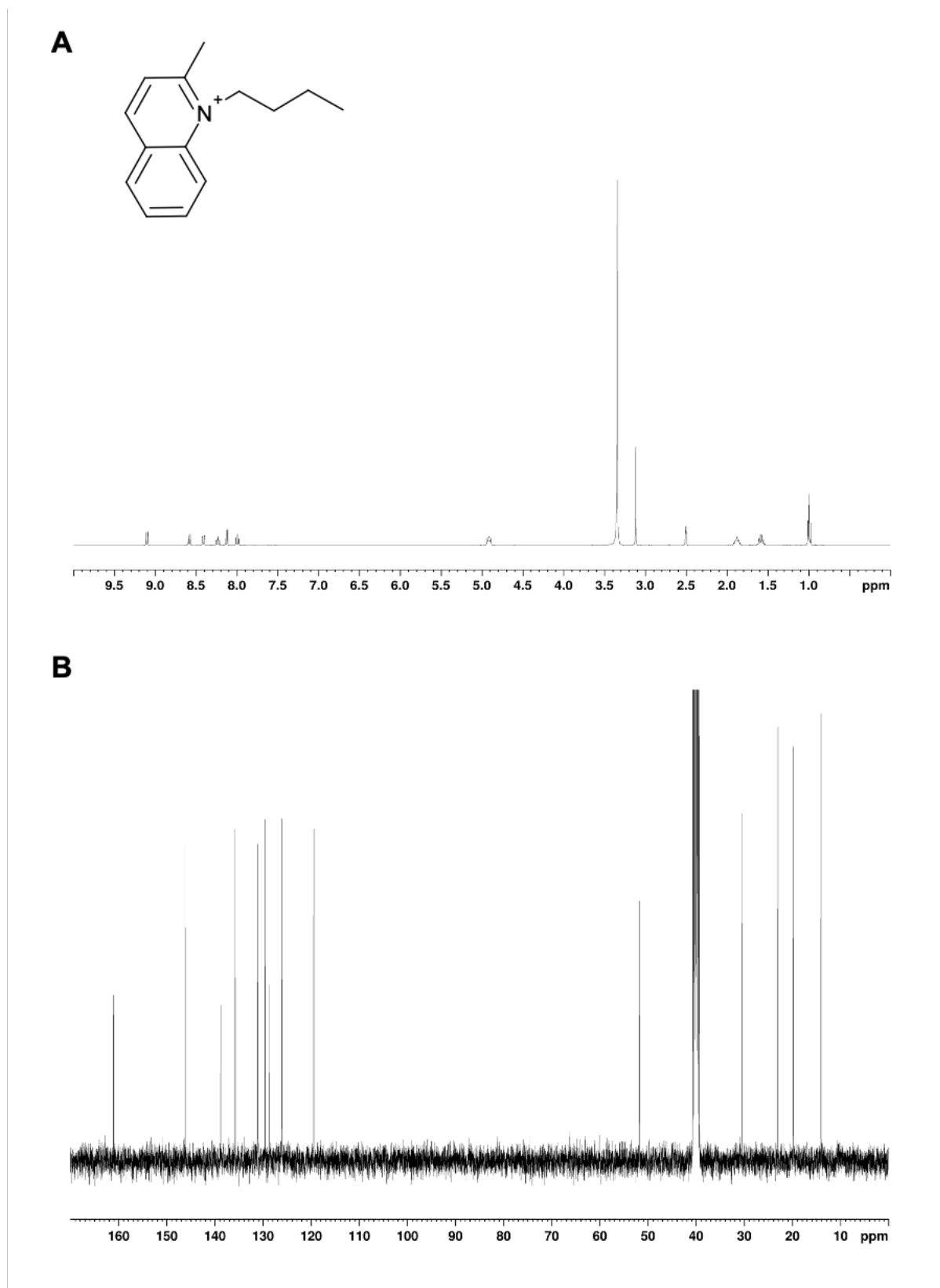
Figure 37 A)^{1}H NMR spectrum of **[C$_4$MeQuin][I]**, B)^{13}C NMR of spectrum of

[C$_4$MeQuin][I].
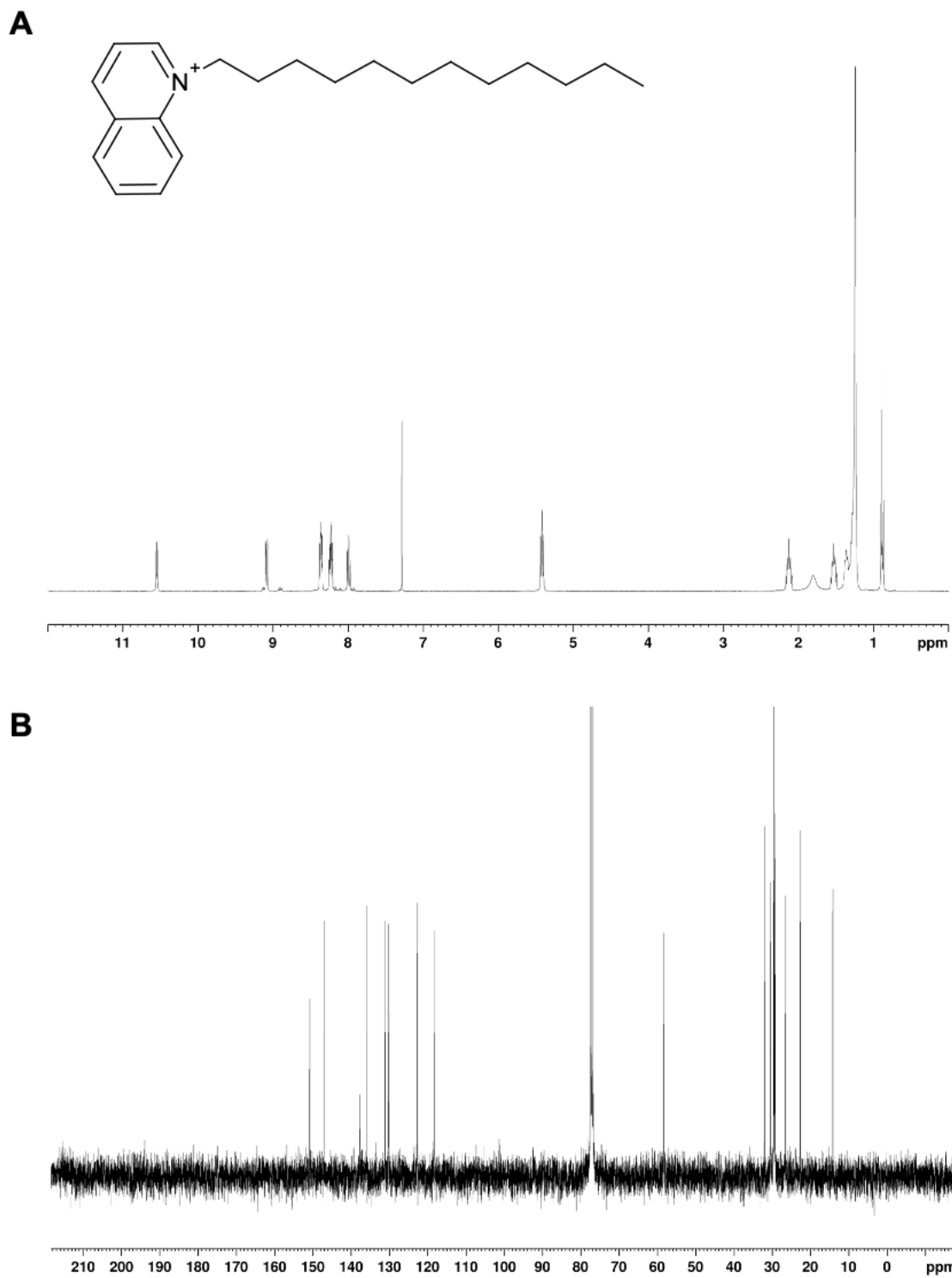
Figure 38 A)^{1}H NMR spectrum of **12**, B)^{13}C NMR spectrum of **12**.
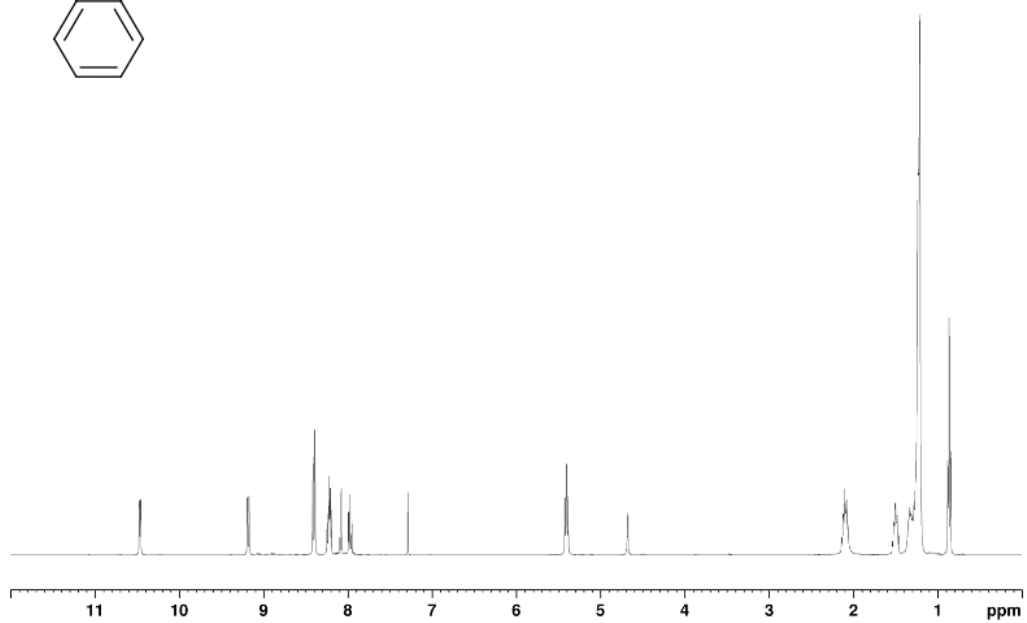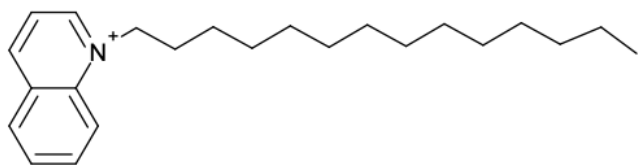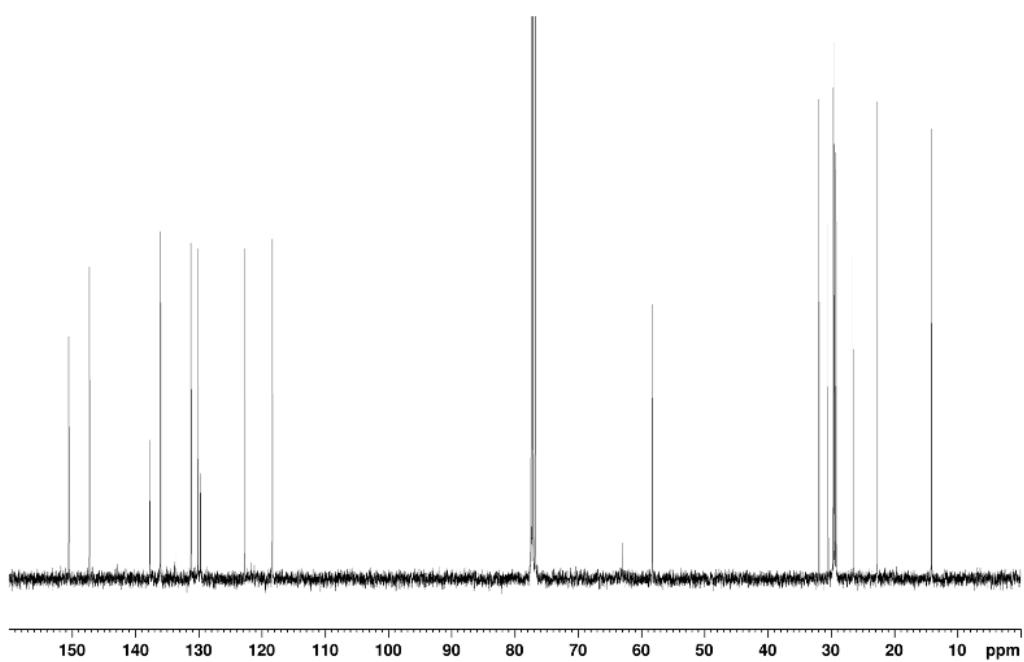
Figure 39 A)^{1}H NMR spectrum of **13**, B)^{13}C NMR spectrum of **13**.
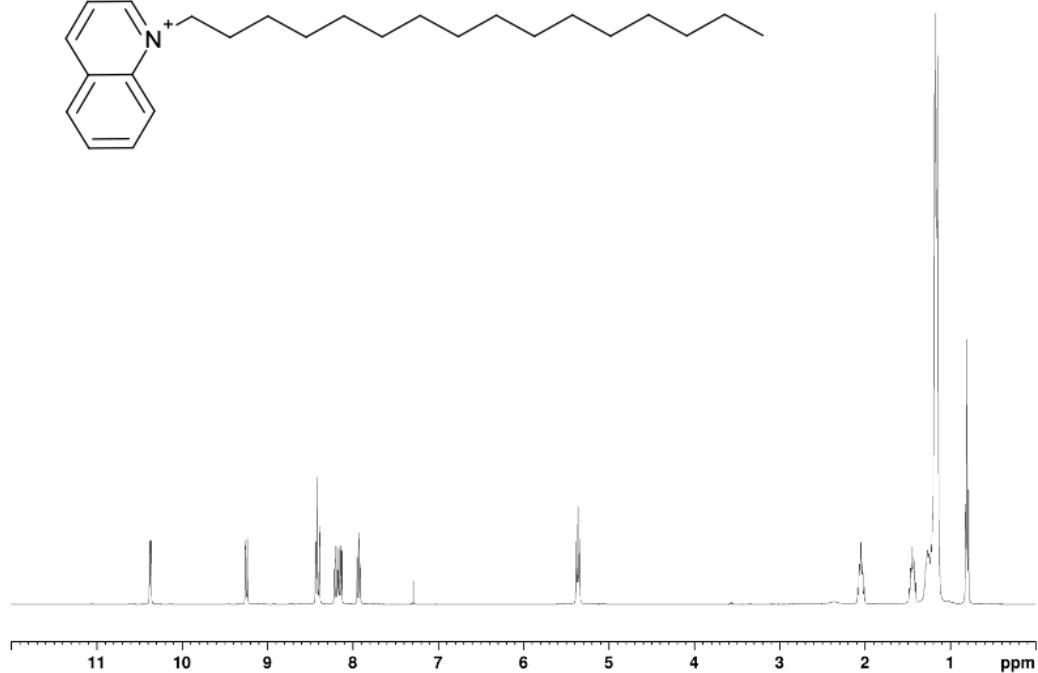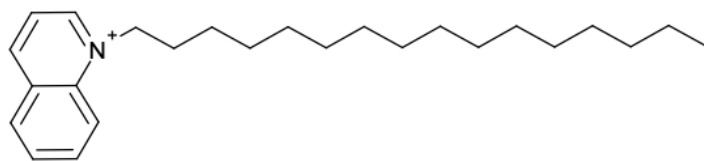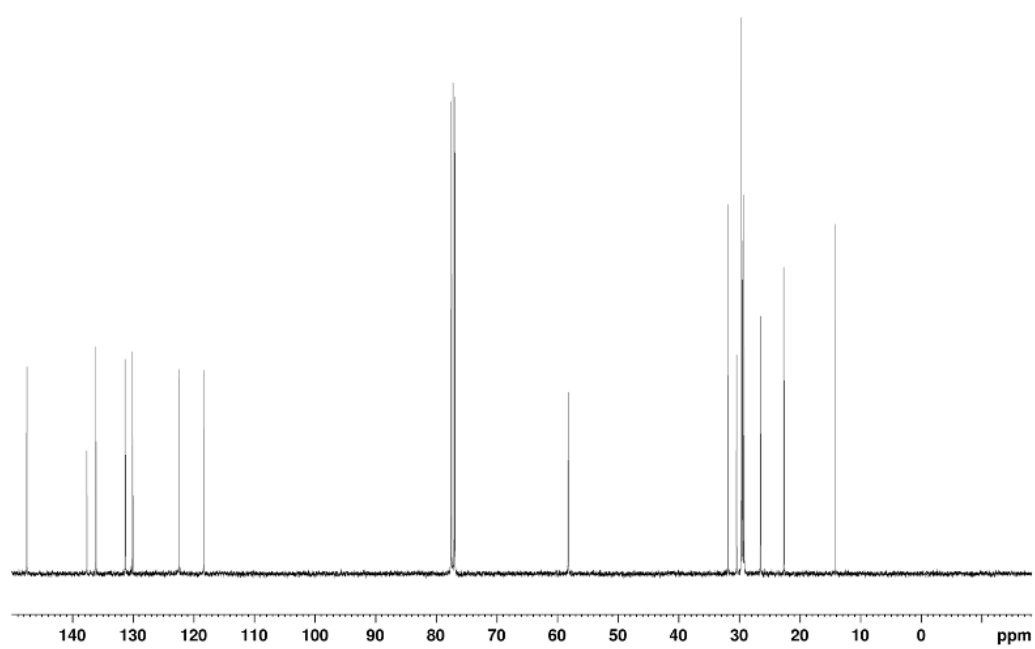
Figure 40 A)^{1}H NMR spectrum of **14**, B)^{13}C NMR spectrum of **14**.
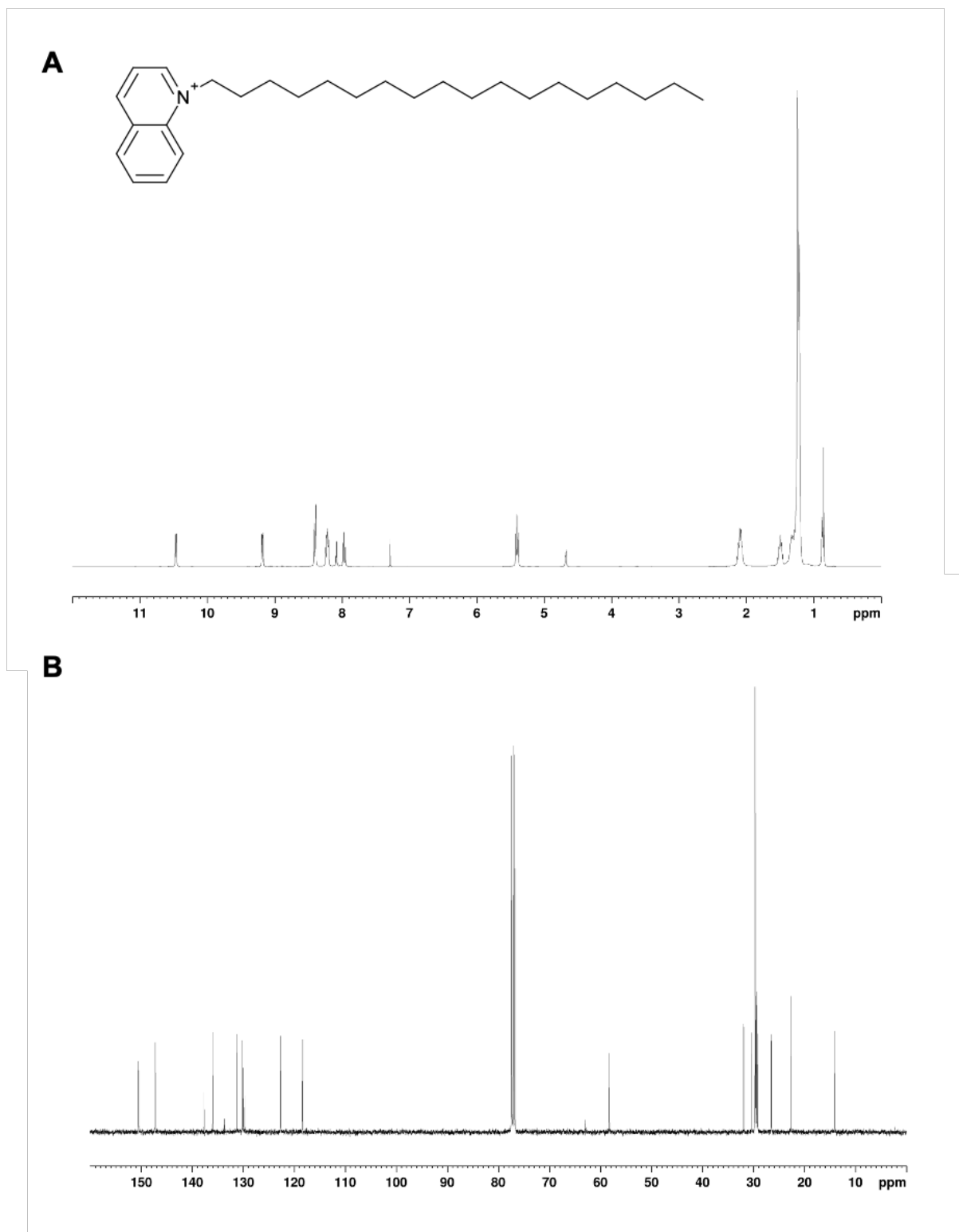
Figure 41 A)^{1}H NMR spectrum of **15**, B)^{13}C NMR spectrum of **15**.
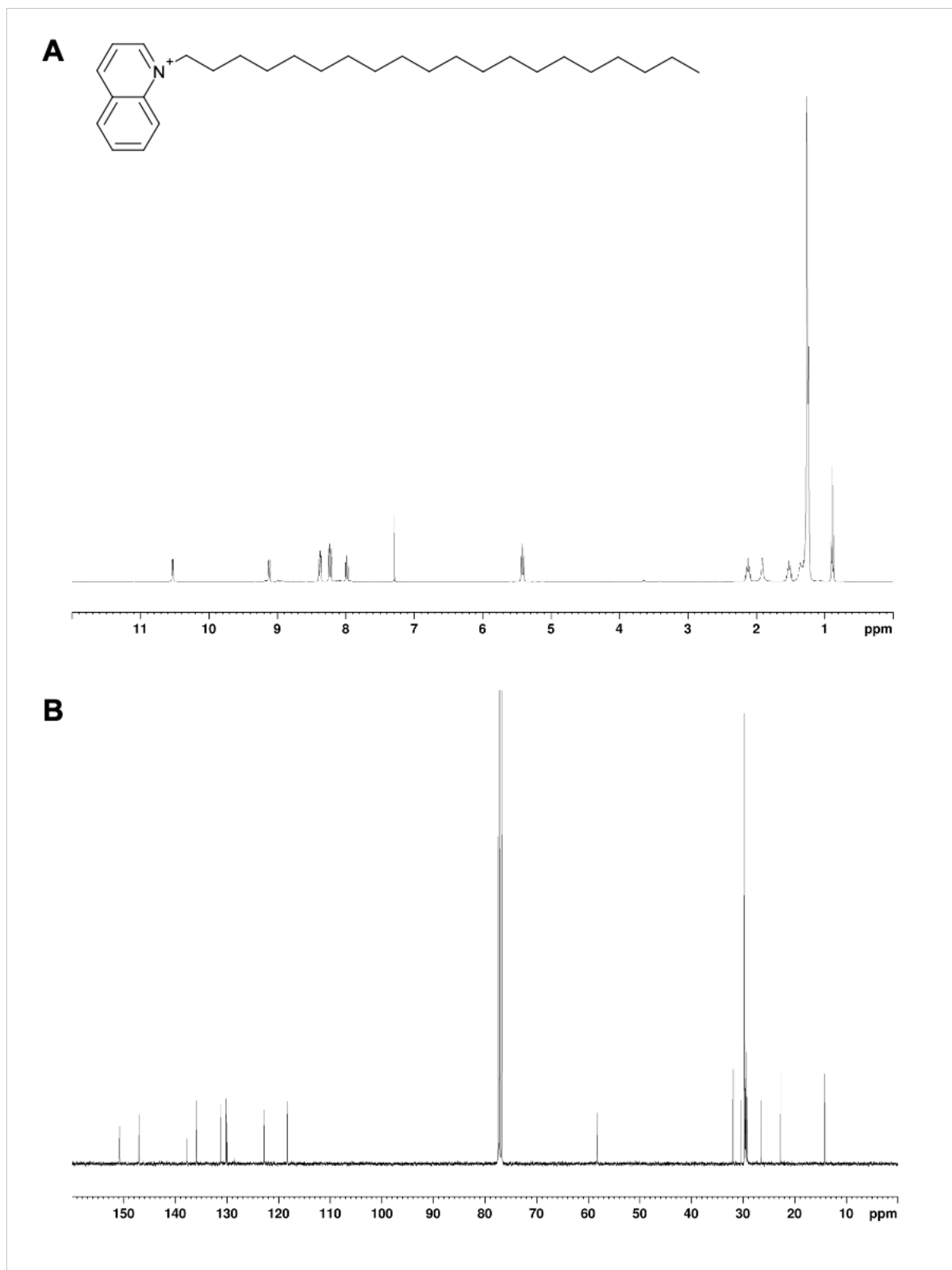
Figure 42 A)^{1}H NMR spectrum of **16**, B)^{13}C NMR spectrum of **16**.
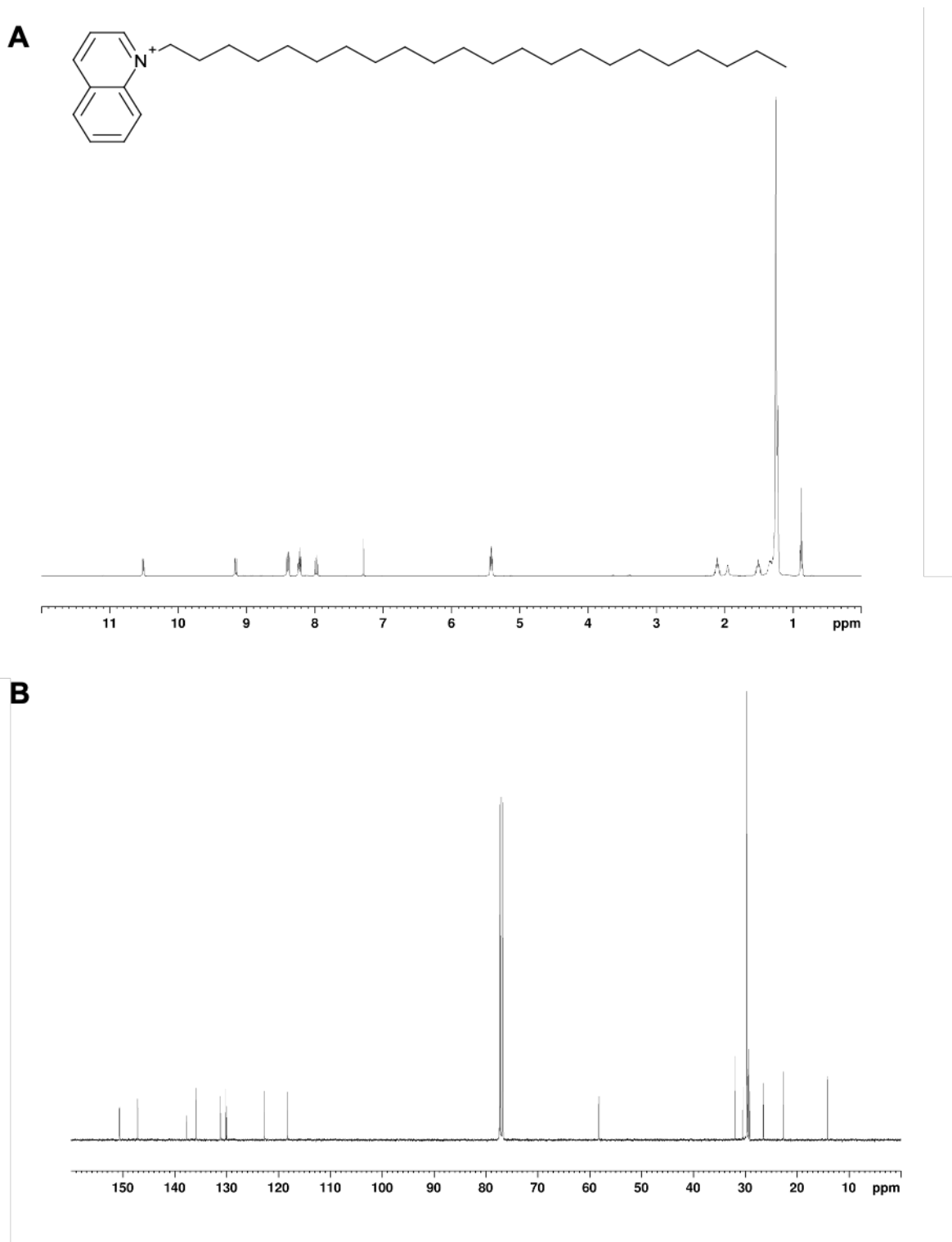
Figure 43 A)^{1}H NMR spectrum of **17**, B)^{13}C NMR spectrum of **17**.
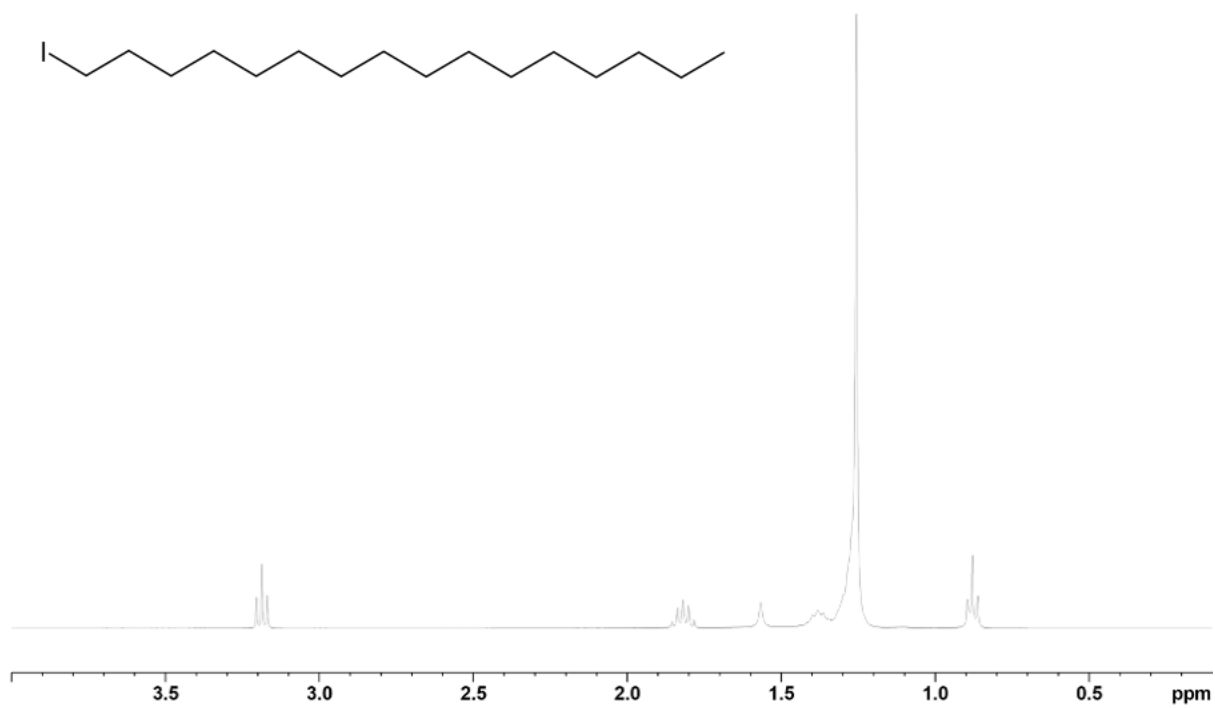
Figure 44 A)^{1}H NMR spectrum of 1-Iodohexadecane **27**.
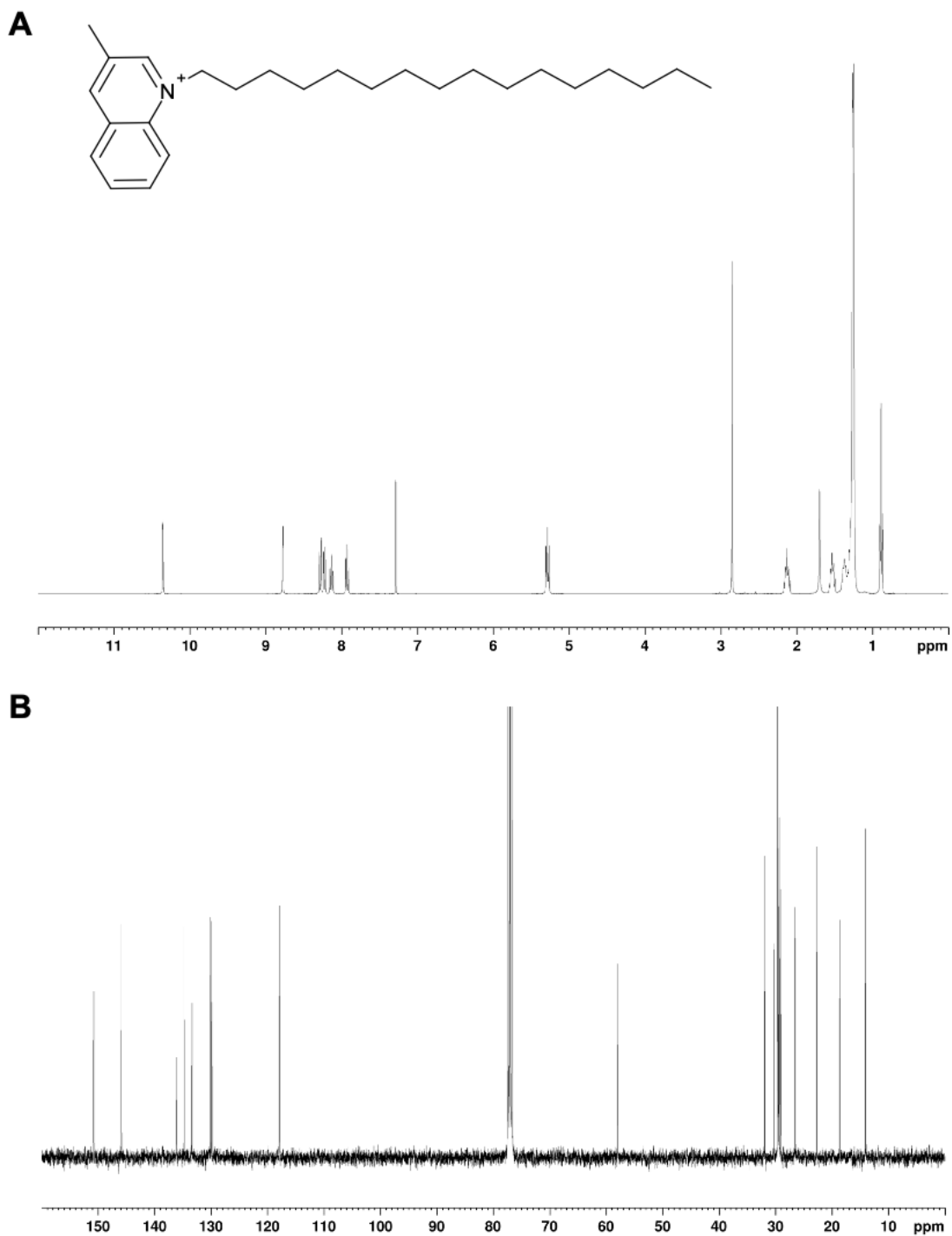
Figure 45 A)^{1}H NMR spectrum of **29**, B)^{13}C NMR spectrum of **29**.
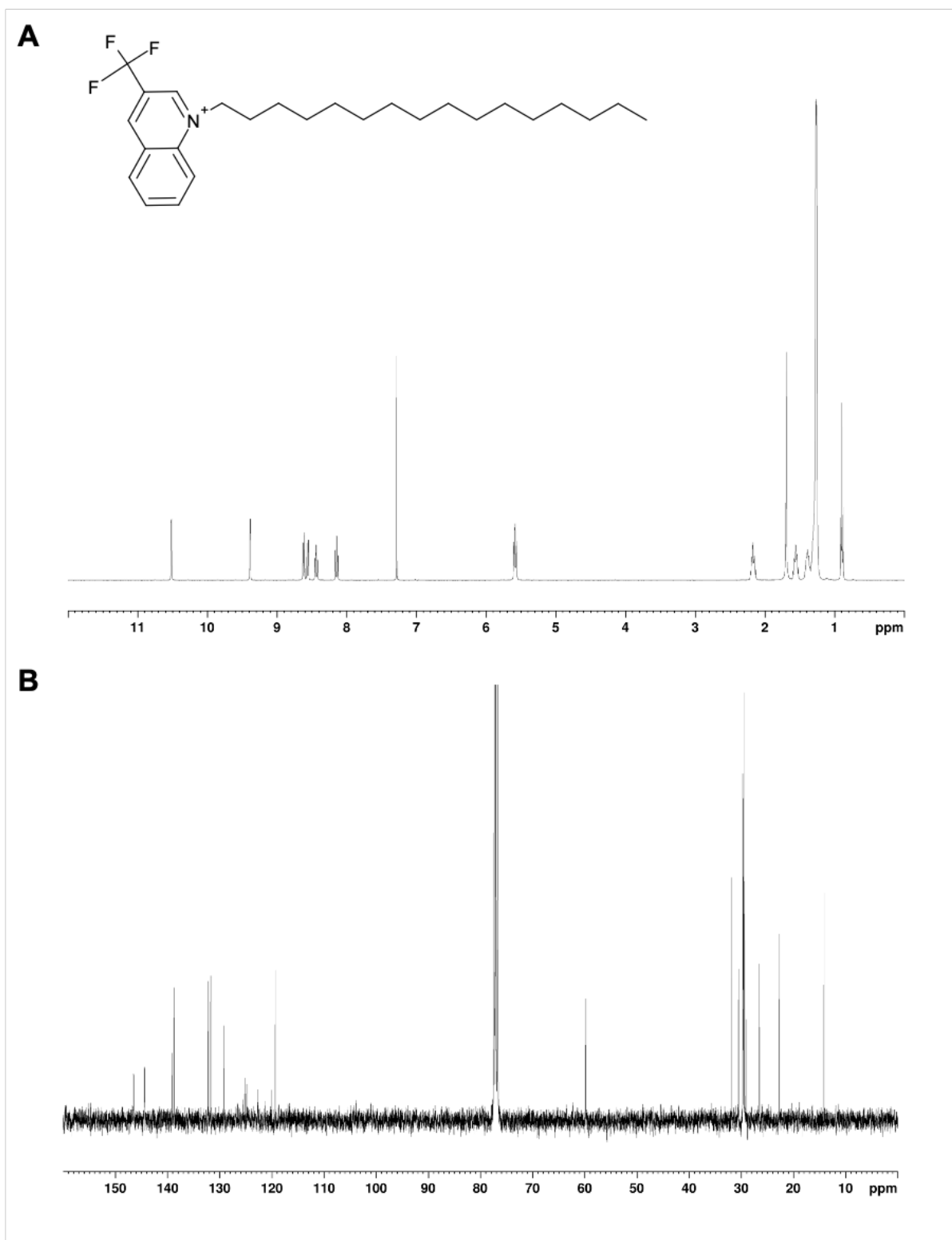
Figure 46 A)^{1}H NMR spectrum of **30**, B)^{13}C NMR spectrum of **30**.

119
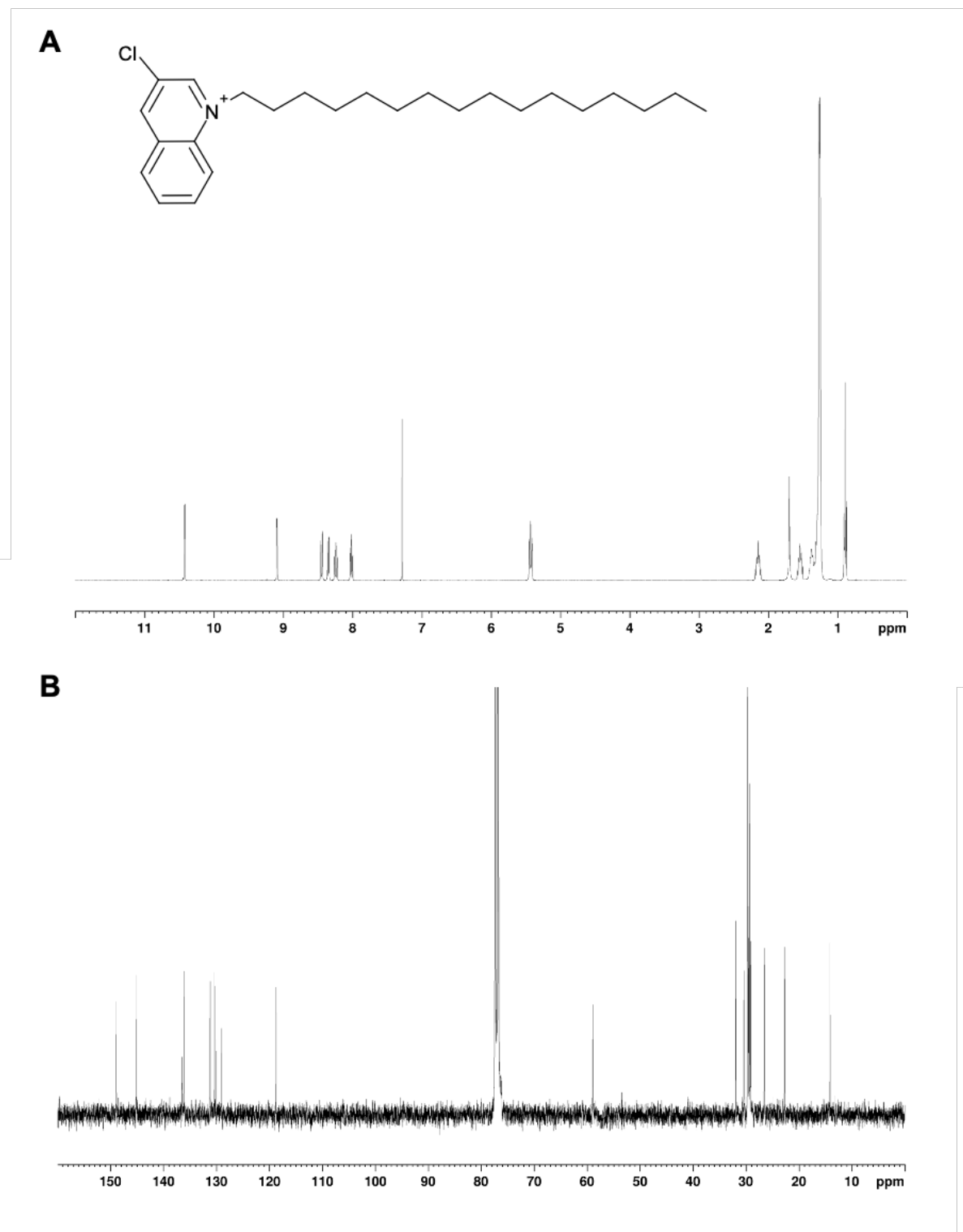
Figure 47 A)^{1}H NMR spectrum of **31**, B)^{13}C NMR spectrum of **31**.
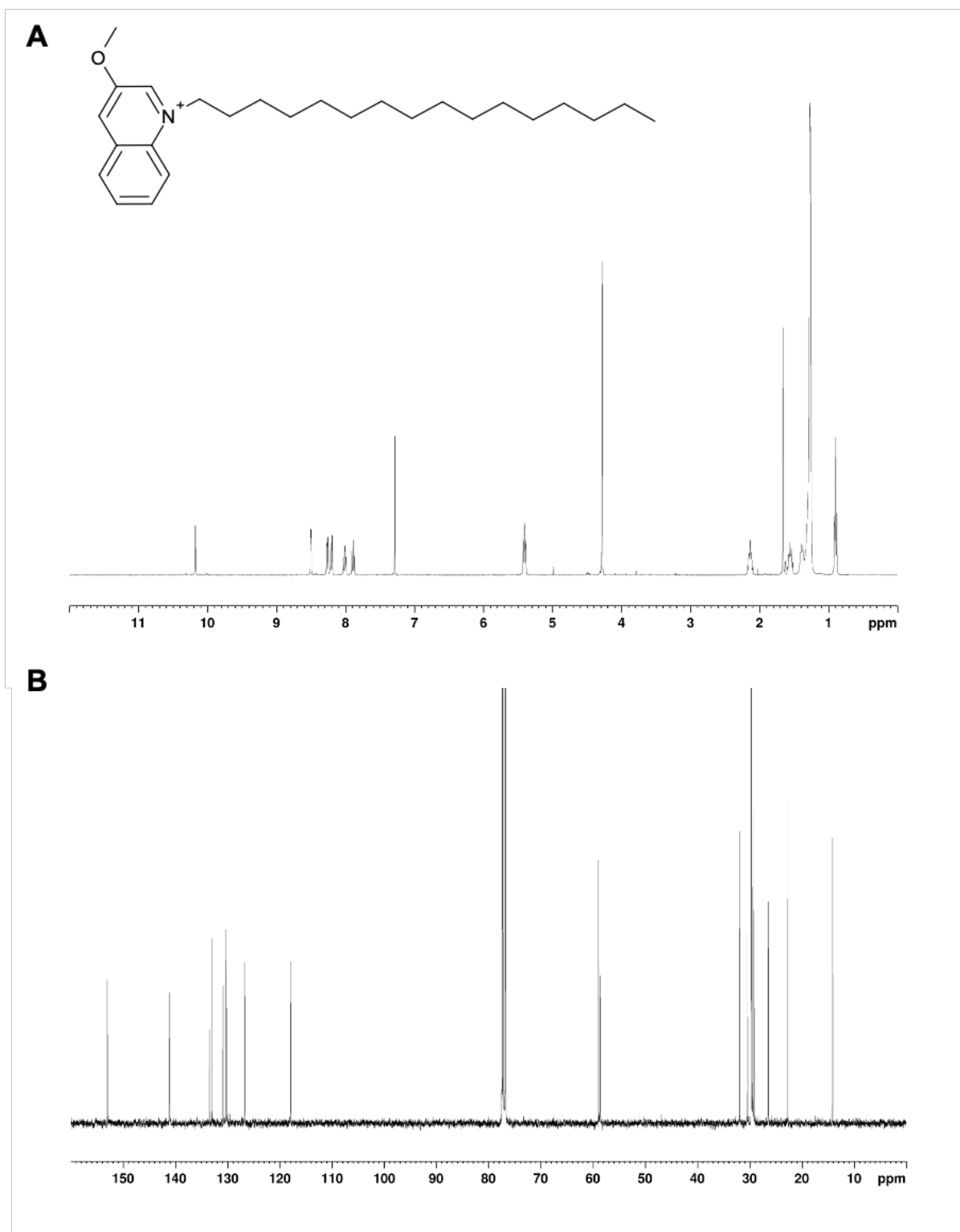
Figure 48 A)^{1}H NMR spectrum of **32**, B)^{13}C NMR spectrum of **32**.
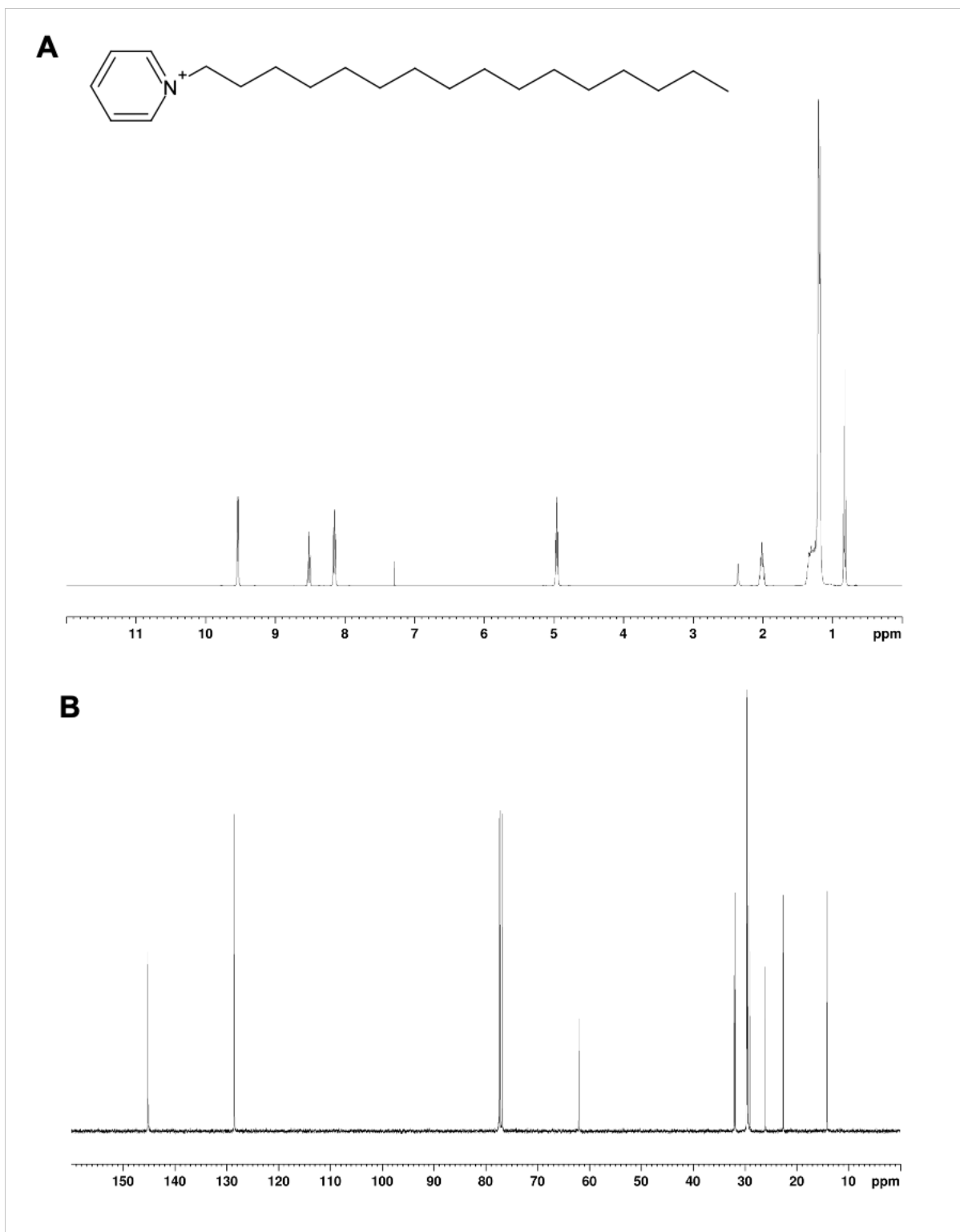
Figure 49 A)^{1}H NMR spectrum of **34**, B)^{13}C NMR spectrum of **34**.

Figure 50 A)^{1}H NMR spectrum of **35**, B)^{13}C NMR spectrum of **35**.
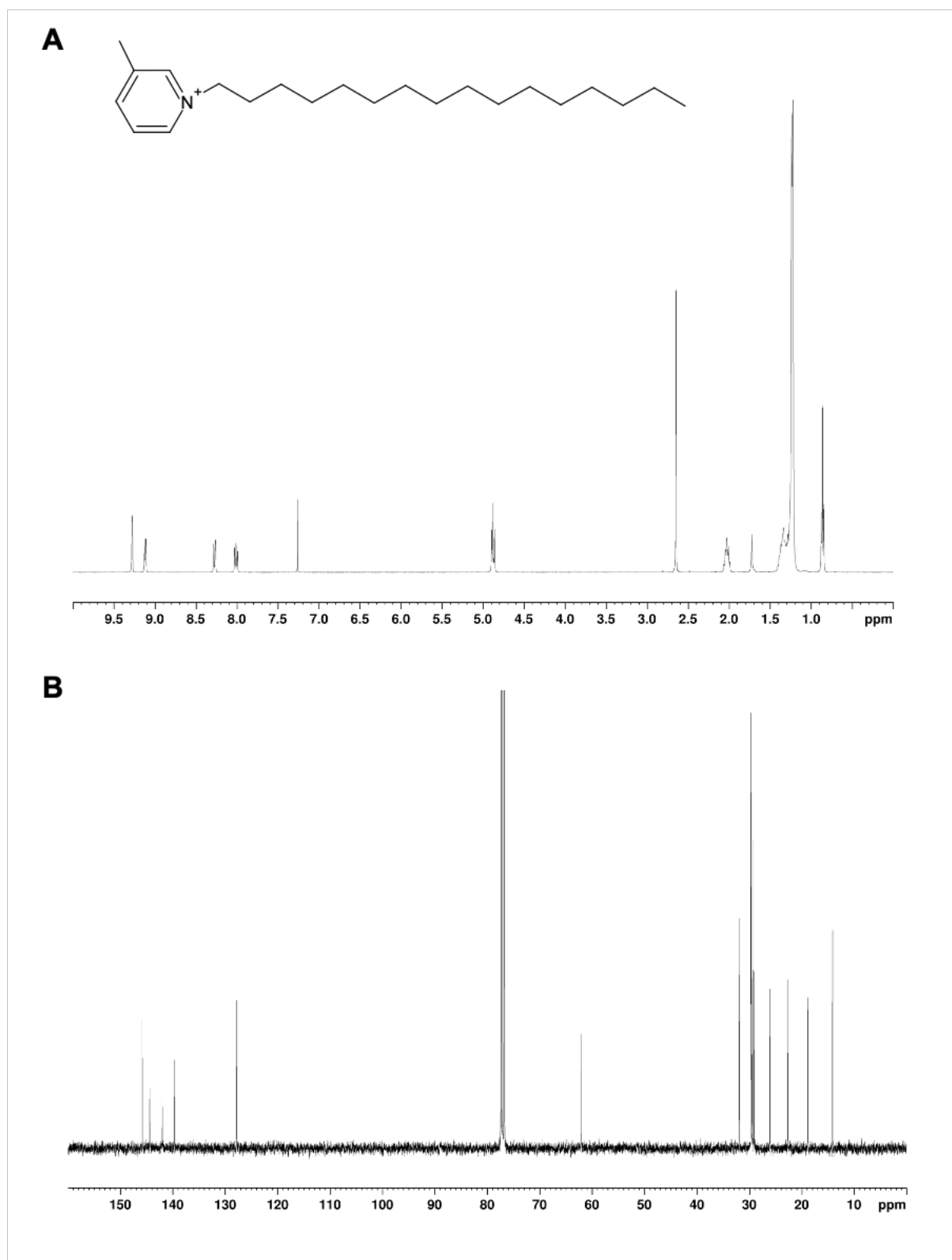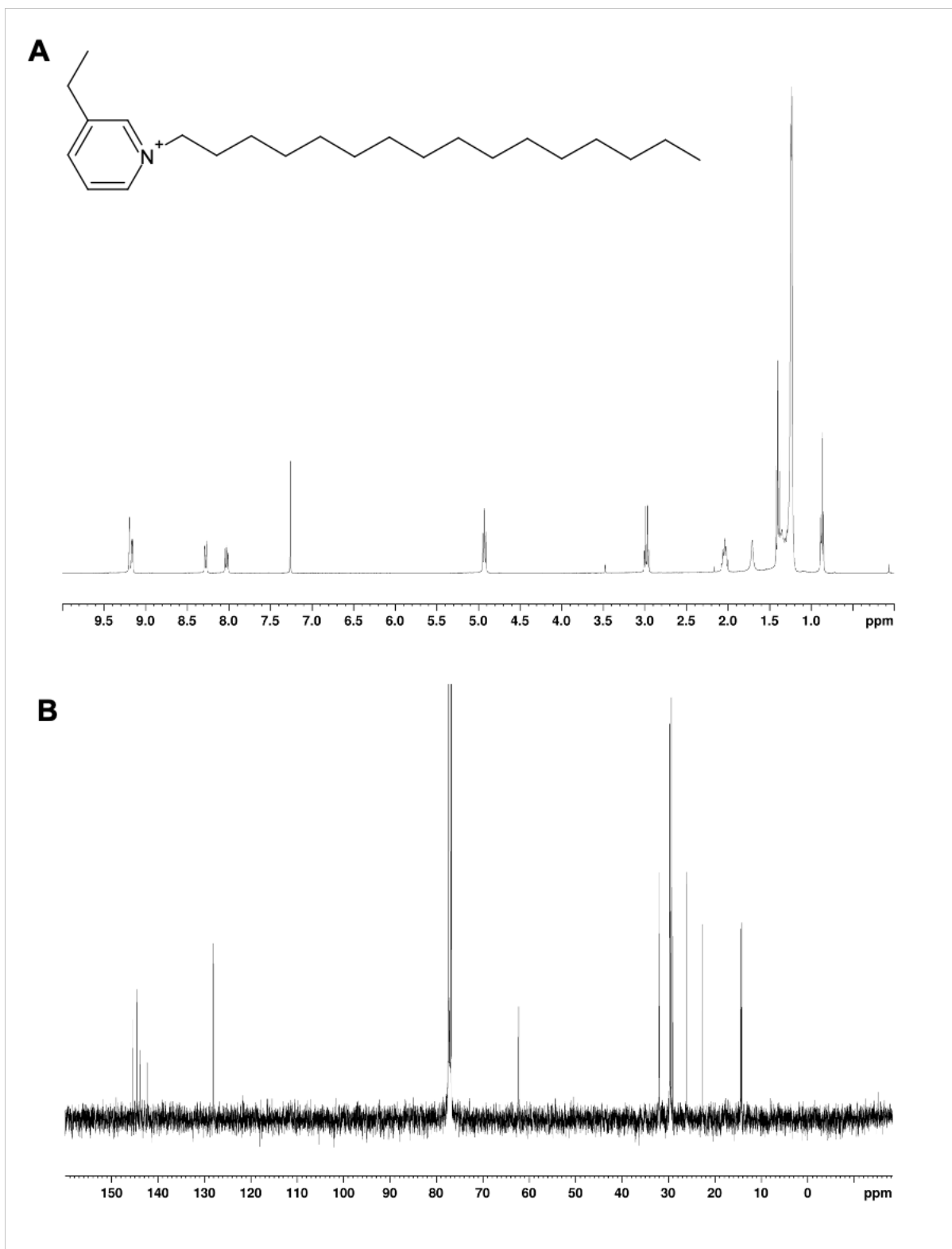
Figure 51 A)^{1}H NMR spectrum of **36**, B)^{13}C NMR spectrum of **36**.
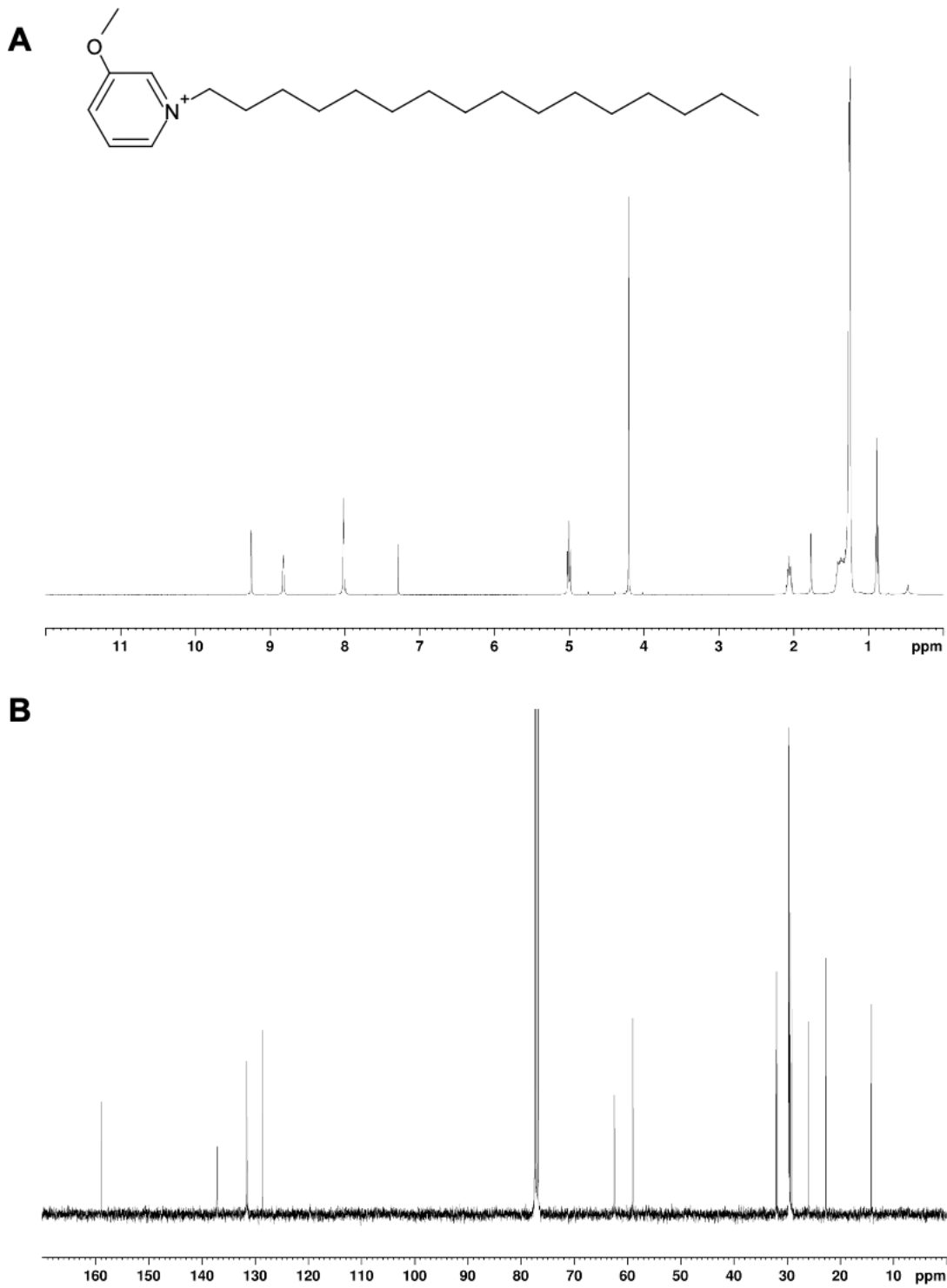
Figure 52 A)¹H NMR spectrum of **37**, B)¹³C NMR spectrum of **37**.
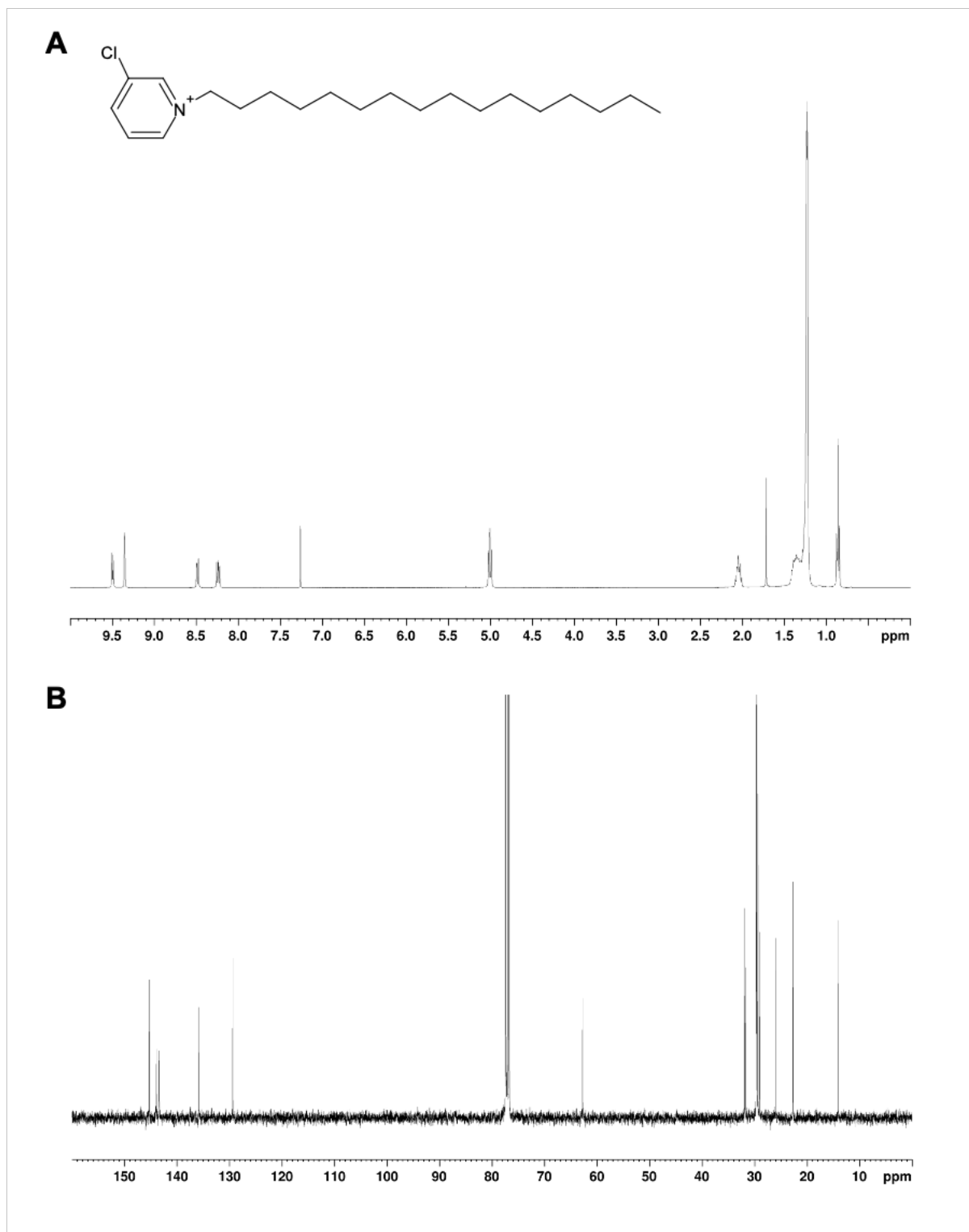
Figure 53 A)^{1}H NMR spectrum of **38**, B)^{13}C NMR spectrum of **38**.
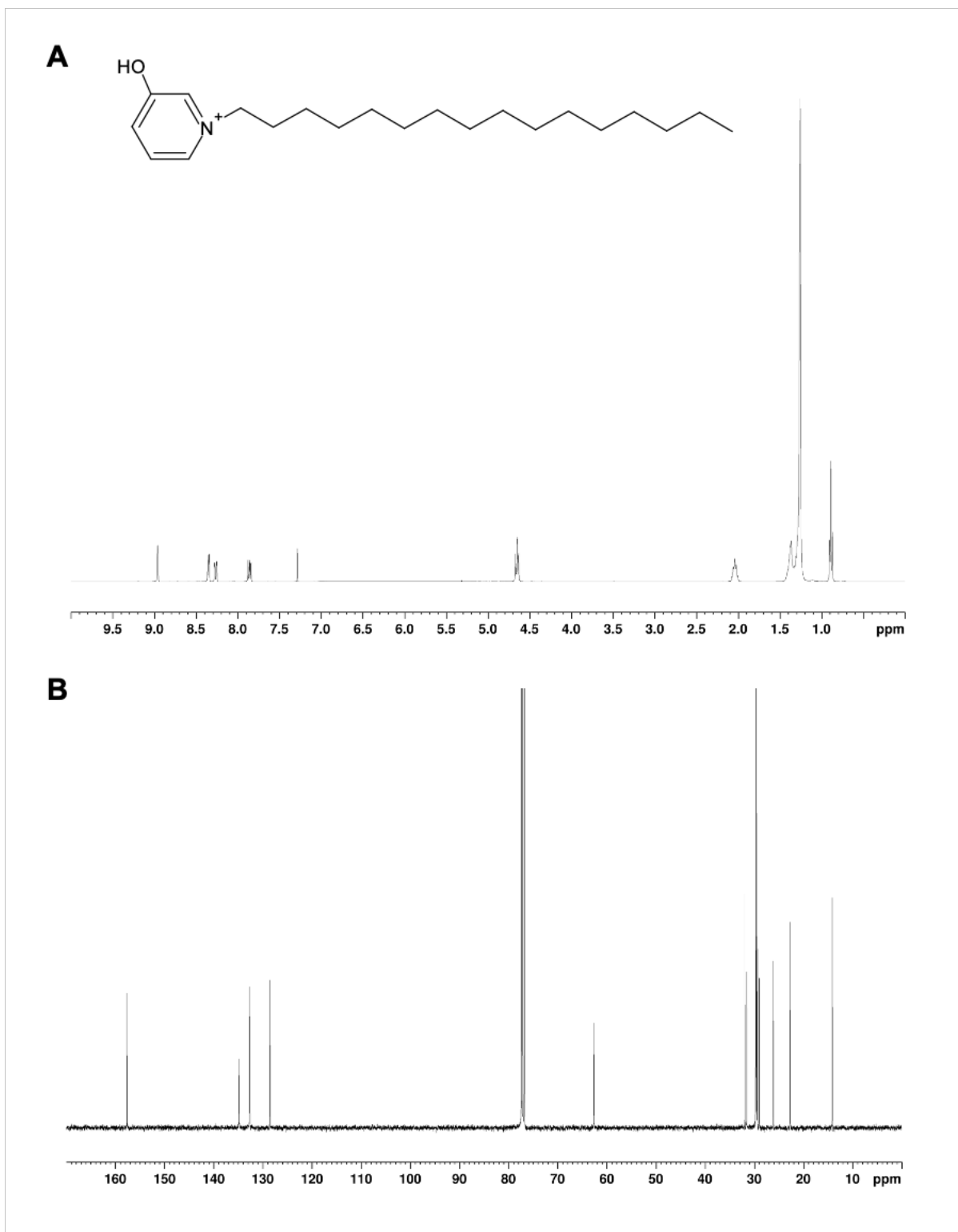
Figure 54 A)^{1}H NMR spectrum of **39**, B)^{13}C NMR spectrum of **39**.
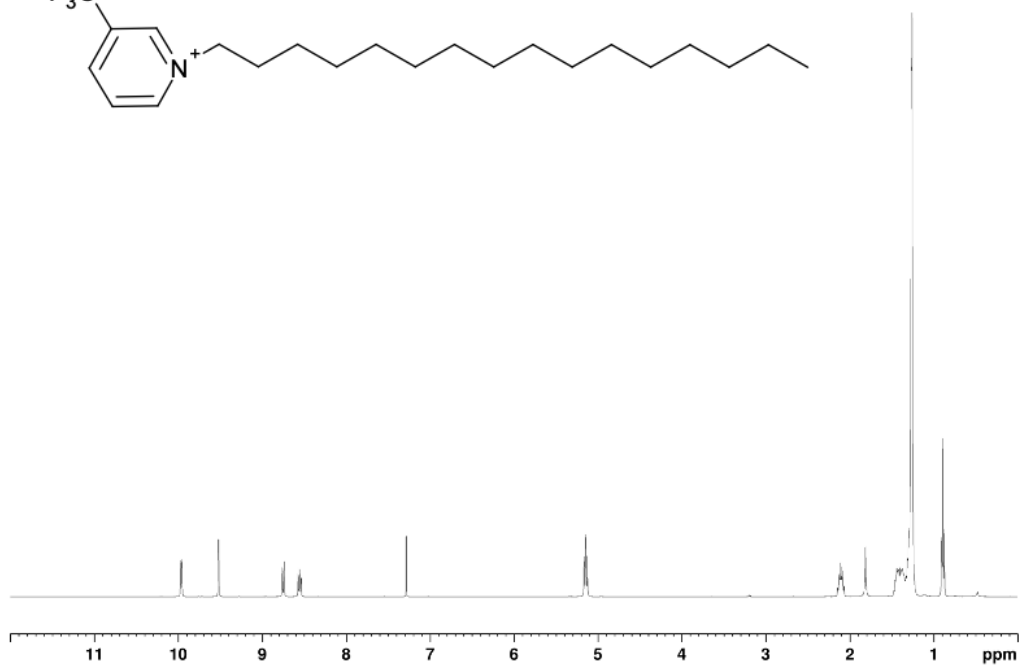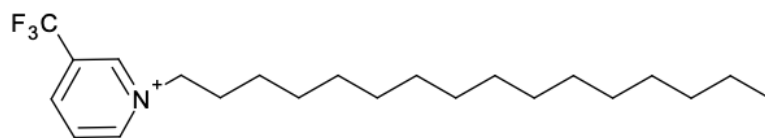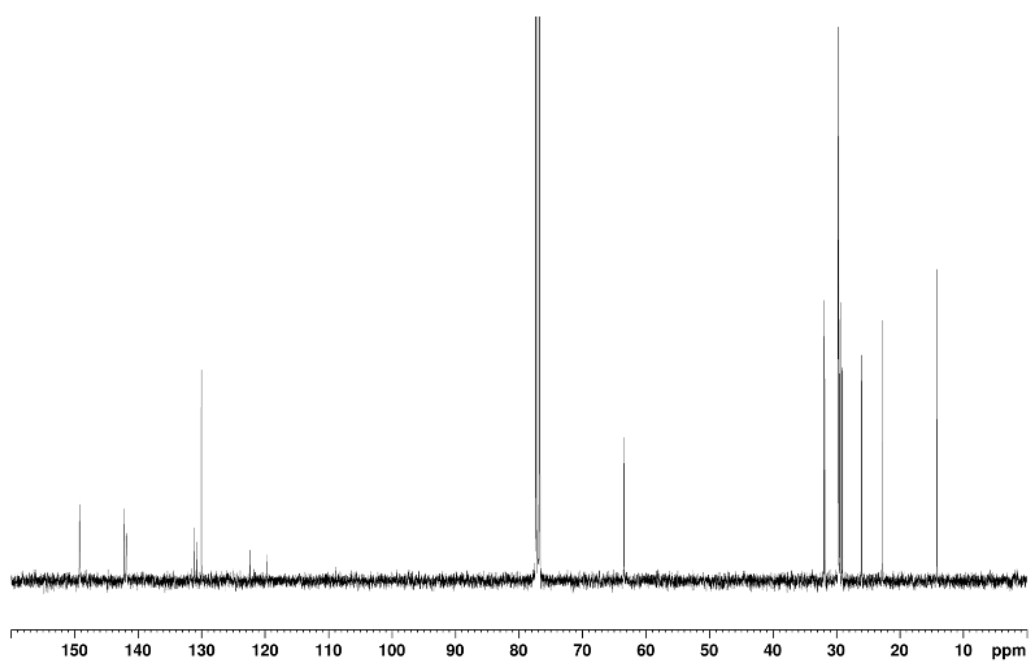
Figure 55 A)^{1}H NMR spectrum of **40**, B)^{13}C NMR spectrum of **40**.
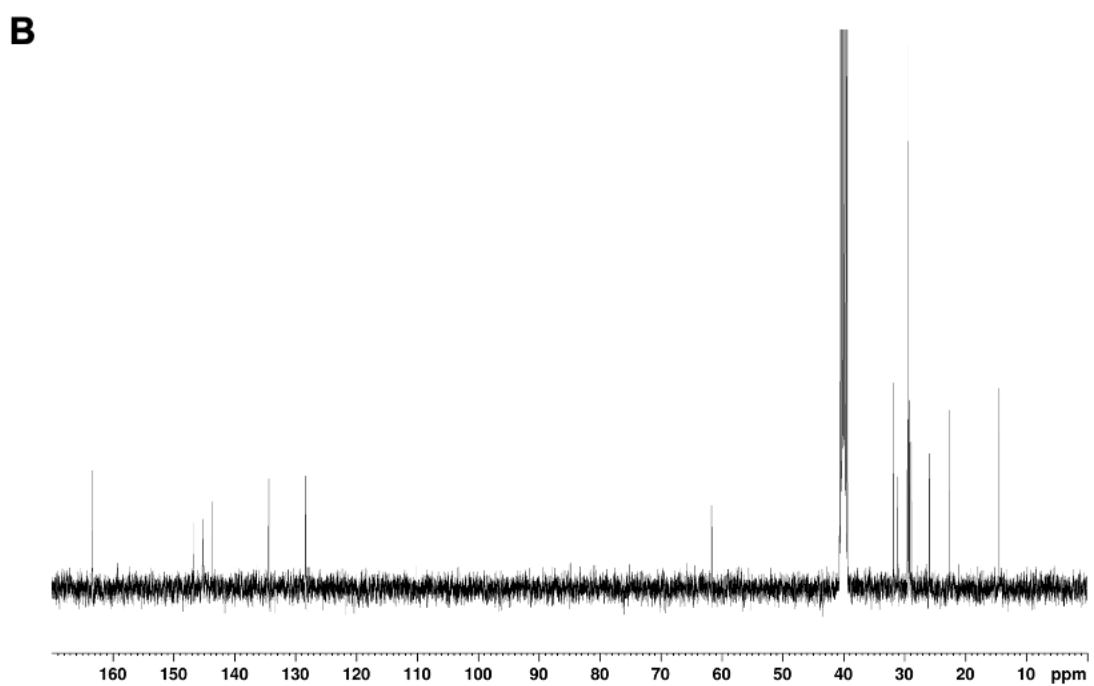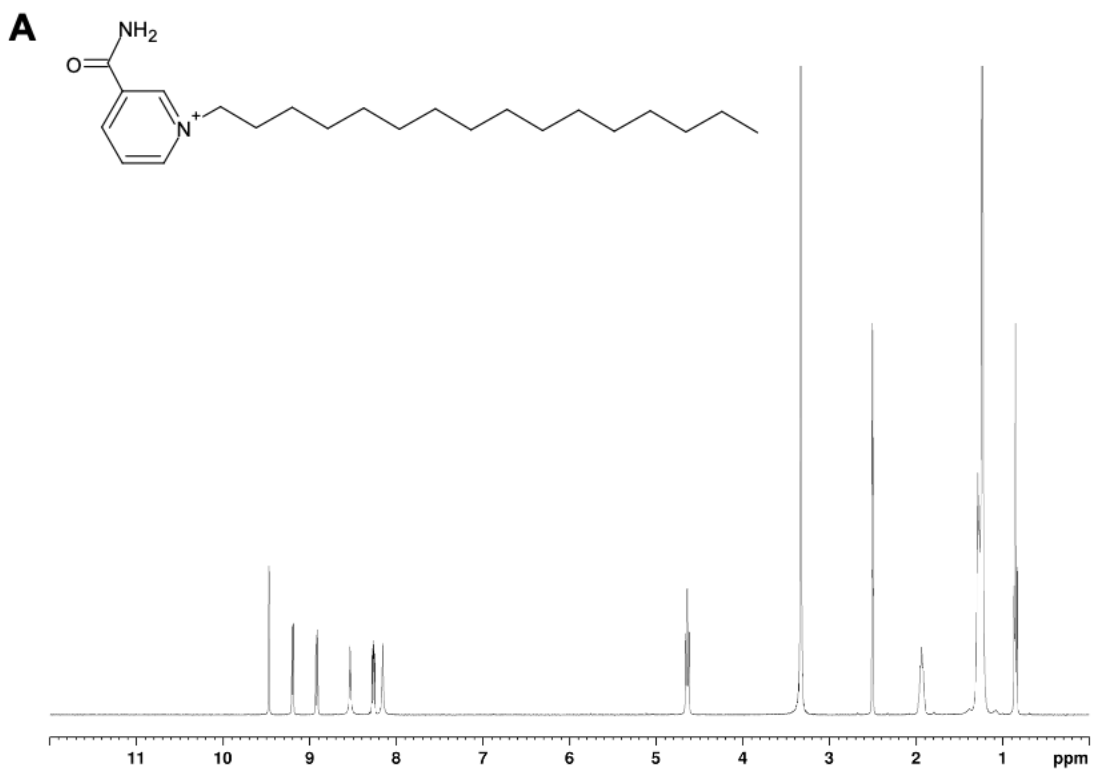
Figure 56 A)^{1}H NMR spectrum of **41**, B)^{13}C NMR spectrum of **41**.
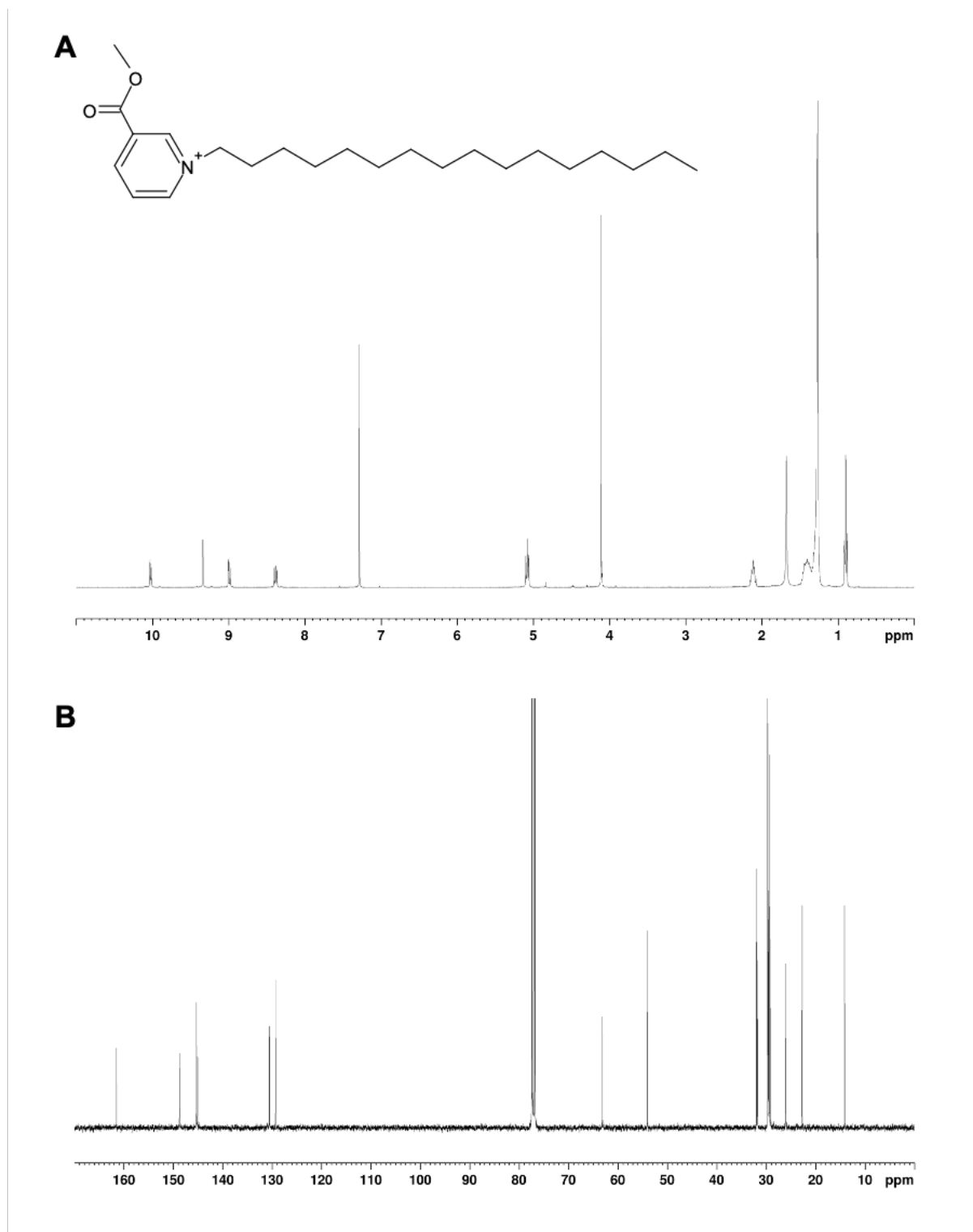
Figure 57 A)^{1}H NMR spectrum of **42**, B)^{13}C NMR spectrum of **42**.
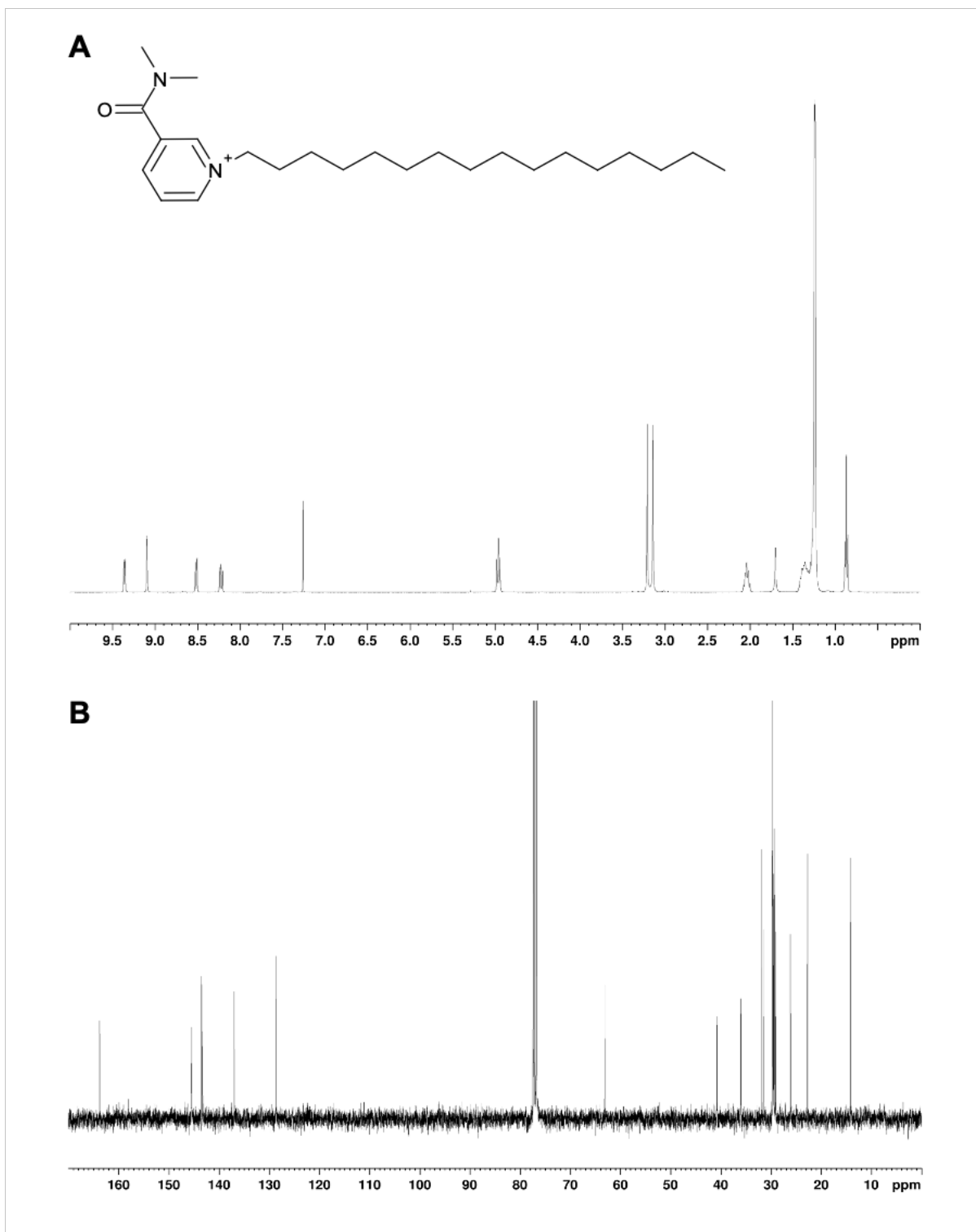
Figure 58 A)^{1}H NMR spectrum of **43**, B)^{13}C NMR spectrum of **43**.
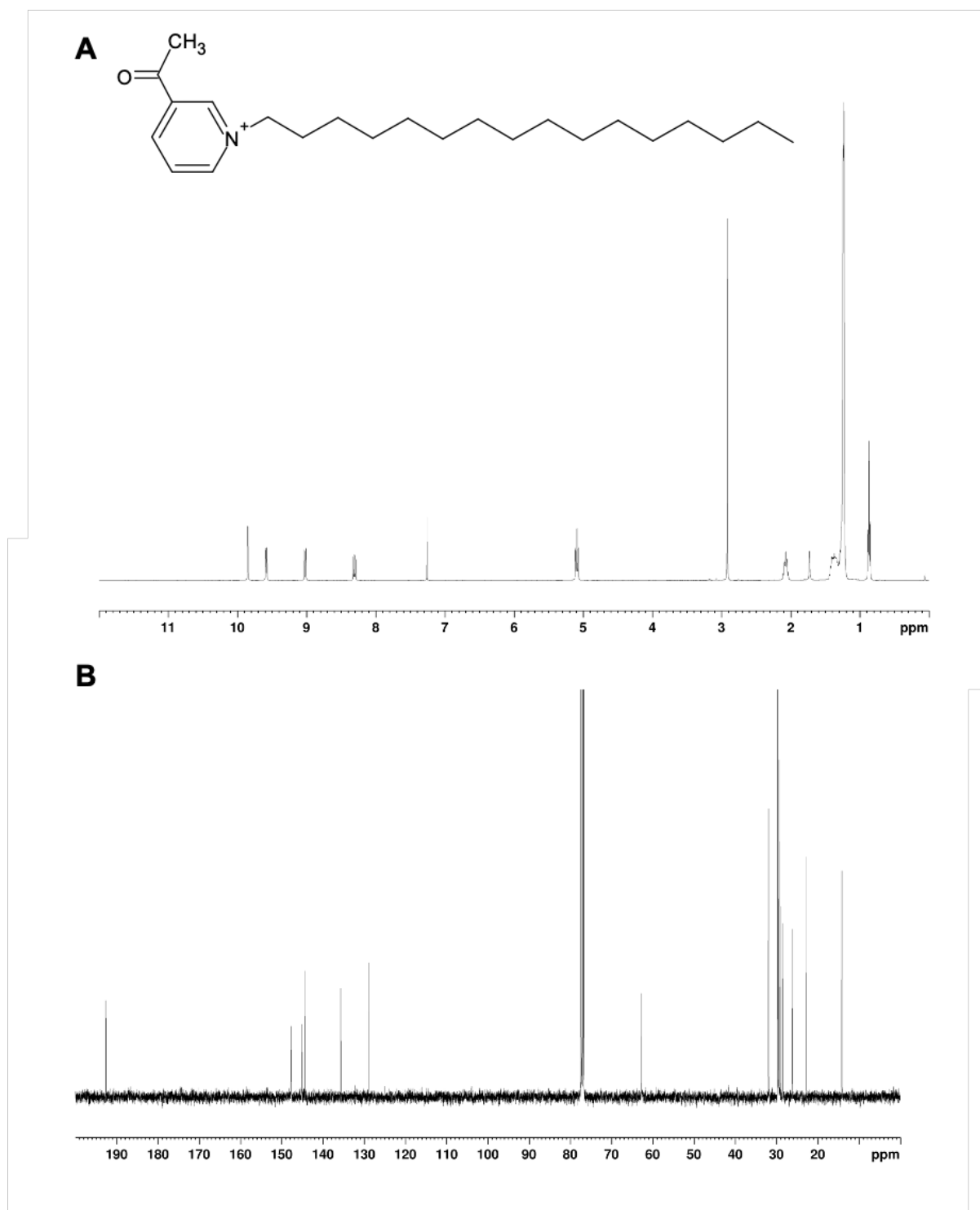
Figure 59 A)^{1}H NMR spectrum of **44**, B)^{13}C NMR spectrum of **44**.
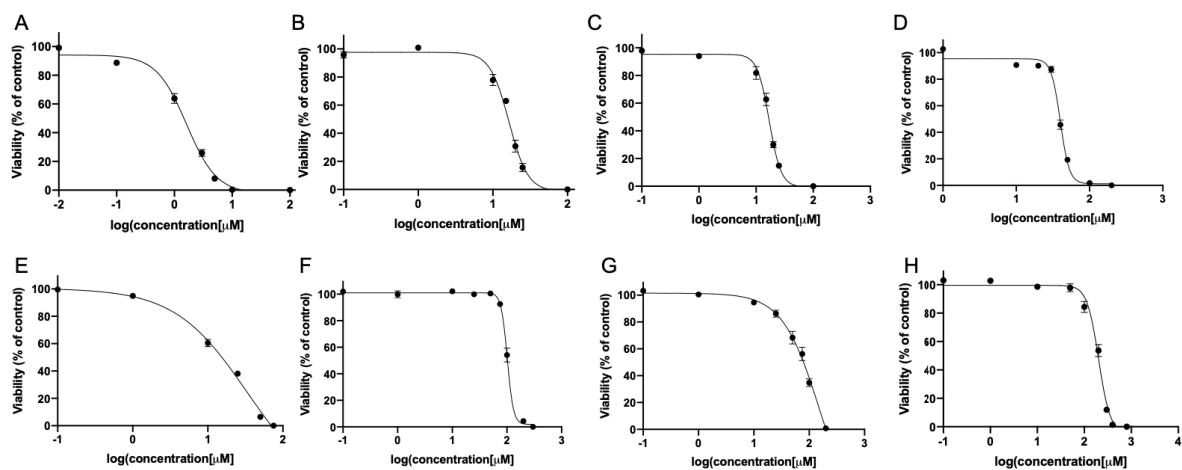
Figure 60 Dose-response curves showing the effect of ILs on the cell viability of Beas-2b cells after 48 h treatment. A) **[C₄Quin][Br]**, B) **[C₄Py][Br]**, C) **[C₄Mim][Br]**, D) **[C₄TMA][Br]**, E) **[C₁₀Quin][Br]**, F) **[C₁₀Py][Br]**, G) **[C₁₀Mim][Br]** and H) **[C₁₀TMA][Br]**. Data represents the mean ± SEM of 3 independent experiments.

Chapter 7 - Reference

(1)   Kumari, P.; Pillai, V. V. S.; Benedetto, A. Mechanisms of action of ionic liquids on living cells: the state of the art. *Biophysical Reviews* **2020**.

(2)   Introduction: Ionic Liquids. *Chemical Reviews* **2017,** *117* (10), 6633.

(3)   Walden, P. Ueber die Molekulargrösse und elektrische Leitfähigkeit einiger geschmolzenen. *Bull. L'Académie Impériale Des Sci. St.-Pétersbourg* **1914,** *8*, 405.

(4)   Greer, A. J.; Jacquemin, J.; Hardacre, C. Industrial Applications of Ionic Liquids. *Molecules (Basel, Switzerland)* **2020,** *25* (21), 5207.

(5)   Rogers, R. D.; Seddon, K. R. Ionic Liquids--Solvents of the Future? *Science* **2003,** *302* (5646), 792.

(6)   Welton, T. Room-Temperature Ionic Liquids. Solvents for Synthesis and Catalysis. *Chemical Reviews* **1999,** *99* (8), 2071.

(7)   Zhao, D.; Wu, M.; Kou, Y.; Min, E. Ionic Liquids: Applications in Catalysis. *Catalysis Today - CATAL TODAY* **2002,** *74*, 157.

(8)   Toledo Hijo, A. A. C.; Maximo, G. J.; Costa, M. C.; Batista, E. A. C.; Meirelles, A. J. A. Applications of Ionic Liquids in the Food and Bioproducts Industries. *ACS Sustainable Chemistry & Engineering* **2016,** *4* (10), 5347.

(9)   Qi, H.; Ren, Y.; Guo, S.; Wang, Y.; Li, S.; Hu, Y.; Yan, F. High-Voltage Resistant Ionic Liquids for Lithium-Ion Batteries. *ACS Applied Materials & Interfaces* **2020,** *12* (1), 591.

(10)   Kumar, V.; Malhotra, S. V. Synthesis of nucleoside-based antiviral drugs in ionic liquids. *Bioorg Med Chem Lett* **2008,** *18* (20), 5640.

(11)   Kaushik, N. K.; Attri, P.; Kaushik, N.; Choi, E. H. Synthesis and antiproliferative activity of ammonium and imidazolium ionic liquids against T98G brain cancer cells. *Molecules (Basel, Switzerland)* **2012,** (17), 13727.

(12)   Jessop, P. G. Searching for green solvents. *Green Chemistry* **2011,** *13* (6), 1391.

(13)   Cevasco, G.; Chiappe, C. Are ionic liquids a proper solution to current environmental challenges? *Green Chemistry* **2014,** *16* (5), 2375.

(14)   Clark, J. H.; Tavener, S. J. Alternative Solvents: Shades of Green. *Organic Process Research & Development* **2007,** *11* (1), 149.

(15)   Cvjetko, M.; Radošević, K.; Tomica, A.; Slivac, I.; Vorkapić-Furač, J.; Srček, V. G. Cytotoxic effects of imidazolium ionic liquids on fish and human cell lines. *Arh Hig Rada Toksikol* **2012,** *63*, 15.

(16)   Stepnowski, P.; Składanowski, A. C.; Ludwiczak, A.; Laczyńska, E. Evaluating the cytotoxicity of ionic liquids using human cell line HeLa. *Human & Experimental Toxicology* **2004,** *23*, 513.

(17)   Wang, X.; Ohlin, C. A.; Lu, Q.; Fei, Z.; Hub, J.; Dysonc, P. J. Cytotoxicity of ionic liquids and precursor compounds towards human cell line HeLa. *Green Chemistry* **2007,** (9), 1191.

(18)   Patel, D. D.; Lee, J.-M. Applications of ionic liquids. *The Chemical Record* **2012,** *12* (3), 329.

(19)   Hallett, J. P.; Welton, T. Room-Temperature Ionic Liquids: Solvents for Synthesis and Catalysis. 2. *Chemical Reviews* **2011,** *111* (5), 3508.

(20)   Kaur, G.; Kumar, H.; Singla, M. Diverse applications of ionic liquids: A comprehensive review. *Journal of Molecular Liquids* **2022,** *351*, 118556.

(21)   Nessim, M. I.; Zaky, M. T.; Deyab, M. A. Three new gemini ionic liquids: Synthesis, characterizations and anticorrosion applications. *Journal of Molecular Liquids* **2018,** *266*, 703.

(22)   Kunze, M.; Jeong, S.; Paillard, E.; Schönhoff, M.; Winter, M.; Passerini, S. New Insights to Self-Aggregation in Ionic Liquid Electrolytes for High-Energy Electrochemical Devices. *Advanced Energy Materials* **2011,** *1* (2), 274.

(23)   Mittal, H.; Al Alili, A.; Alhassan, S. M. Adsorption isotherm and kinetics of water vapors on novel superporous hydrogel composites. *Microporous and Mesoporous Materials* **2020,** *299*, 110106.

(24)   Yang, G.; Song, Y.; Wang, Q.; Zhang, L.; Deng, L. Review of ionic liquids containing, polymer/inorganic hybrid electrolytes for lithium metal batteries. *Materials & Design* **2020,** *190*, 108563.

(25)   Isikli, S.; Ryan, K. M. Recent advances in solid-state polymer electrolytes and innovative ionic liquids based polymer electrolyte systems. *Current Opinion in Electrochemistry* **2020,** *21*, 188.

(26)   Li, X.; Zheng, Y.; Li, C. Y. Dendrite-free, wide temperature range lithium metal batteries enabled by hybrid network ionic liquids. *Energy Storage Materials* **2020,** *29*, 273.

(27)   Angell, M.; Zhu, G.; Lin, M.-C.; Rong, Y.; Dai, H. Ionic Liquid Analogs of AlCl3 with Urea Derivatives as Electrolytes for Aluminum Batteries. *Advanced Functional Materials* **2020,** *30* (4), 1901928.

(28)   Rehman, A.; Zeng, X. Interfacial composition, structure, and properties of ionic liquids and conductive polymers for the construction of chemical sensors and biosensors: a perspective. *Current Opinion in Electrochemistry* **2020,** *23*, 47.

(29)   Ding, S.; Lyu, Z.; Niu, X.; Zhou, Y.; Liu, D.; Falahati, M.; Du, D.; Lin, Y. Integrating ionic liquids with molecular imprinting technology for biorecognition and biosensing: A review. *Biosensors and Bioelectronics* **2020,** *149*, 111830.

(30)   Zhao, X.; Zhou, K.; Zhong, Y.; Liu, P.; Li, Z.; Pan, J.; Long, Y.; Huang, M.; Brakat, A.; Zhu, H. Hydrophobic ionic liquid-in-polymer composites for ultrafast, linear response and highly sensitive humidity sensing. *Nano Research* **2021,** *14* (4), 1202.

(31)   Yu, L.; Liu, J.; Yin, W.; Yu, J.; Chen, R.; Song, D.; Liu, Q.; Li, R.; Wang, J. Ionic liquid combined with NiCo2O4/rGO enhances electrochemical oxygen sensing. *Talanta* **2020,** *209*, 120515.

(32)   D'Anna, F.; Grilli, M. L.; Petrucci, R.; Feroci, M. WO3 and Ionic Liquids: A Synergic Pair for Pollutant Gas Sensing and Desulfurization. *Metals* **2020,** *10* (4), 475.

(33)   Predel, T.; Pohrer, B.; Schlücker, E. Ionic Liquids as Alternative Lubricants for Special Applications. *Chemical Engineering & Technology* **2010,** *33* (1), 132.

(34)   Nasirpour, N.; Mohammadpourfard, M.; Zeinali Heris, S. Ionic liquids: Promising compounds for sustainable chemical processes and applications. *Chemical Engineering Research and Design* **2020,** *160*, 264.

(35)   Mittal, H.; Al Alili, A.; Alhassan, S. M. Solid polymer desiccants based on poly(acrylic acid-co-acrylamide) and Laponite RD: Adsorption isotherm and kinetics studies. *Colloids and Surfaces A: Physicochemical and Engineering Aspects* **2020,** *599*, 124813.

(36)   Marrucho, I. M.; Branco, L. C.; Rebelo, L. P. N. Ionic Liquids in Pharmaceutical Applications. *Annual Review of Chemical and Biomolecular Engineering* **2014,** *5* (1), 527.

(37)   Zhao, Q.; Anderson, J. L. In *Comprehensive Sampling and Sample Preparation*; Pawliszyn, J., Ed.; Academic Press: Oxford, 2012, DOI:https://doi.org/10.1016/B978-0-12-381373-2.00053-3 https://doi.org/10.1016/B978-0-12-381373-2.00053-3.

(38)   Mai, N. L.; Ahn, K.; Koo, Y.-M. Methods for recovery of ionic liquids—A review. *Process Biochemistry* **2014,** *49* (5), 872.

(39)   Dołżonek, J.; Kowalska, D.; Maculewicz, J.; Stepnowski, P. In *Encyclopedia of Ionic Liquids*; Zhang, S., Ed.; Springer Singapore: Singapore, 2020, DOI:10.1007/978-981-10-6739-6_58-1 10.1007/978-981-10-6739-6_58-1.

(40)   Tan, J. S.; Lee, S. Y.; Chew, K. W.; Lam, M. K.; Lim, J. W.; Ho, S.-H.; Show, P. L. A review on microalgae cultivation and harvesting, and their biomass extraction processing using ionic liquids. *Bioengineered* **2020,** *11* (1), 116.

(41)   Rodrigues, R. D. P.; de Castro, F. C.; Santiago-Aguiar, R. S. d.; Rocha, M. V. P. Ultrasound-assisted extraction of phycobiliproteins from Spirulina (Arthrospira) platensis using protic ionic liquids as solvent. *Algal Research* **2018,** *31*, 454.

(42)   Ika Aulia, R.; Mahdi, J.; Abdul, M. i. Extraction of Quercetin from Nothopanax scutellarium Leaves via Ionic Liquid-based Microwave-assisted Extraction. *Pharmacognosy Journal* **2020,** *12* (6s).

(43)   Amde, M.; Liu, J.-F.; Pang, L. Environmental Application, Fate, Effects, and Concerns of Ionic Liquids: A Review. *Environmental Science & Technology* **2015,** *49* (21), 12611.

(44)   Pendleton, J. N.; Gilmore, B. F. The antimicrobial potential of ionic liquids: A source of chemical diversity for infection and biofilm control. *International Journal of Antimicrobial Agents* **2015,** *46* (2), 131.

(45)   Naushad, M.; Alothman, Z. A. Separation of toxic Pb2+ metal from aqueous solution using strongly acidic cation-exchange resin: analytical applications for the removal of metal ions from pharmaceutical formulation. *Desalination and Water Treatment* **2015,** *53* (8), 2158.

(46)   Dutta, R.; Kundu, S.; Sarkar, N. Ionic liquid-induced aggregate formation and their applications. *Biophys Rev* **2018,** *10* (3), 861.

(47)   Shamshina, J. L.; Kelley, S. P.; Gurau, G.; Rogers, R. D. Chemistry: Develop ionic liquid drugs. *Nature* **2015,** *528* (7581), 188.

(48)   L., H. W.; D., R. R. Ionic Liquids Then and Now: From Solvents to Materials to Active Pharmaceutical Ingredients. *Bulletin of the Chemical Society of Japan* **2007,** *80* (12), 2262.

(49)   Ferraz, R.; Branco, L. C.; Prudêncio, C.; Noronha, J. P.; Petrovski, Ž. Ionic Liquids as Active Pharmaceutical Ingredients. *ChemMedChem* **2011,** *6* (6), 975.

(50)   Araújo, J. M. M.; Florindo, C.; Pereiro, A. B.; Vieira, N. S. M.; Matias, A. A.; Duarte, C. M. M.; Rebelo, L. P. N.; Marrucho, I. M. Cholinium-based ionic liquids with pharmaceutically active anions. *RSC Advances* **2014,** *4* (53), 28126.

(51)   Egorova, K. S.; Seitkalieva, M. M.; Posvyatenko, A. V.; Khrustalev, V. N.; Ananikov, V. P. Cytotoxic Activity of Salicylic Acid-Containing Drug Models with Ionic and Covalent Binding. *ACS Medicinal Chemistry Letters* **2015,** *6* (11), 1099.

(52)   Md Moshikur, R.; Chowdhury, M. R.; Fujisawa, H.; Wakabayashi, R.; Moniruzzaman, M.; Goto, M. Design and Characterization of Fatty Acid-Based Amino Acid Ester as a New "Green" Hydrophobic Ionic Liquid for Drug Delivery. *ACS Sustainable Chemistry & Engineering* **2020,** *8* (36), 13660.

(53)   Moshikur, R. M.; Chowdhury, M. R.; Wakabayashi, R.; Tahara, Y.; Kamiya, N.; Moniruzzaman, M.; Goto, M. Ionic liquids with N-methyl-2-pyrrolidonium cation as an enhancer for topical drug delivery: Synthesis, characterization, and skin-penetration evaluation. *Journal of Molecular Liquids* **2020,** *299*, 112166.

(54)   Organisation, W. H., Febuary 2022.

(55)   Ranke, J.; Mölter, K.; Stock, F.; Bottin-Weber, U.; Poczobutt, J.; JHoffmann; Ondruschka, B.; Filsera, J.; Jastorffa, B. Biological effects of imidazolium ionic liquids

with varying chain lengths in acute Vibrio fischeri and WST-1 cell viability assays. *Ecotoxicology and Environmental Safety* **2004,** *58* (3), 396.

(56) Salminen, J.; Papaiconomou, N.; Kumara, R. A.; Lee, J.-M.; Kerr, J.; Newman, J.; Prausnitz, J. M. Physicochemical properties and toxicities of hydrphobic piperidinium and pyrrolidinium ionic liquids. *Fluid phase equilibria* **2007,** *261* (1-2), 421.

(57) Kumar, R. A.; Papaïconomou, N.; Lee, J.-M.; Salminen, J.; Clark, D. S.; Prausnitz, J. M. In vitro cytotoxicities of ionic liquids: effect of cation rings, functional groups, and anions. *Environ Toxicol* **2009,** *24* (4), 388.

(58) García-Lorenzo, A.; Tojo, E.; Tojo, J.; Teijeira, M.; Rodríguez-Berrocal, F. J.; Gonzálezbd, M. P.; Martínez-Zorzano, V. S. Cytotoxicity of selected imidazolium-derived ionic liquids in the human Caco-2 cell line. Sub-structural toxicological interpretation through a QSAR study. *Green Chemistry* **2008,** *10*, 508.

(59) Li, X.; Ma, J.; Wang, J. Cytotoxicity, oxidative stress, and apoptosis in HepG2 cells induced by ionic liquid 1-methyl-3-octylimidazolium bromide. *Ecotoxicology and Environmental Safety* **2015,** *120*, 342.

(60) Malhotra, S. V.; Kumar, V.; Velez, C.; Zayas, B. Imidazolium-derived ionic salts induce inhibition of cancerous cell growth through apoptosis. *MedChemComm* **2014,** *5* (9), 1404.

(61) Malhotra, S. V.; Kumar, V. A profile of the in vitro anti-tumor activity of imidazolium-based ionic liquids. *Bioorganic & Medicinal Chemistry Letters* **2010,** *20* (2), 581.

(62) Zhong-bo, Z.; Shi-bo, F.; Hai-feng, D.; Ying-jie, L.; Ying, Y. Brand-new function of well-designed ionic liquid: Inhibitor of tumor cell growth. *Chemical Research in Chinese Universities* **2010,** *26* (5), 757.

(63)   Abdelghany, T. M.; Leitch, A. C.; Nevjestić, I.; Ibrahim, I.; Miwa, S.; Wilson, C.; Heutz, S.; Wright, M. C. Emerging risk from "environmentally-friendly" solvents: Interaction of methylimidazolium ionic liquids with the mitochondrial electron transport chain is a key initiation event in their mammalian toxicity. *Food and Chemical Toxicology* **2020,** *145*, 111593.

(64)   Frade, R. F. M.; Matias, A.; Branco, L. C.; Afonso, C. A. M.; Duarte, C. M. M. Effect of ionic liquids on human colon carcinoma HT-29 and CaCo-2 cell lines. *Green Chemistry* **2007,** *9* (8), 873.

(65)   Ali, I.; Hozaifa, M.; Ali, S.; Malik, A.; Locatelli, M. Advances in ionic liquids as future anti-cancer drugs. *Journal of Molecular Liquids* **2023,** *388*, 122823.

(66)   Li, X.-Y.; Jing, C.-Q.; Lei, W.-L.; Li, J.; Wang, J.-J. Apoptosis caused by imidazolium-based ionic liquids in PC12 cells. *Ecotoxicology and Environmental Safety* **2012,** *83*, 102.

(67)   Rahman, M.; O'Donnell, J. M.; Brazel, C. S. Cytotoxicity of Plasticizers and Ionic Liquids Using Drosophila melanogaster S2 Cell Culture. *Chemical Engineering & Technology* **2011,** *34* (3), 429.

(68)   Costa, S. P. F.; Pinto, P. C. A. G.; Lapa, R. A. S.; Saraiva, M. L. M. F. S. Toxicity assessment of ionic liquids with Vibrio fischeri: An alternative fully automated methodology. *Journal of Hazardous Materials* **2015,** *284*, 136.

(69)   Liu, H.; Zhang, S.; Zhang, X.; Chen, C. Growth inhibition and effect on photosystem by three imidazolium chloride ionic liquids in rice seedlings. *J Hazard Mater* **2015,** *286*, 440.

(70)   Dzhemileva, L. U.; D'Yakonov, V. A.; Seitkalieva, M. M.; Kulikovskaya, N. S.; Egorova, K. S.; Ananikov, V. P. A large-scale study of ionic liquids employed in chemistry and

energy research to reveal cytotoxicity mechanisms and to develop a safe design guide. *Green Chemistry* **2021,** *23* (17), 6414.

(71) Kulacki, K. J.; Lamberti, G. A. Toxicity of imidazolium ionic liquids to freshwater algae. *Green Chemistry* **2008,** *10* (1), 104.

(72) Latała, A.; Nędzi, M.; Stepnowski, P. Toxicity of imidazolium and pyridinium based ionic liquids towards algae. Chlorella vulgaris, Oocystis submarina (green algae) and Cyclotella meneghiniana, Skeletonema marinoi (diatoms). *Green Chemistry* **2009,** *11* (4), 580.

(73) Chen, H.; Zou, Y.; Zhang, L.; Wen, Y.; Liu, W. Enantioselective toxicities of chiral ionic liquids 1-alkyl-3-methylimidazolium lactate to aquatic algae. *Aquatic Toxicology* **2014,** *154*, 114.

(74) Deng, X. Y.; Hu, X. L.; Cheng, J.; Ma, Z. X.; Gao, K. Growth inhibition and oxidative stress induced by 1-octyl-3-methylimidazolium bromide on the marine diatom Skeletonema costatum. *Ecotoxicol Environ Saf* **2016,** *132*, 170.

(75) Biczak, R.; Pawłowska, B.; Bałczewski, P.; Rychter, P. The role of the anion in the toxicity of imidazolium ionic liquids. *Journal of Hazardous Materials* **2014,** *274*, 181.

(76) Cvjetko Bubalo, M.; Hanousek, K.; Radošević, K.; Gaurina Srček, V.; Jakovljević, T.; Radojčić Redovniković, I. Imidiazolium based ionic liquids: effects of different anions and alkyl chains lengths on the barley seedlings. *Ecotoxicol Environ Saf* **2014,** *101*, 116.

(77) Matzke, M.; Stolte, S.; Arning, J.; Uebers, U.; Filser, J. Imidazolium based ionic liquids in soils: effects of the side chain length on wheat (Triticum aestivum) and cress (Lepidium sativum) as affected by different clays and organic matter. *Green Chemistry* **2008,** *10* (5), 584.

(78)   Pawłowska, B.; Biczak, R. Evaluation of the effect of tetraethylammonium bromide and chloride on the growth and development of terrestrial plants. *Chemosphere* **2016,** *149*, 24.

(79)   Biczak, R.; Telesiński, A.; Pawłowska, B. Oxidative stress in spring barley and common radish exposed to quaternary ammonium salts with hexafluorophosphate anion. *Plant Physiology and Biochemistry* **2016,** *107*, 248.

(80)   Ventura, S. P.; e Silva, F. A.; Gonçalves, A. M.; Pereira, J. L.; Gonçalves, F.; Coutinho, J. A. Ecotoxicity analysis of cholinium-based ionic liquids to Vibrio fischeri marine bacteria. *Ecotoxicol Environ Saf* **2014,** *102*, 48.

(81)   Walkiewicz, F.; Materna, K.; Kropacz, A.; Michalczyk, A.; Gwiazdowski, R.; Praczyk, T.; Pernak, J. Multifunctional long-alkyl-chain quaternary ammonium azolate based ionic liquids. *New Journal of Chemistry* **2010,** *34* (10), 2281.

(82)   Ismail Hossain, M.; El-Harbawi, M.; Noaman, Y. A.; Bustam, M. A. B.; Alitheen, N. B. M.; Affandi, N. A.; Hefter, G.; Yin, C.-Y. Synthesis and anti-microbial activity of hydroxylammonium ionic liquids. *Chemosphere* **2011,** *84* (1), 101.

(83)   Frade, R. F. M.; Afonso, C. A. M. Impact of ionic liquids in environment and humans: an overview. *Human & Experimental Toxicology* **2010,** *29* (12), 1038.

(84)   Bubalo, M. C.; Radošević, K.; Srček, V. G.; Das, R. N.; PaulPopelier; KunalRoy. Cytotoxicity towards CCO cells of imidazolium ionic liquids with functionalized side chains: Preliminary QSTR modeling using regression and classification based approaches. *Ecotoxicology and Environmental Safety* **2015,** *112*, 22.

(85)   Chen, H. L.; Kao, H. F.; Wang, J. Y.; Wei, G. T. Cytotoxicity of Imidazole Ionic Liquids in Human Lung Carcinoma A549 Cell Line. *Journal Of The Chinese Chemical Society* **2014,** *61* (7), 763.

(86)   Rusiecka, I.; Składanowski, A. C. Induction of the multixenobiotic/multidrug resistance system in HeLa cells in response to imidazolium ionic liquids. *Acta Biochimica Polonice* **2011,** *58* (2), 187.

(87)   Delgado-Mellado, N.; Ayuso, M.; Villar-Chavero, M. M.; García, J.; Rodríguez, F. Ecotoxicity evaluation towards Vibrio fischeri of imidazolium- and pyridinium-based ionic liquids for their use in separation processes. *SN Applied Sciences* **2019,** *1* (8), 896.

(88)   Frade, R. F. M.; Rosatella, A. A.; Marques, C. S.; Branco, L. C.; Kulkarni, P. S.; Mateus, N. M. M.; Afonsob, C. A. M.; Duartea, C. M. M. Toxicological evaluation on human colon carcinoma cell line (CaCo-2) of ionic liquids based on imidazolium, guanidinium, ammonium, phosphonium, pyridinium and pyrrolidinium cations. *Green Chemistry* **2009,** *11*, 1660.

(89)   Kumar, V.; Malhotra, S. V. Study on the potential anti-cancer activity of phosphonium and ammonium-based ionic liquids. *Bioorganic & Medicinal Chemistry Letters* **2009,** *19*, 4643.

(90)   Frade, R. F.; Afonso, C. A. Impact of ionic liquids in environment and humans: An overview. *Human and Experimental Toxicology* **2010,** *19* (12), 1038.

(91)   Egorova, K. S.; Gordeev, E. G.; Ananikov, V. P. Biological Activity of Ionic Liquids and Their Application in Pharmaceutics and Medicine. *Chemical Reviews* **2017,** *117*, 7132.

(92)   van Meer, G. Lipid traffic in animal cells. *Annu Rev Cell Biol* **1989,** *5*, 247.

(93)   Singer, S. J.; Nicolson, G. L. The fluid mosaic model of the structure of cell membranes. *Science* **1972,** *175* (4023), 720.

(94)   Kumar, S.; Scheidt, H. A.; Kaur, N.; Kang, T. S.; Gahlay, G. K.; Huster, D.; Mithu, V. S. Effect of the Alkyl Chain Length of Amphiphilic Ionic Liquids on the Structure and Dynamics of Model Lipid Membranes. *Langmuir* **2019,** *35* (37), 12215.

(95)   Benedetto, A.; Heinrich, F.; Gonzalez, M. A.; Fragneto, G.; Watkins, E.; Ballone, P.
Structure and Stability of Phospholipid Bilayers Hydrated by a Room-Temperature
Ionic Liquid/Water Solution: A Neutron Reflectometry Study. *The Journal of Physical
Chemistry B* **2014,** *118* (42), 12192.

(96)   Kaur, N.; Fischer, M.; Kumar, S.; Gahlay, G. K.; Scheidt, H. A.; Mithu, V. S. Role of
cationic head-group in cytotoxicity of ionic liquids: Probingchanges in bilayer
architecture using solid-state NMR spectroscopy. *Journal of Colloid and Interface
Science* **2021,** *581*, 954.

(97)   Jing, B.; Lan, N.; Qiu, J.; Zhu, Y. Interaction of Ionic Liquids with a Lipid Bilayer: A
Biophysical Study of Ionic Liquid Cytotoxicity. *The Journal of Physical Chemistry B* **2016,**
120 (10), 2781.

(98)   Yoo, B.; Jing, B.; Jones, S. E.; Lamberti, G. A.; Zhu, Y.; Shah, J. K.; Maginn, E. J. Molecular
mechanisms of ionic liquid cytotoxicity probed by an integrated experimental and
computational approach. *Scientific Reports* **2016,** *6* (1), 19889.

(99)   Yoo, B.; Shah, J. K.; Zhu, Y.; Maginn, E. J. Amphiphilic interactions of ionic liquids with
lipid biomembranes: a molecular simulation study. *Soft Matter* **2014,** *10* (43), 8641.

(100)   Stolte, S.; Arning, J.; Bottin-Weber, U.; Matzke, M.; Thiele, F. S. K.; Uerdingen, M.;
Welz-Biermann, U.; Jastorffa, B.; Ranke, J. Anion effects on the cytotoxicity of ionic
liquids. *Green Chemistry* **2006,** *8* (7), 621.

(101)   Gal, N.; Malferarri, D.; Kolusheva, S.; Galletti, P.; Tagliavini, E.; Jelinek, R. Membrane
interactions of ionic liquids: Possible determinants for biological activity and toxicity.
Biochimica et Biophysica Acta (BBA) - Biomembranes **2012,** *1818* (12), 2967.

(102)   B, J.; N, L.; Qiu, J.; Zhu, Y. Interaction of Ionic Liquids with a Lipid Bilayer: A Biophysical
Study of Ionic Liquid Cytotoxicity. *The Journal of Physical Chemistry B* **2016,** *120*, 2781.

(103) Cook, K.; Tarnawsky, K.; Swinton, A. J.; Yang, D. D.; Senetra, A. S.; Caputo, G. A.; Carone, B. R.; Vaden, T. D. Correlating Lipid Membrane Permeabilities of Imidazolium Ionic Liquids with Their Cytotoxicities on Yeast, Bacterial, and Mammalian Cells. *Biomolecules* **2019,** *9* (6), 251.

(104) Li, X.-Y.; Jing, C.-Q.; Zang, X.-Y.; Yang, S.; Wang, J.-J. Toxic cytological alteration and mitochondrial dysfunction in PC12 cells induced by 1-octyl-3-methylimidazolium chloride. *Toxicology in Vitro* **2012,** *26* (7), 1087.

(105) Wu, S.; Zeng, L.; Wang, C.; Yang, Y.; Zhou, W.; Li, F.; Tan, Z. Assessment of the cytotoxicity of ionic liquids on Spodoptera frugiperda 9 (Sf-9) cell lines via in vitro assays. *Journal of Hazardous Materials* **2018,** *348*, 1.

(106) Austin, R. P.; Barton, P.; Davis, A. M.; Manners, C. N.; Stansfield, M. C. The Effect of Ionic Strength on Liposome–Buffer and 1-Octanol–Buffer Distribution Coefficients. *Journal of Pharmaceutical Sciences* **1998,** *87* (5), 599.

(107) Chellappan, D. K.; Paudel, K. R.; Tan, N. W.; Cheong, K. S.; Khoo, S. S. Q.; Seow, S. M.; Chellian, J.; Candasamy, M.; Patel, V. K.; Arora, P.et al. Targeting the mitochondria in chronic respiratory diseases. *Mitochondrion* **2022,** *67*, 15.

(108) Brenner, C.; Kroemer, G. Mitochondria--the Death Signal Integrators. *Science* **2000,** *289* (5482), 1150.

(109) McBride, H. M.; Neuspiel, M.; Wasiak, S. Mitochondria: more than just a powerhouse. *Current Biology* **2006,** *16* (14), 551.

(110) Milane, L.; Trivedi, M.; Singh, A.; Talekar, M.; Amiji, M. Mitochondrial biology, targets, and drug delivery. *Journal of Controlled Release* **2015,** *207* (10), 40.

(111) Nolfi-Donegana, D.; Braganzaa, A.; Shiva, S. Mitochondrial electron transport chain: Oxidative phosphorylation, oxidant production, and methods of measurement. *Redox Biology* **2020,** *37*, 2213.

(112) Childress, E. S.; Alexopoulos, S. J.; Hoehn, K. L.; Santos, W. L. Small Molecule Mitochondrial Uncouplers and Their Therapeutic Potential. *Journal of Medicinal Chemistry* **2018,** *61* (11), 4641.

(113) Li, A.; Gao, M.; Liu, B.; Qin, Y.; chen, L.; Liu, H.; Wu, H.; Gong, G. Mitochondrial autophagy: molecular mechanisms and implications for cardiovascular disease. *Cell Death & Disease* **2022,** *13* (5), 444.

(114) Ma, J.; Li, X. Insight into the negative impact of ionic liquid: A cytotoxicity mechanism of 1-methyl-3-octylimidazolium bromide. *Environmental Pollution* **2018,** *242*, 1337.

(115) Zorova, L. D.; Popkov, V. A.; Plotnikov, E. Y.; Silachev, D. N.; Pevzner, I. B.; Jankauskas, S. S.; Babenko, V. A.; Zorov, S. D.; Balakireva, A. V.; Juhaszova, M.et al. Mitochondrial membrane potential. *Analytical biochemistry* **2018,** *552*, 50.

(116) Hu, L.-X.; Xiong, Q.; Shi, W.-J.; Huang, G.-Y.; Liu, Y.-S.; Ying, G.-G. New insight into the negative impact of imidazolium-based ionic liquid [C10mim]Cl on Hela cells: From membrane damage to biochemical alterations. *Ecotoxicology and Environmental Safety* **2021,** *208*, 111629.

(117) Smith, R. A.; Hartley, R. C.; Murphy, M. P. Mitochondria-targeted small molecule therapeutics and probes, Antioxid. *Redox Signal* **2011,** *15*, 3021.

(118) Guzman-Villanueva, D.; Mendiola, M. R.; Nguyen, H. X.; Weissig, V. Influence of Triphenylphosphonium (TPP) Cation Hydrophobization with Phospholipids on Cellular Toxicity and Mitochondrial Selectivity. *SOJ Pharmacy & Pharmaceutical Sciences* **2015,** *2* (1), 1.

(119)   Zielonka, J.; Joseph, J.; Sikora, A.; Hardy, M.; Ouari, O.; Vasquez-Vivar, J.; Cheng, G.; Lopez, M.; Kalyanaraman, B. Mitochondria-Targeted Triphenylphosphonium-Based Compounds: Syntheses, Mechanisms of Action, and Therapeutic and Diagnostic Applications. *Chemical Reviews* **2017,** *117* (15), 10043.

(120)   Jeena, M. T.; Kim, S.; Jin, S.; Ryu, J.-H. Recent Progress in Mitochondria-Targeted Drug and Drug-Free Agents for Cancer Therapy. *Cancers* **2020,** *12* (1).

(121)   Prag, H. A.; Kula-Alwar, D.; Pala, L.; Caldwell, S. T.; Beach, T. E.; James, A. M.; Saeb-Parsy, K.; Krieg, T.; Hartley, R. C.; Murphy, M. P. Selective Delivery of Dicarboxylates to Mitochondria by Conjugation to a Lipophilic Cation via a Cleavable Linker. *Molecular pharmaceutics* **2020,** *17*, 3526.

(122)   Biasutto, L.; D, L.-F.; Zoratti, M.; Neuzil, J. Mitochondrially targeted anti-cancer agents. *Mitochondrion* **2010,** *10* (6), 670.

(123)   Murphy, M. P.; Smith, R. A. Targeting antioxidants to mitochondria by conjugation to lipophilic cations. *Annu Rev Pharmacol Toxicol* **2007,** *47*, 629.

(124)   Kurtoglu, M.; Lampidis, T. J. From delocalized lipophilic cations to hypoxia: blocking tumor cell mitochondrial function leads to therapeutic gain with glycolytic inhibitors. *Mol Nutr Food Res* **2009,** *53* (1), 68.

(125)   Modica-Napolitano, J. S.; Aprille, J. R. Delocalized lipophilic cations selectively target the mitochondria of carcinoma cells. *Advanced Drug Delivery Reviews* **2001,** *49* (1–2), 63.

(126)   Trachootham, D.; Alexandre, J.; Huang, P. Targeting cancer cells by ROS-mediated mechanisms: a radical therapeutic approach? *Nature reviews drug discovery* **2009,** *8*, 579

(127) Liou, G.-Y.; Storz, P. Reactive oxygen species in cancer. *Free Radical Research* **2010,** *44* (5), 479.

(128) Heller, A.; Brockhoff, G.; Goepferich, A. Targeting drugs to mitochondria. *European Journal of Pharmaceutics and Biopharmaceutics* **2012,** *82*, 1.

(129) Lu, P.; Bruno, B. J.; Rabenau, M.; Lim, C. S. Delivery of Drugs and Macromolecules to the Mitochondria for Cancer Therapy. *Journal of Controlled Release* **2016,** *240*, 38.

(130) Battogtokh, G.; Choi, Y. S.; Kang, D. S.; Park, S. J.; Shim, M. S.; Huh, K. M.; Cho, Y.-Y.; Lee, J. Y.; Lee, H. S.; Kang, H. C. Mitochondria-targeting drug conjugates for cytotoxic, anti-oxidizing and sensing purposes: current strategies and future perspectives. *Acta Pharmaceutica Sinica B* **2018,** *8* (6), 862.

(131) Neuzil, J.; Weber, T.; Schröder, A.; Lu, M.; Ostermann, G.; Gellert, N.; Mayne, G. C.; Olejnicka, B.; Nègre-Salvayre, A.; Stícha, M.et al. Induction of cancer cell apoptosis by alpha-tocopheryl succinate: molecular pathways and structural requirements. *Faseb j* **2001,** *15* (2), 403.

(132) Dong, L.-F.; Jameson, V. J. A.; Tilly, D.; Prochazka, L.; Rohlena, J.; Valis, K.; Truksa, J.; Zobalova, R.; Mahdavian, E.; Kluckova, K.et al. Mitochondrial targeting of α-tocopheryl succinate enhances its pro-apoptotic efficacy: A new paradigm for effective cancer therapy. *Free Radical Biology and Medicine* **2011,** *50* (11), 1546.

(133) Millard, M.; Gallagher, J. D.; Olenyuk, B. Z.; Neamati, N. A selective mitochondrial-targeted chlorambucil with remarkable cytotoxicity in breast and pancreatic cancers. *J Med Chem* **2013,** *56* (22), 9170.

(134) Menschutkin, N. Beiträge zur Kenntnis der Affinitätskoeffizienten der Alkylhaloide und der organischen Amine. *Zeitschrift für Physikalische Chemie* **1890,** *5U* (1), 589.

(135) Bubalo, M. C.; Radošević, K.; Srček, V. G.; Das, R. N.; Popelier, P.; Roy, K. Cytotoxicity towards CCO cells of imidazolium ionic liquids with functionalized side chains: Preliminary QSTR modeling using regression and classification based approaches. *Ecotoxicology and Environmental Safety* **2015,** *112*, 22.

(136) Kumar, V.; Malhotra, S. V. Study on the potential anti-cancer activity of phosphonium and ammonium-based ionic liquids. *Bioorganic Medicinal Chemistry Letters* **2009,** *19*, 4643.

(137) Bernot, R. J.; Brueseke, M. A.; Evans-White, M. A.; Lamberti, G. A. Acute and chronic toxicity of imidazolium-based ionic liquids on Daphnia magna. *Environmental Toxicology and Chemistry* **2005,** *24* (1), 87.

(138) Garcia, M. T.; Gathergood, N.; Scammells, P. J. Biodegradable ionic liquids. part II: effect of the anion and toxicology. *Green Chemistry* **2005,** *7*, 9.

(139) Dias, A. R.; Costa-Rodrigues, J.; Fernandes, M. H.; Ferraz, R.; Prudêncio, C. The Anticancer Potential of Ionic Liquids. *ChemMedChem* **2017,** *12*, 11.

(140) Pham, T. P.; Chul-WoongCho; Yeoung-SangYun. Environmental fate and toxicity of ionic liquids: a review. *Water Research* **2010,** *44* (2), 352.

(141) Cranfield, C.; Carne, S.; Martinac, B.; Cornell, B. The assembly and use of tethered bilayer lipid membranes (tBLMs). *Methods Mol Biol* **2015,** *1232*, 45.

(142) Cranfield, C. G.; Berry, T.; Holt, S. A.; Hossain, K. R.; Brun, A. P. L.; Carne, S.; Khamici, H. A.; Coster, H.; Valenzuela, S. M.; Cornell, B. Evidence of the Key Role of H3O+ in Phospholipid Membrane Morphology. *Langmuir* **2016,** *32* (41), 10725.

(143) Horvath, S. E.; Daum, G. Lipids of mitochondria. *Prog Lipid Res* **2013,** *52* (4), 590.

(144) Bakshi, K.; Mitra, S.; Sharma, V. K.; Jayadev, M. S. K.; Sakai, V. G.; Mukhopadhyay, R.; Gupta, A.; Ghosh, S. K. Imidazolium-based ionic liquids cause mammalian cell death

due to modulated structures and dynamics of cellular membrane. *Biochimica et Biophysica Acta (BBA) - Biomembranes* **2020,** *1862* (2), 183103.

(145)   Busschaert, N.; Bradberry, S. J.; Wenzel, M.; Haynes, C. J. E.; Hiscock, J. R.; Kirby, I. L.; Karagiannidis, L. E.; Moore, S. J.; Wells, N. J.; Herniman, J.et al. Towards predictable transmembrane transport: QSAR analysis of anion binding and transport. *Chemical Science* **2013,** *4* (8), 3036.

(146)   Xu, J.; He, H.; Zhou, L. J.; Liu, Y. Z.; Li, D. W.; Jiang, F. L.; Liu, Y. Pyridinium and indole orientation determines the mitochondrial uncoupling and anti-cancer efficiency of F16. *Eur J Med Chem* **2018,** *154*, 305.

(147)   Chen, H.; Wang, J.; Feng, X.; Zhu, M.; Hoffmann, S.; Hsu, A.; Qian, K.; Huang, D.; Zhao, F.; Liu, W.et al. Mitochondria-targeting fluorescent molecules for high efficiency cancer growth inhibition and imaging. *Chem Sci* **2019,** *10* (34), 7946.

(148)   Saha, P. C.; Chatterjee, T.; Pattanayak, R.; Das, R. S.; Mukherjee, A.; Bhattacharyya, M.; Guha, S. Targeting and Imaging of Mitochondria Using Near-Infrared Cyanine Dye and Its Application to Multicolor Imaging. *ACS Omega* **2019,** *4* (11), 14579.

(149)   Fulda, S.; Galluzzi, L.; Kroemer, G. Targeting mitochondria for cancer therapy. *Nat Rev Drug Discov* **2010,** *9* (6), 447.

(150)   Shrestha, R.; Johnson, E.; Byrne, F. L. Exploring the therapeutic potential of mitochondrial uncouplers in cancer. *Mol Metab* **2021,** *51*, 101222.

(151)   Abdelghany, T. M.; Leitch, A. C.; Nevjestić, I.; Ibrahim, I.; Miwa, S.; Wilson, C.; Heutz, S.; Wright, M. C. Emerging risk from "environmentally-friendly" solvents: Interaction of methylimidazolium ionic liquids with the mitochondrial electron transport chain is a key initiation event in their mammalian toxicity. *Food and Chemical Toxicology* **2020,** *145*, 111593.

(152) de Moura, M. B.; Van Houten, B. Bioenergetic analysis of intact mammalian cells using the Seahorse XF24 Extracellular Flux analyzer and a luciferase ATP assay. *Methods Mol Biol* **2014,** *1105*, 589.

(153) Probert, P. M.; Leitch, A. C.; Dunn, M. P.; Jones, D. E.; Blain, P. G.; Wright, M. C. Identification of a xenobiotic as a potential environmental trigger in primary biliary cholangitis. *Journal of Hepatology* **2018,** *69*, 1123.

(154) Lofaro, F. D.; Boraldi, F.; Garcia-Fernandez, M.; Estrella, L.; Valdivielso, P.; Quaglino, D. Relationship Between Mitochondrial Structure and Bioenergetics in Pseudoxanthoma elasticum Dermal Fibroblasts. *Frontiers in Cell and Developmental Biology* **2020,** *8*.

(155) Decleer, M.; Jovanovic, J.; Vakula, A.; Udovicki, B.; Agoua, R. E. K.; Madder, A.; De Saeger, S.; Rajkovic, A. Oxygen Consumption Rate Analysis of Mitochondrial Dysfunction Caused by Bacillus cereus Cereulide in Caco-2 and HepG2 Cells. *Toxins (Basel)* **2018,** *10* (7).

(156) Brand, M. D.; Nicholls, D. G. Assessing mitochondrial dysfunction in cells. *Biochem J* **2011,** *435* (2), 297.

(157) Chen, Y.; Gibson, S. B. Is mitochondrial generation of reactive oxygen species a trigger for autophagy? *Autophagy* **2008,** *4* (2), 246.

(158) Finkel, T.; Holbrook, N. J. Oxidants, oxidative stress and the biology of ageing. *Nature* **2000,** *408* (6809), 239.

(159) Finkel, T.; Holbrook, N. J. Oxidants, oxidative stress and the biology of ageing. *Nature* **2000,** *408*, 239.

(160) Korge, P.; John, S. A.; Calmettes, G.; Weiss, J. N. Reactive oxygen species production induced by pore opening in cardiac mitochondria: The role of complex II. *J Biol Chem* **2017,** *292* (24), 9896.

(161) Aldeghi, M.; Malhotra, S.; Selwood, D. L.; Chan, A. W. E. Two- and Three-dimensional Rings in Drugs. *Chemical Biology & Drug Design* **2014,** *83* (4), 450.

(162) Polêto, M. D.; Rusu, V. H.; Grisci, B. I.; Dorn, M.; Lins, R. D.; Verli, H. Aromatic Rings Commonly Used in Medicinal Chemistry: Force Fields Comparison and Interactions With Water Toward the Design of New Chemical Entities. *Frontiers in Pharmacology* **2018,** *9*.

(163) Madaan, P.; Tyagi, V. K. Quaternary pyridinium salts: a review. *J Oleo Sci* **2008,** *57* (4), 197.

(164) Bonhôte, P.; Dias, A.-P.; Papageorgiou, N.; Kalyanasundaram, K.; Grätzel, M. Hydrophobic, Highly Conductive Ambient-Temperature Molten Salts. *Inorganic Chemistry* **1996,** *35* (5), 1168.

(165) Duffin, G. F. In *Advances in Heterocyclic Chemistry*; Katritzky, A. R., Ed.; Academic Press, 1964; Vol. 3.

(166) Hansch, C.; Leo, A.; Taft, R. W. A survey of Hammett substituent constants and resonance and field parameters. *Chemical Reviews* **1991,** *91* (2), 165.

(167) McDaniel, D. H.; Brown, H. C. An Extended Table of Hammett Substitutent Constants Based on the Ionization of Substituted Benzoic Acids. *The Journal of Organic Chemistry* **1958,** *23* (3), 420.

(168) C, C.; S, C.; B, M.; B, C. The Assembly and Use of Tethered Bilayer Lipid Membranes (tBLMs). *Methods Mol Biol* **2015,** *1232*, 45.

(169) G, C. C.; T, B.; B, C. Nanoscale Ion Sequestration To Determine the Polarity Selectivity of Ion Conductance in Carriers and Channels. *Langmuir* **2015,** *31*, 292.